Diamondoid 2-Substituted 1,3-butadienes: Synthesis and Characterization of Thermal and Mechanical Properties

A Dissertation
Presented in Partial Fulfillment of the Requirements for the
Degree of Doctor of Philosophy
with a
Major in Chemical Engineering
in the
College of Graduate Studies
University of Idaho
by
Connor J. Hill

Major Professor: Mark Roll, Ph.D.
Committee Members: Armando McDonald, Ph.D.; Kristopher Waynant, Ph.D.;
James Moberly, Ph.D.
Department Administrator: Dev Shrestha, Ph.D.

August 2021

Authorization to Submit Dissertation

This dissertation of Connor J. Hill, submitted for the degree of Doctor of Philosophy with a Major in Chemical Engineering and titled "Diamondoid 2-Substituted 1,3-butadienes: Synthesis and Characterization of Thermal and Mechanical Properties," has been reviewed in final form. Permission, as indicated by the signatures and dates below, is now granted to submit final copies to the College of Graduate Studies for approval.

Major Professor:	Mark Roll, Ph.D.	Date: 7/20/2021
Committee Members:	Armando McDonald, Ph.D.	Date: 07/23/2021
	Kristopher Waynant, Ph.D.	Date: 07/20/2021
	James Moberly, Ph.D.	Date: 07/20/21
Department Administrator:	Dev Shrestha, Ph.D.	Date: 07/20/2021

Abstract

An improved monomer synthesis for diamondoid 2-substituted 1,3-butadienes is presented. Heterogenous dehydration of 2-(1-adamantyl)-3-buten-2-ol using Amberlyst®-15 cationic exchange resin at ambient temperature gave 2-(1-adamantyl)-1,3-butadiene (**1**) in excellent yield. An improved UV photoacetylation of diamantane was also identified and the dehydration of 2-(4-diamantyl)-3-buten-2-ol afforded 2-(4-diamantyl)-1,3-butadiene (**2**) in good yields. Overall, heterogeneous dehydration with Amberlyst®-15 presents an attractive monomer synthesis route for diamondoid 2-substituted 1,3-butadienes in quantities necessary for comprehensive polymerization studies.

Emulsion polymerization of **1** and mixtures of **1** and isoprene was carried out at room temperature using redox pair-type hydroperoxide initiator. All poly(**1)** and poly(**1**-*ran*-isoprene) samples were soluble in common organic solvents and exhibited high 1,4-microstructure. A continuous increase in glass transition temperature (T_g) from -63 to 172°C was observed by increasing the ratio of **1** in the comonomer feed of poly(**1**-*ran*-isoprene), and T_g values were in good agreement with the Fox equation. After complete hydrogenation to poly(**1**-vinyladamantane-*alt*-ethylene-*ran*-propylene-*alt*-ethylene) a continuous increase in T_g was observed from -55 to 152°C. The high solubility and improved access to 2-(1-admantyl)-1,3-butadiene open the door for the exploration of diene polymers with enhanced high temperature properties.

The first mechanical characterization of the poly(**1**) and the rubbery poly(**1**-*ran*-isoprene) system is reported here. Bulk samples were hot pressed and analyzed with dynamic mechanical analysis in a 3-point bend geometry. In conjunction with rheometry, a more complete characterization of the glass transition, rubbery plateau, and rubbery flow regions with respect to wt% of **1** was achieved. Rheology of poly(**1**) before and after complete hydrogenation of the backbone was performed to understand the effect that backbone rigidity has on flow properties.

Nitroxide mediated polymerization was investigated as a potential route for poly(**1**) block copolymers. However, it was determined that the formation of monoterpene side products was favored at required reaction temperatures. A novel living anionic polymerization technique using 4,5-methylenephenanthrene an indicator to titrate impurities prior to initiation with *sec*-butyllithium was then used to synthesize poly(**1**) and poly(**1**-*block*-isoprene). A comparison of anionic to emulsion poly(**1**) prompted an investigation into the insolubility of the former. Powder x-ray diffraction experiments revealed distinct diffraction peaks in anionic poly(**1**). NMR and GPC analysis suggests the presence of branching in emulsion poly(**1**) while anionic poly(**1**) was confirmed to be completely linear. It is hypothesized that branching in emulsion poly(**1**) contributes its observed solubility.

Acknowledgements

The following individuals have been instrumental to my doctoral research and my ability to maintain any semblance of family life, for which I am deeply grateful. First, I would like to thank my committee members, Prof. McDonald, Dr. Waynant, and Dr. Moberly for their expertise, feedback, funding, equipment, and patience over the last half decade. A special thanks goes to all the other faculty and staff that have guided my work, especially Alex Blumenfeld, Tom Willams, Dave MacPherson, Charles Cornwall, and Brian Petty.

Throughout my time at the U of I, I have interacted with people who have left a deeply positive impact on my life. Although too numerous to mention individually, I would like to specifically thank Stephanie Haag and Carson Silsby for their support and friendship.

I have been remarkably fortunate to have maintained funding throughout my graduate studies. This would not have been possible without the efforts of people like Prof. Brian Johnson, Prof. Eric Aston, and generous contributions from the Walter C. Hayes Engineering Scholarship, the Richard V. Roehl Jr. Memorial Scholarship, and the Almquist family. Thank you.

Lastly, I would like to acknowledge my advisor, Dr. Mark Roll for his continued mentorship throughout an often tumultuous 5 years. This has been a journey for us both, but I will be forever grateful that you encouraged me to pursue my Ph.D.

Dedication

To my incredibly loving and patient family. This would not have been possible without you.

Table of Contents

Authorization to Submit Dissertation ii

Abstract iii

Acknowledgements iv

Dedication v

Table of Contents vi

List of Tables ix

List of Figures x

List of Schemes xii

Chapter 1: Introduction 1

- Polyisoprene Rubbers 1
- Introduction to Polymers 4
- Bulk Polymer Morphology and Thermal Transitions 7
- Thermoplasticity and Dynamic Mechanical Analysis 9
- Block Copolymer Self-Assembly 12
- Natural vs. Synthetic rubbers 14
- Designed 2-Subsitutents in Polydienes 15
- Diamondoids 16
- Diamondoids in Polymers: State of the Art 17
- Summary of Work 19

Chapter 2: Straightforward Synthesis of Diamondoid Substituted 1,3-Butadiene Monomers with Amberlyst®-15 23

- Abstract 23
- Introduction 23
- Experimental 26
- Results and Discussion 32
- Conclusions 41

Chapter 3: Poly(2-(1-adamantyl)-1,3-butadiene and Random Copolymers with Isoprene via Redox-emulsion Polymerization and their Hydrogenation 43
Abstract 43
Introduction 43
Methods and Materials 45
Results and Discussion 47
Conclusions 55
Chapter 4: Mechanical Characterization of poly(**1**) and poly(**1**-*ran*-isoprene) 57
Abstract 57
Introduction 57
Methods and Materials 59
Results and Discussion 60
Conclusions 66
Chapter 5: Anionic Polymerization of poly(2-(1-adamantyl)-1,3-butadiene) 67
Abstract 67
Introduction 67
Experimental 69
Results and Discussion 70
Conclusions 80
Chapter 6: Conclusions and Future Work 82
Summary 82
Broader Impacts and Future Work 82
Chapter 7: References 86
Appendix A - Chapter 2 Supporting Information 91
UV Photoacetylation of Diamantane 91
Monoterpene Characterization 94
NMR Spectra of Isolated Compounds 100

Appendix B - Chapter 3 Supporting Information 116
    Microstructure Characterization 116
    Determination of Adamantyl Content in poly(**1**-*ran*-isoprene) by ^{1}H NMR 118
    Differential Scanning Calorimetry of Copolymer and Physical Mixture 119
    Variation of T_g with M_n for poly(**1**) 119

List of Tables

Table 2.1: Monoterpene concentration at endpoint 36
Table 2.2: Dehydration of 2-(1-adamantyl)-1,3-butadiene in the presence of various desiccants 39
Table 2.3: Dehydration of alkyl and phenyl 2-substituted tertiary alcohols with Amberlyst®-15 40
Table 3.1: NMP copolymerization with TIPAL[a] 50
Table 3.2: Emulsion polymerization of **1**[a] 51
Table 3.3: Random copolymerization of 1 with isoprene[a] 52
Table 3.4: Polymer microstructure and thermal properties 53
Table 4.1: Emulsion polymerized poly(**1**) and poly(**1**-*ran*-isoprene)[a] 61
Table 5.1: Anionic polymerization and block copolymerization of **1** 72
Table 7.1: UV Acetylation of diamantane[a] 93

List of Figures

Figure 1.1: Rubber products from *Hevea brasiliensis* and *Palaquium gutta* trees 3

Figure 1.2: Structure of linear, branched, and crosslinked polymers adapted from ref. 21 4

Figure 1.3: Schematic of four classes of copolymers 5

Figure 1.4: Visual representation of chain vs. step polymerization 5

Figure 1.5: Molecular weight distribution in a typical polymer sample adapted from ref. 21 6

Figure 1.6: Morphology of a semicrystalline linear polymer where discrete crystalline regions (a) are connected by amorphous regions (b). Adapted from ref 21 8

Figure 1.7: Temperature vs specific volume for amorphous and semicrystalline polymer from ref 21. 9

Figure 1.8: The five regions of thermoplasticity adapted from ref 22 10

Figure 1.9: Oscillatory stress versus strain in a viscoelastic material from ref 25 11

Figure 1.10: Moduli relationships in DMA. Adapted from ref 25 11

Figure 1.11: LCST and UCST generalized phase diagrams. Taken from ref 22 13

Figure 1.12: Graphical map of self-assembled morphologies in diblock copolymers. From ref 28 13

Figure 1.13: Theoretical and experimental phase maps of diblock copolymers (adapted from ref. 29) 14

Figure 1.14: Configurational isomers in synthetic polyisoprene 15

Figure 1.15: The lower order diamondoids 16

Figure 1.16: T_g variations with addition of adamantyl containing monomers. Data from refs 53,60,61 18

Figure 1.17: Stained TEM images of microphase separation of hydrogenated poly(isoprene-*block*-**1**-*block*-isoprene). Taken from ref. 53 19

Figure 2.1: Relative concentration 2-methyl-3-buten-2-ol at various $[S]_0/[H+]$ 34

Figure 2.2: Relative isoprene concentration at various$[S]_0/[H+]$ 34

Figure 2.3: Composition of dehydrations in various solvents. **2**: ●, **1**: ●, **3a**: ○**, 3**b: ○ 36

Figure 2.4: Relative acidity of protonated functional groups 38

Figure 2.5: Dehydration of 2-adamantyl-3-buten-2-ol with and without desiccant 39

Figure 3.1: Relationship between T_g and the weight composition of adamantyl containing monomer with Fox prediction lines. ● and solid line: poly(**1**-*ran*-isoprene). ○ and dashed line: poly(1-vinyladamantane-*alt*-ethylene-*ran*-propylene-*alt*-ethylene) 54

Figure 4.1: Storage modulus (E') of poly(**1**) and poly(**1**-*ran*-isprene) at varying wt% **1** 62

Figure 4.2: Storage (G') and loss (G") modulus versus temperature 63

Figure 4.3: Top: angular frequency (ω) versus storage modulus (G’) at 220 °C. Middle: angular frequency (ω) versus loss modulus (G”) at 220 °C**.** Bottom: angular frequency (ω) versus dynamic viscosity (η*) at 220 °C 64
Figure 4.4: Dynamic viscosity (η*) versus angular velocity (ω) of poly(**1**) (Run 8) before and after hydrogenation as well as poly(**1**-*ran*-isoprene) (Run 5) at 220 °C........ 65
Figure 5.1: Stages of the anionic polymerization of **1** with MPT indicator: a) at titration endpoint b) during polymerization c) after quenching with degassed methanol 71
Figure 5.2: Solidification of quenched anionic polymerization of 1 (Entry 3)........ 71
Figure 5.3: DSC overlay of anionic poly(**1**) before and after hydrogenation........ 74
Figure 5.4: Powder x-ray diffraction patterns of anionic and emulsion poly(**1**) before (black) and after (grey) hydrogenation 75
Figure 5.5: Visual representation of intramolecular and intermolecular chain transfer to polymer in polyethylene (from ref 136)........ 76
Figure 5.6 ^{13}C NMR comparison of emulsion and anionic poly(**1**)........ 77
Figure 5.7: ^{13}C and DEPT 135 NMR of hydrogenated poly(**1**) (Run 8) 78
Figure 5.8: Mark-Houwink plots of hydrogenated poly(**1**) (red) and linear polystyrene standard (black). Left: emulsion Run 8, right: anionic Run 1 80
Figure 6.1: Theoretical Phase Map taken from ref 123 83
Figure 7.1: Transmission of UV light in various materials. Taken from ref 152 91
Figure 7.2: UV/Vis spectrum of 2,3-butanedione 92
Figure 7.3: Visual comparison of penetration depth at various reactor IDs........ 93
Figure 7.6: HSQC NMR spectrum of **3a** (^{1}H and DEPT 135) 98
Figure 7.7: COSY NMR spectrum of **3a**........ 99
Figure 7.8: ^{1}H NMR spectra of poly(**1**) (Run 3) and microstructure assignments in the olefinic region 116
Figure 7.9: ^{13}C NMR spectra of poly(**1**) (Run 3)........ 116
Figure 7.10: ^{1}H NMR spectra of poly(**1**-*ran*-isoprene) (Run 14) and microstructure assignments in the olefinic region........ 117
Figure 7.11: ^{13}C NMR spectra of poly(**1**-*ran*-isoprene) (Run 14) 117
Figure 7.12: poly(**1**-*ran*-isoprene) structure 118
Figure 7.13: Differential Scanning Calorimetry of Copolymer and Physical Mixture 119
Figure 7.14: Compiled variations of in T_g vs. M_n found for poly(**1**)........ 120

List of Schemes

Scheme 2.1: Reported syntheses of 2-(1-adamantyl)-1,3-butadiene 24
Scheme 2.2: Synthesis of 2-(1-adamantyl)-3-buten-2-ol 33
Scheme 2.3: Dehydration of 2-(1-adamantyl)-3-buten-2-ol and formation of terpenes 35
Scheme 2.4: E1 mechanism of tertiary alcohol dehydration 37
Scheme 2.5: Formation of protonated solvent species 37
Scheme 3.1: Synthesis of **1** 48
Scheme 3.2: Copolymerization of **1** and isoprene and subsequent dehydration 51
Scheme 5.1: Anionic polymerization of 1 using 4,5-methylenephenanthrene indicator 68
Scheme 5.2: Carbon environments of emulsion poly(**1**) before and after branching 79

Chapter 1: Introduction

A polymer is a macromolecule composed of many smaller structural repeat units called monomers that are covalently bonded together. Although the idea of long chain-like macromolecules is well accepted in the contemporary scientific community, this was not always the case. The field of polymer science can trace it origins to the industrial revolution, when in 1861 Scottish chemist Thomas Graham noted the differences between what he termed crystalloid substances, which would diffuse easily in solution, and colloidal compounds that would not crystallize and exhibited very slow diffusion in solutions.[1] He posited that these gluey colloidal substances were composed of large molecules, an idea that was not well accepted at the time. A fierce debate ensued as to whether materials like latex rubber were merely large aggregates of otherwise crystalline molecules or were, in fact, large chemically linked molecules (i.e. polymers). It took until the late 1920's for the work of German chemist, Herman Staudinger, to begin to convince even the most ardent sceptics that materials like rubber, cellulose and starch were actually string-like molecules of variable lengths comprised of discrete molecular units that are covalently bonded together.[1,2] By the time his modern theory of polymers had earned him a Nobel Prize in chemistry in 1953, synthetic plastics like nylon, polyethylene, polypropylene, polycarbonate, and polystyrene were being industrially produced by companies like Dow Chemical, Dupont and General Electric.[3] Today it is estimated that over 300 million metric tons of commodity plastics are generated annually,[3–5] a testament to the ubiquity of polymers in our daily lives.[6]

Polyisoprene Rubbers

Though the utilization of polyisoprene rubber by Mesoamerican peoples has been confirmed as far back as 1600 B.C.,[7] Western civilizations did not become aware of the malodorous gum of the *Hevea brasiliensis* tree until around the 18th century.[2] Despite assertions from famous English chemist Joseph Priestley that natural rubber was an excellent material for "wiping from paper the black marks of a pencil", it found few uses.[2] In 1823 Charles Macintosh patented a process for making waterproof fabrics with natural rubber. Though the word "mackintosh" eventually became a synonym for raincoat, his products revealed the principal shortcoming of natural rubber; the material melted in hot weather and was brittle at low temperatures.

The industrial significant of natural rubber was not realized until 1839, when Charles Goodyear accidentally dropped a sample of natural rubber compounded with sulfur on a hot stove.[8] Instead of melting, the material acquired a tough leathery consistency while maintaining elasticity. Goodyear had inadvertently crosslinked natural rubber, converting its linear polymer chains into a three-dimensional network, a process which came to be known as vulcanization. Although delays in his patent application denied him the opportunity to profit fully from his discovery, vulcanization transformed natural rubber from a novelty to a global commodity. Increase in rubber consumption from 25 tons in 1830 to 6000 tons in 1860 reflect the explosion of vulcanized rubber products.[2] The advent of the pneumatic tire and telegraph wire further added to the increasing demand for natural rubber.

By the late 19th century, Brazil, the center of global rubber production, had an estimated output of 42,000 tons of natural rubber harvested exclusively from the *Hevea brasiliensis* tree.[9] Envious of the Brazilian rubber monopoly, British scientists clandestinely developed higher-yield, more disease-resistant varieties, and established plantations in their colonial territories.[10] By the early 20th century, cheaper British rubber produced in the Malaysian Peninsula brought an end to the "Rubber Boom" in Northern Brazil. By the 1930's, the emergence of the first epidemic of South American leaf blight (SALB), a fungal disease native to the Amazon region, halted any further attempts by the Brazilian government to revive its rubber industry.[11] Even today, no effective treatment or prevention methods for SALB exist, and the fungus still poses a serious threat to global supply chains of natural rubber.

Though largely forgotten, another "rubber boom" existed throughout the 19th century. Gutta-percha, as it came to be known, is an isomer of polyisoprene that is harvested primarily from the sap of the P*alaquium gutta* tree, although up to eight species of gutta-producing trees were native to Southeast Asia.[12] Unlike natural *Hevea* rubber, gutta-percha exists as a tough impact resistant solid. In fact, when it was first discovered by British explorers to Malaysia in the 17th century it was mistaken for a type of wood.[13] The key feature of gutta-percha, however, was that it could be easily worked and shaped when heated. The unique potential of gutta-percha became apparent in 1847 when the German engineer Werner von Siemens used it as an insulator for an electric telegraph cable. By the 1860's, gutta-percha was a household name in Victorian England and was used to make toys, furniture, decorations, shoes, pipes, medical devices and building materials.[12] Its most consequential use, however, was as insulation for newly the developed undersea telegraph cables. Natural rubber rapidly degrades in salt water, and until the emergence of gutta-percha, no viable material existed. By the end of the 19th century, over 115,000 nautical miles of undersea cables crisscrossed the globe, allowing Western powers to better administrate and economically exploit their massive colonial empires.[12]

Massive demand for undersea cables outpaced the primitive methods of extraction of gutta-percha latex. Harvesting methods were archaic, inefficient, and unsustainable. After cutting down the entire tree, the thick gutta-percha latex, which coagulated in air, was slowly drained into a bowl. An entire 60-foot tree yielded less than a pound of gutta-percha latex on average, and the majority remained in the discarded tree. By the 1890's wild gutta-percha producing trees were nearly extinct, and the market for gutta-percha had nearly collapsed.[12] Following the invention of the wireless telegraph in

1901, undersea cables were rendered obsolete, and gutta-percha faded from memory. Unfortunately, gutta-percha has been largely absent from the world of modern materials[12] save for its use in endodontics as a filling material for root canal therapy.[14,15]

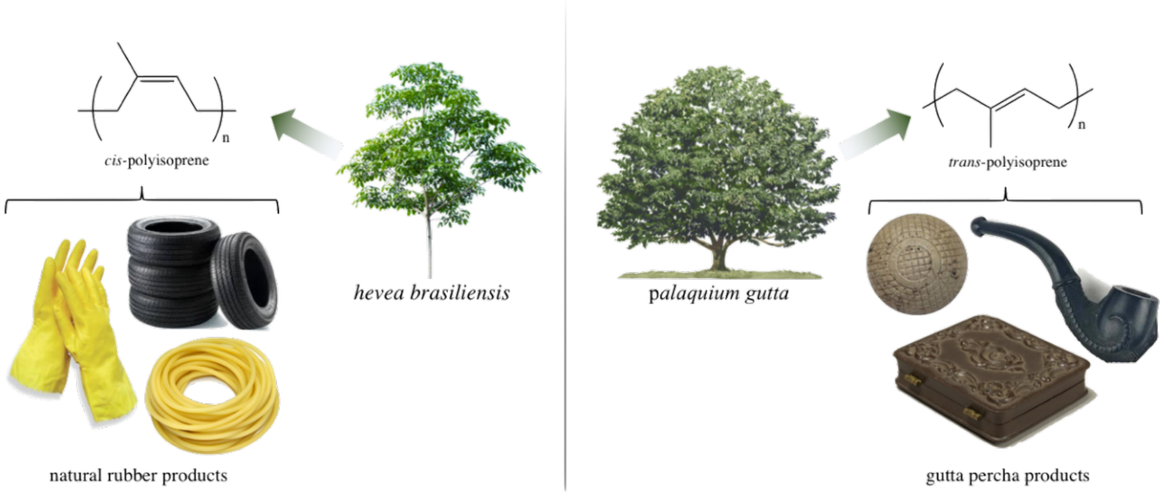

Figure 1.1: Rubber products from *Hevea brasiliensis* and *Palaquium gutta* trees

Although scientists had identified isoprene as a primary structural component of natural rubber as early as the 1880's, polyisoprene synthesis remained mostly an academic interest. Synthesis of isoprene also remained prohibitively expensive. The Allied blockade of Germany during the First World War highlighted the strategic importance of a natural rubber supply. Despite plummeting natural rubber prices following the war, Germany and Russia poured resources into synthetic rubber alternatives.[16] Work was concentrated on polymers from 1,3-butadiene, which was significantly cheaper to produce. The result was the production of sodium catalyzed polybutadiene, labelled SK Rubber in Russia, or Buna in Germany. Block copolymers of butadiene with styrene (Buna S) and acrylonitrile (Buna N) were also developed, but these materials were hard, tough, and difficult to process.[16] The United States produced more than 700,000 tons of styrene-butadiene rubber (SBR) throughout the war.[16]

Despite the explosion of the synthetic rubber industry following the Second World War, a true replacement for natural rubber has remained formidable challenges even with contemporary polymerization techniques.[17–20] To understand these challenges, and the scope of this research effort, an introduction to polymer science, specifically the relationship between polymer synthesis, structure, morphology, and physical and mechanical behavior is necessary. The following sections will introduce the concepts necessary to understand the scope of this dissertation.

Introduction to Polymers

At the molecular level, polymers are made through chemical reactions called polymerizations. During polymerization, monomers are linked together to form a polymer. The overall structure of the resulting polymer is determined by the functionality of the monomer, which refers to the number of reactive sites on a monomer that can form a covalent linkage. Polymers can be classified as linear, branched, or crosslinked as illustrated in Figure 1.2. Linear polymers are formed from difunctional monomers. Increasing the functionality to more than two will lead to branching and crosslinking. Branched polymers can be comb-like with either long (Figure 1.2a) or short (Figure 1.2b) branches. Extensive branching will result in a dendritic structure (Figure 1.2c).[21] When linear polymer chains are connected, they are said to be crosslinked. Crosslinking can become so extensive that it leads to a dense three-dimensional network.[1]

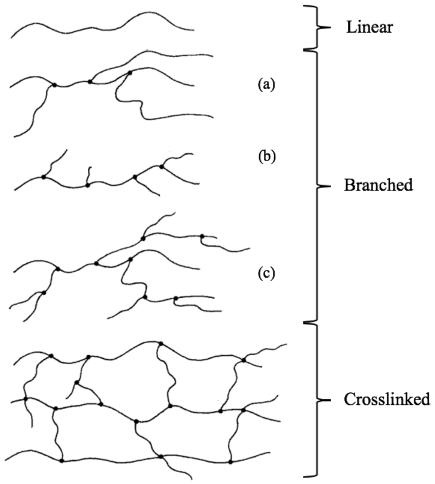

Figure 1.2: Structure of linear, branched, and crosslinked polymers adapted from ref. 21

A polymer which consists of chains made entirely from a single monomer type is referred to as a homopolymer. Copolymers, however, contain two or more monomer types, which can be combined in various ways to obtain interesting and often highly useful materials.[22] Copolymers are classified by the arrangement of each monomeric repeat structure along the backbone. For a copolymer system consisting of two monomeric types, four of the simplest configurations are presented in Figure 1.3.

a) *Statistical copolymers*: formed by the statistically random incorporation of each monomer during polymerization.

b) *Alternating copolymers*: characterized by a regular alternating sequence of each comonomer in the polymer chain.

c) *Block copolymers*: comprised of long sequences, or blocks, of each monomer.

d) *Graft copolymer*: Consists of a backbone species and a sidechain species that is grafted to the backbone.

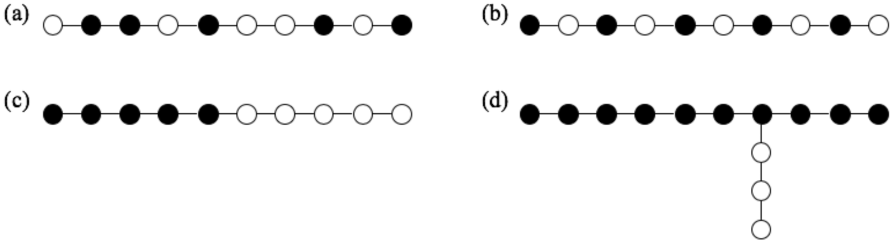

Figure 1.3: Schematic of four classes of copolymers

Carothers was the first to classify polymers as either condensation or addition polymers based upon the compositional differences between the polymer and the monomers from which it was synthesized.[23] Condensation polymers are those formed from polyfunctional monomers that undergo a condensation reaction to form the polymer chain resulting in the loss of a small molecule, often water. This classification was sufficient for the range of polymers known at the time of publication, in 1929.[23] We now, however, more generally describe condensation polymers as those that possess functional groups as the polymer linkages (e.g. amide, ester, urethane, sulfide or ether).

The second class of polymers classified by Carothers were addition polymers, which are formed without the loss of a molecule.[21] Most addition polymers are formed by the conversion of carbon-carbon double bonds to saturated linkages. Common addition polymers include those of vinylic compounds such as styrene, ethylene, propylene, and diene systems like isoprene.

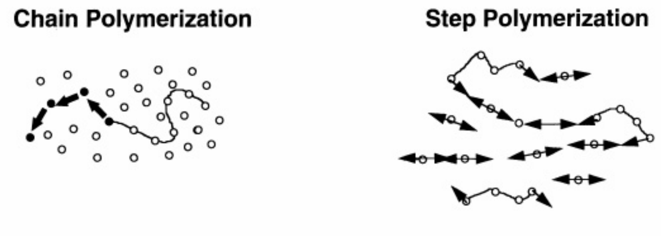

Figure 1.4: Visual representation of chain vs. step polymerization

Flory refined these two classifications to reflect the actual mechanism of polymerization.[24] He classified polymers into those that undergo step and chain polymerization, though in most cases step-growth polymers are synonymous with condensation polymers as chain-growth is to addition. The characteristic of step polymerization that distinguishes it from chain polymerization is that reaction occurs between any of the different sized species in the reaction.[21] For example, a tetramer (4 monomer units) can result from the condensation of a monomer and a trimer or two dimers. Chain polymerization occurs exclusively as addition of a single monomer to the growing polymer chain. Chain and step polymerizations are illustrated in Figure 1.4.

The inability to assign an exact molecular weight distinguishes many synthetic polymers from small molecules. This is because the length of each polymer chain in a polymerization reaction is determined by random events, resulting in a mixture of chains of varying length. Molecular weight of a polymer is, consequently, represented as a statistical distribution of molar masses. Number average molar mass (M_n) provides an average molecular weight based on the *number* of molecules, while weight average molar mass (M_w) is the average molecular weight based on the *size* of the molecules. Eq. 1.1 and 1.2 describe M_n and M_w in terms of the number of moles of each polymer species (N_i) and the molar mass (M_i) of that species. Polydispersity ($Đ$) is the measure of the breadth of molecular weight distribution in a polymer sample and is defined by eq. 1.3. Figure 1.5 depicts M_n and M_w in a typical molecular weight distribution.

$$M_n = \frac{\sum N_i M_i}{\sum N_i} \tag{1.1}$$

$$M_w = \frac{\sum N_i {M_i}^2}{\sum N_i M_i} \tag{1.2}$$

$$Đ = \frac{M_w}{M_n} \tag{1.3}$$

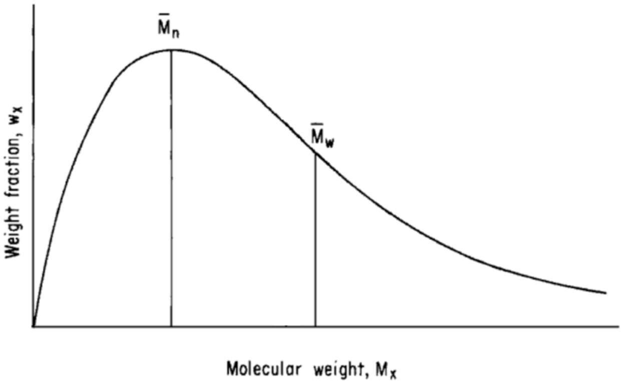

Figure 1.5: Molecular weight distribution in a typical polymer sample adapted from ref. 21

Polymer configuration refers to the organization of atoms along the polymer chain and is also termed the microstructure. Unlike conformation, which refers to the different arrangements of the atoms and substituents of the polymer brought about by rotations about single bonds, configuration can only be altered by the breaking and reforming of primary chemical bonds.[22] Like small molecules these configurations are termed isomers as each has the same chemical formula but vary in the arrangement of atoms. Configurational isomers can be classified as two types: stereo- and geometric isomers. Stereoisomerism occurs when the polymer chain contains asymmetric centers, resulting in three possible configurations also known as the polymer tacticity: isotactic, syndiotactic and atactic. Geometric isomerism occurs when polymerization results in double bonds with *cis* and *trans* configurations in the backbone. Four configurational isomers are present in polyisoprene. The content of each of these isomers is often termed the microstructure and greatly influences the thermal and mechanical properties of the polymer.[21]

Bulk Polymer Morphology and Thermal Transitions

Polymers in the bulk state, or the absence of solvent, are categorized as either crystalline or amorphous. Crystalline polymer domains consist of chains that form ordered crystal lattices that scatter x-rays in a distinct pattern and exhibit the first-order thermal transition known as melting. Conversely, the amorphous state is characterized by a complete lack of short and long-range conformational ordering of the polymer chains. Consequently, amorphous polymers will not scatter x-rays in a distinct pattern, nor will they undergo melting.[22] One major difference between crystalline polymers and small molecules is that polymers are virtually never *purely* crystalline. This is attributed to their long chain nature. Crystallization requires polymer chains to be able to slide past each other and fold onto themselves to form ordered crystal lattices. The long-chain nature of polymers, however, leads to entanglements which results in a finite amount of amorphous material in the bulk (Figure 1.6). Thus, we refer to polymers as semicrystalline and report the amount of crystallinity present in a sample as a percent or degree of crystallinity.[22] Because crystallization requires polymer chains to assemble in an ordered repeating pattern, randomness in the polymer chain from configurational and stereoisomerism greatly influences the ability of a polymer to crystallize. Thus, isotactic and syndiotactic polymers usually exhibit crystallinity, whereas atactic polymers almost never do.[1,22] For this reason, statistical copolymers and branched polymers are also usually amorphous.

Polymers are characterized by two major thermal transition temperatures: the crystalline melting temperature (T_m) and the glass transition temperature (T_g). At temperatures above T_m the crystalline domains in bulk polymers melt, while below the T_g amorphous domains behave as stiff, brittle glasses. These thermal transitions can be understood more clearly by considering the example of a hypothetical liquid polymer as it cools. The translational, rotational, and vibrational energy of polymer chains decrease on cooling. At the point where translational and rotational energies are essentially zero, crystallization becomes possible.[21] If symmetry requirements can be met, the polymer chains will pack into an ordered lattice arrangement (i.e. crystallize). However, if symmetry requirements are not met (e.g. due to configurational isomerism or branching), crystallization is not possible, and the energies of the chains will continue to decrease with temperature. At T_g, the energy has become low enough that all long-range molecular motion of the amorphous polymer chains has ceased. Though completely amorphous polymers will exhibit only a T_g, semicrystalline polymers will exhibit both a T_m and a T_g.

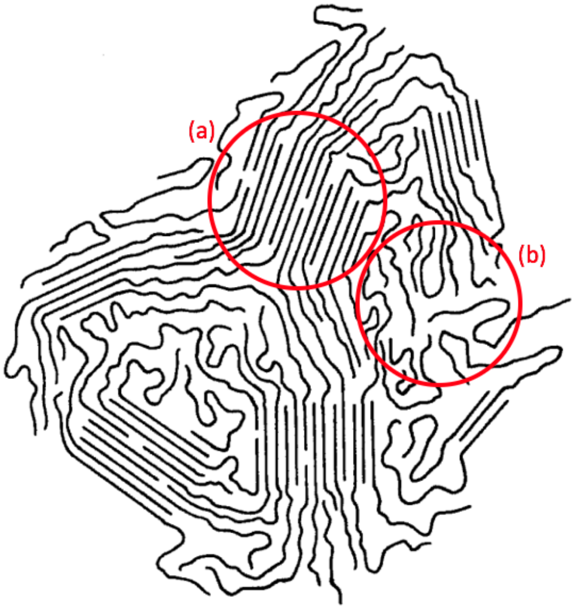

Figure 1.6: Morphology of a semicrystalline linear polymer where discrete crystalline regions (a) are connected by amorphous regions (b). Adapted from ref 21

Identifying the T_m and T_g can be accomplished by observing the changes in properties such as specific volume that occur as polymers undergo thermal transitions. Figure 1.7 shows the change in specific volume with temperature for an amorphous and semicrystalline polymer. T_m can be identified because it is a first-order transition with a discontinuous change in specific volume at the transition temperature, while T_g is a second-order transition involving only a change in the temperature coefficient of the specific volume. Thermal transitions can also be identified by observing changes in properties like heat capacity or dielectric constant with respect to temperature. In fact, the most commonly used method to identify thermal transitions is differential scanning calorimetry (DSC). DSC determines heat capacity of a sample as a function of temperature by measuring heat flow required to maintain a zero temperature differential between an inert refence material and the polymer sample.[22]

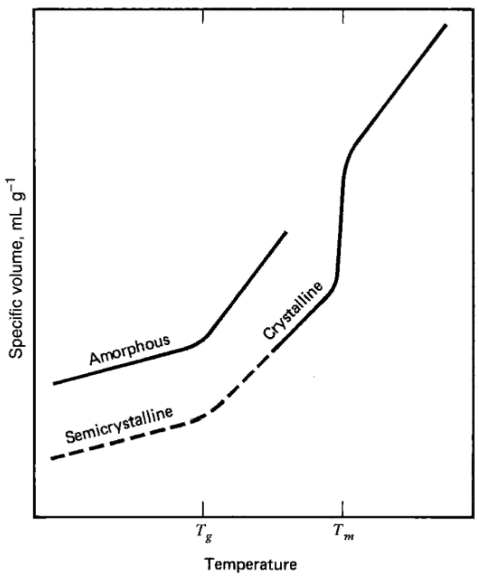

Figure 1.7: Temperature vs specific volume for amorphous and semicrystalline polymer from ref 21

Thermoplasticity and Dynamic Mechanical Analysis

Viscous materials, like water, resist shear flow and strain linearly with respect to time as a stress is applied where viscosity is the measure of this resistance. Perfectly elastic materials, on the other hand, strain when a stress is applied but return to their original state when the stress is removed. Viscoelastic materials exhibit a combination of viscous and elastic characteristics when undergoing deformation.[22] Though viscoelasticity is observed in nearly all materials to some degree, it is extremely pronounced in polymers.

Young's modulus (E) is a property often used to quantify the stiffness of a material and describes the relationship between a linear (or non-linearly) applied stress (σ) and the resulting strain (ε) as shown in eq. 1.4. Under small stresses solid materials will undergo reversible elastic deformation and a plot of stress-strain will initially be linear with a slope of E. Though E is dependent on temperature and the applied stress, it generally indicates whether a polymer is suitable for a given application and temperature range.[25]

$$E = \frac{\sigma}{\varepsilon} \tag{1.4}$$

The modulus of polymers varies drastically across thermal transitions. As temperature is increased, a linear amorphous polymer will exhibit five distinct regions of viscoelasticity. Below the T_g, a polymer exists in the glassy region (Figure 1.8 #1). Polymers in the glassy region are often quite brittle and generally have a modulus around $3E^9$ Pa. In the glass transition region (Figure 1.8 #2) the modulus typically drops by a factor of 1000 over a span of 20 to 30°C.[22] The consistency of polymers in this region is often described as leathery and is highly dependent on even small changes in temperature. After the precipitous drop in modulus during the glass transition, the modulus becomes nearly constant around $2E^6$ Pa in the rubbery plateau region (Figure 1.8 #3).

For linear polymers in the rubbery plateau, the modulus will slowly decrease with increased temperature. This decrease is related to molecular weight, where higher molecular weight polymers have a broader plateau region. When crosslinking is present, however, the ability of the polymer chains to flow is eliminated, and the modulus in the rubbery plateau will be constant. Chemically crosslinked materials, such as vulcanized rubber, which possess covalently linked polymer chains, are represented by the dotted line in (Figure 1.8). Crystalline domains can also act as physical crosslinks and inhibit the flow of polymer chains in the rubbery plateau. Since crystalline domains also act as a filler material the modulus in the rubbery plateau increases with increased degree of crystallinity. At temperatures above T_m, the modulus will fall precipitously as the sample begins to flow (dashed line in Figure 1.8).[22]

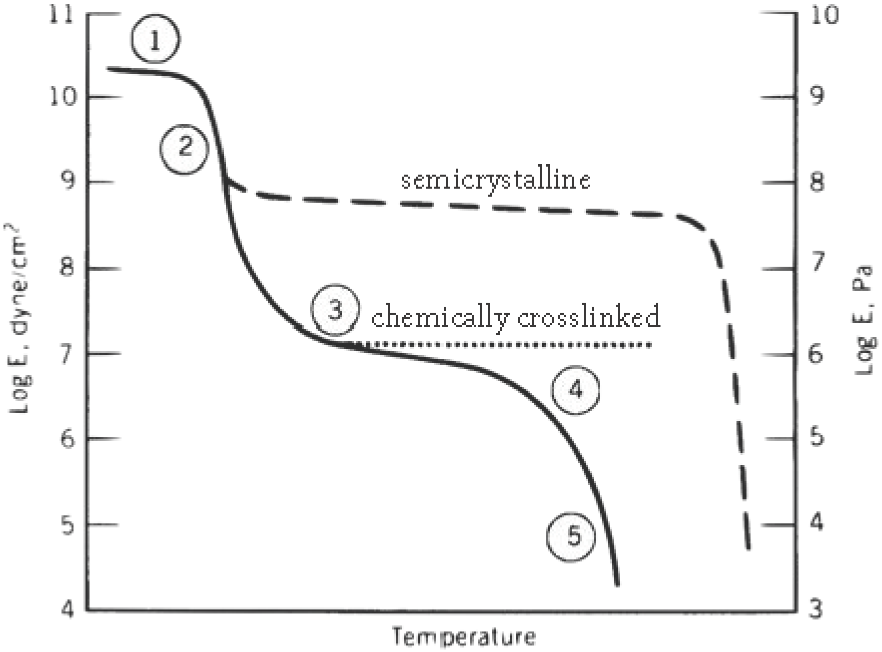

Figure 1.8: The five regions of thermoplasticity adapted from ref 22

As temperatures exceed the rubbery plateau region, linear amorphous polymers enter the rubbery flow region (Figure 1.8 #4). Depending on the time scale of the stress applied, polymers in the rubbery flow region will exhibit both rubber elasticity and flow characteristics.[25] Under rapid stress, polymer chains do not have sufficient time to relax, and the material will behave rubbery, while under prolonged stress the sample will flow.[22] A classic example of a material in the rubbery flow region is Silly Putty™, which behaves as a solid under rapid stress, but flows when stress is applied over a long timescale. At high enough temperatures polymer chains have sufficient energy to overcome entanglements and behave as individual molecules. This region is known as the liquid flow region (Figure 1.8 #5).[22]

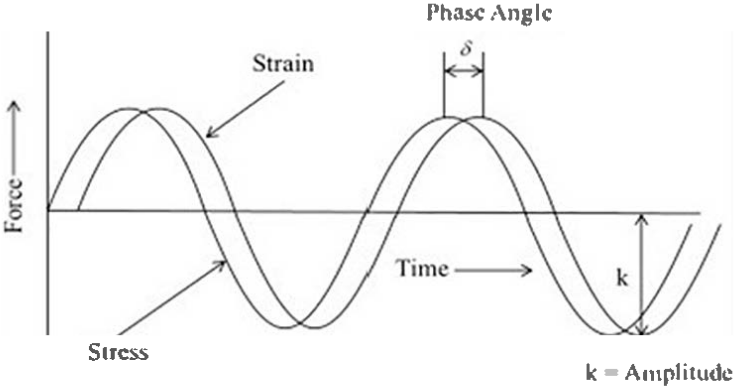

Figure 1.9: Oscillatory stress versus strain in a viscoelastic material from ref 25

Although Young's modulus provides a useful measure of a material stiffness, for polymers exhibiting viscoelasticity, dynamic mechanical analysis (DMA) offers a more complete picture of the material properties.[25] Unlike a conventional stress-strain curve, DMA applies a sinusoidal oscillating stress to the sample meaning that a modulus value can be recorded for every stress cycle (e.g. every second for a 1Hz oscillation rate). DMA allows for moduli to be acquired continuously over a temperature range, an especially useful feature when characterizing rubbery materials.[25]

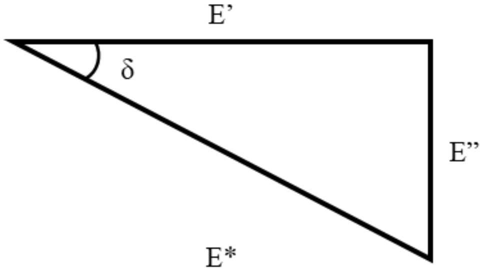

Figure 1.10: Moduli relationships in DMA. Adapted from ref 25

If an oscillating sinusoidal stress is applied to a material, it will deform sinusoidally, and this deformation will be reproducible so long as the material is within its purely elastic region. The shape of the strain response depends on the amount of elastic and viscous behavior present, where the difference between applied stress and strain is an angle, δ. For a perfectly elastic material, $\delta = 0$ as the deformation is perfectly reversible, while $\delta = 90°$ for a purely viscous liquid. The phase angle in viscoelastic materials falls between these two extremes and the complex modulus (E*) obtained in

DMA can be broken into its in-phase and out-of-phase components, the storage (E') and loss (E") moduli. The relationship δ, E' and E" and E* is depicted in Figure 1.10. As a material become more elastic, δ decreases and E' approaches E*.[25]

Block Copolymer Self-Assembly

When two polymers are mixed, the most common result is complete phase separation. Qualitatively, this can be explained in terms of the reduced combinatorial entropy of mixing. Solubility of any given solvent-solute pair is dictated by the free energy of mixing as shown in eq. 1.5.

$$\Delta G_M = \Delta H_M - T\Delta S_M \tag{1.5}$$

Where ΔG_M is the Gibbs free energy of mixing, ΔH_M is the enthalpy of mixing, T is absolute temperature and ΔS_M is the entropy mixing. For mixing to occur ΔG_M must be negative. According to statistical thermodynamics, the entropy of mixing is determined by the number of possible arrangements in space that the molecule can assume.[1] Because polymers exist as long covalently bonded chains, the number of ways they can be arranged in space is drastically reduced compared to small molecules. Consequently, the entropy term in eq. 1.5 becomes negligible and the free energy of mixing will be dependent on ΔH_M. For polymer-polymer mixing, ΔH^M can be approximated using eq. 1.6.

$$\chi_{12} = \frac{V_0}{RT}(\delta_1 - \delta_2)^2 \tag{1.6}$$

Where χ_{12} is the polymer-polymer interaction parameter, V_0 is the volume of a polymer segment, and the solubility parameter (δ) quantifies polymer-polymer interactions. Hildebrand developed a semi-empirical approach to δ based upon the principal that "like dissolves like".[1] It relates ΔH_M to cohesive energy density (CED) and defines δ with eq. 1.7.

$$\delta = \left(\frac{E}{V}\right)^{\frac{1}{2}} \tag{1.7}$$

Where E is the molar energy of vaporization and V is the molar volume of the component. Solubility parameters are readily determined for liquids as enthalpy of vaporization is usually well known.[1] However, for polymers E is not measurable. Consequently, qualitative methods and semiempirical models have been developed to estimate δ. Small and Hoy compiled a series of molar attraction constants that can provide a reasonable estimate.1

When polymers are miscible, they generally phase-separate at some higher temperature called the lower critical solution temperature (LCST). Although *decreased* miscibility with increased temperature may seem counterintuitive, it can be explained by eq. 1.5. LCST behavior is characterized by exothermic heat of mixing ($\Delta H_M < 0$) and a negative excess entropy (ΔS_M).[26] At the critical point, the heat of mixing is equal to the entropy of mixing times the absolute temperature ($\Delta G_M = 0$). This means that at lower temperatures ΔG_M will be negative, indicating miscibility, but at higher temperatures ΔG_M will be positive resulting in phase separation. Upper critical solution temperatures are characteristic of endothermic mixing and positive entropy of mixing and are common in polymers in solution.[26]

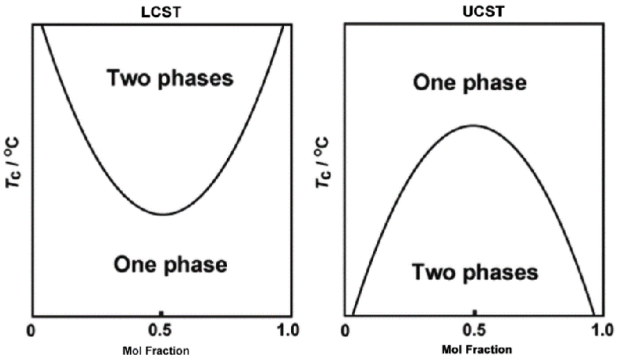

Figure 1.11: LCST and UCST generalized phase diagrams. Taken from ref 22

In diblock copolymers, two chemically distinct chain segments are covalently bonded. This means that even if the blocks are completely immiscible, they cannot macroscopically separate into two discrete phases (e.g. oil and water). The result is microphase separation into ordered morphologies depending on the size and composition of the block copolymer (BCP). Theoretical modeling has identified four basic microphase geometries: body-centered cubic (S, S'), hexagonal cylindrical (C, C'), gyroid (G, G'), and lamellar (L), as shown in Figure 1.12.[28]

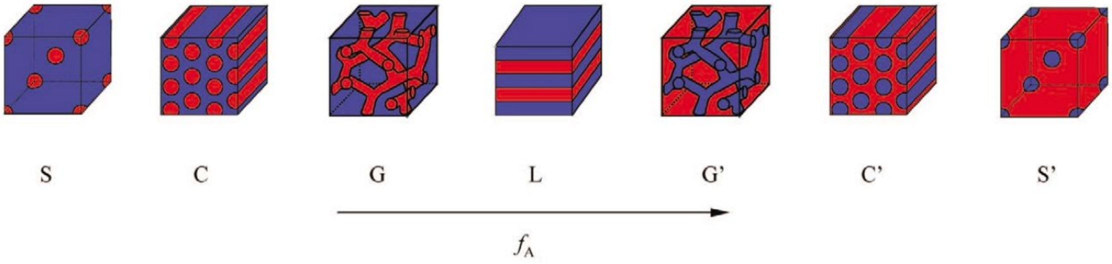

Figure 1.12: Graphical map of self-assembled morphologies in diblock copolymers. From ref 28

Although the enthalpy of mixing is the thermodynamic driving force for self-assembly, the shape and size of the subsequent morphology is a function of overall chain length (***N***) and the volume fraction of each polymer block (***f_i***). Tremendous effort has been dedicated to mapping the thermodynamic microphases both theoretically and experimentally.[29,30] Figure 1.13 depicts the theoretical map of BCP microphase separation using mean-field theory calculations and corresponding experimental results. LCST behavior is observed in BCP systems and the critical temperature (i.e. where $\Delta G_M = 0$) is referred to as the order-disorder transition temperature (T_{ODT}).

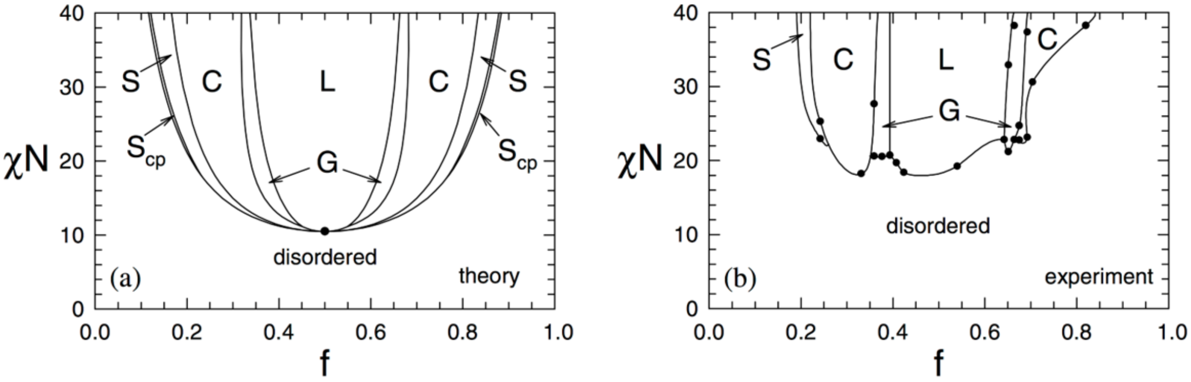

Figure 1.13: Theoretical and experimental phase maps of diblock copolymers (adapted from ref. 29)

Natural vs. Synthetic rubbers

The exceptional properties of natural rubber (i.e. rubber from *Hevea brasiliensis*) and gutta-percha are partly attributed to their microstructure. This is perhaps most evident in the comparison natural rubber and gutta-percha. Natural rubber is virtually entirely comprised of the cis-1,4- isomer resulting in a completely amorphous elastomer with a low glass transition temperature (T_g) of -70°C.[31] Gutta-percha, on the other hand, exhibits complete selectivity for the *trans*-1,4- isomer.[13] Although the *cis*- and *trans*- conformations of polyisoprene have very similar T_gs,[32] the presence of crystallinity in *trans*-1,4-polyisoprene imparts dramatically different mechanical properties. Depending on the kinetics of crystallization, purely *trans*-1,4-polyisoprene will exhibit a melting point between 56°C and 65°C.[13,14] At temperatures between the T_g and T_m, crystalline domains, acting as physical crosslinks, impart rigidity and strength while amorphous domains provide flexibility resulting in a strong impact-resistant solid.

Despite an ever-increasing demand for polydiene rubbers, high molecular weight (M_n ~1,000,000 g/mol for natural rubber)[33] and complete configurational selectivity have remained formidable challenges even with contemporary polymerization techniques.[17–20] Synthetic polyisoprene is obtained via the addition polymerization mechanism with either anionic or radical initiators.[21] Incorporation of an isoprene molecule to the growing polymer chain results in one of four configurational isomers: *cis*-1,4, *trans*-1,4, 1,2- and 3,4- as illustrated in Figure 1.14. Though high selectivity for *cis*- and *trans*-1,4- can be achieved with a host of catalysts,[34–37] obtaining both complete selectivity and high M_n remain a synthetic challenge.

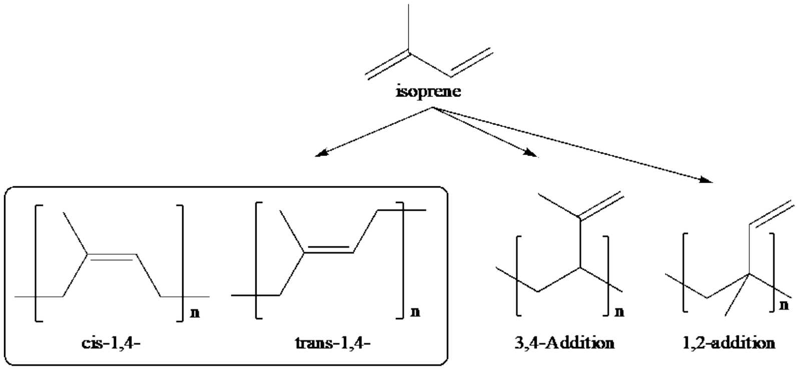

Figure 1.14: Configurational isomers in synthetic polyisoprene

Polyisoprene with *cis*-1,4- content of 94% and M_n = ~2000 – 150,000 g/mol has been obtained with living anionic polymerization using alkyllithium initiators and hydrocarbon solvents.[37,38] Commercially, the closest synthetic mimic to natural rubber is produced by Goodyear under the name Natsyn®, and was polymerized via a Ziegler-Natta type titanium aluminum catalyst giving 98.5% *cis*-1,4- content and M_n= ~200,000 g/mol (Đ = ~3).[39] Significantly less effort has been dedicated to the synthesis of highly *trans*-1,4-polyisoprene, but a recent renewal in interest has been driven by its potential as an additive in tire manufacturing.[19,40] Bonnet et al. have reported 98.5% trans-polyisoprene with M_n ranging from 9500 to 90,000 g/mol.[19] For comparison, gutta-percha typically has a molecular weight of around 30,000 to 60,000 g/mol.[13]

Designed 2-Subsitutents in Polydienes

In addition to configurational isomerism and molecular weight, the presence of a side substituent at the 2-position has a significant effect on thermomechanical properties of rubbers. This is especially evident when comparing *cis*-1,4-polybutadiene to *cis*-1,4-polyisoprene. The low T_g of *cis*-1,4-polybutadiene (-94 °C) provides exceptional flexibility and excellent strong deformation tolerance.[41] In fact polybutadiene is perhaps the most flexible synthetic rubber. Inclusion of a methyl 2-subsitutent in *cis*-1,4-polyisoprene results in an increase in T_g (-64 to -70 °C) and reduced elasticity but enhanced strength.[41] Although the inclusion of designed 2-substituents presents a viable method for tuning rubber properties, polymerization of 1,3-dienes with pendant groups larger that methyl groups (e.g. polyisoprene, (E)- and (Z)- 1,3-pentadiene and 2,3-dimethylbutadiene) have been relatively scarce.

Marvel et al. explored the effect of bulky 2-substituents in polybutadienes shortly after the end of World War II.[3,4] Using the well-established GR-S emulsion polymerization system, homopolymers of ethyl, *n*-propyl and *n*-amyl 2-substituted 1,3-butadienes were synthesized as well as their copolymers with butadiene and styrene. Though the alkyl side chains clearly influenced the thermal and mechanical properties of the compounded rubbers, the results were not a dramatic improvement over existing GR-S rubber. Overberger et al. followed up this work with an examination of the thermal properties of 1,3-butadienes with *tert*-butyl, *n*-heptyl, and *n*-decyl substituents at the 2-position.[5,6] In particular, the addition of a 2-*tert*-butyl group increased T_g by ca. 80 °C, while the poly(2-*n*-decyl-1,3-butadiene) exhibited a T_g increase of only ca. 10 °C, indicating that the addition of sterically bulky, branched chains at the 2-position of butadiene is fundamentally different to purely linear chains. Marconi et. al investigated the effect of stereospecific polymerization of 2-isopropyl and 2-*tert*-butyl 1,3-butadienes and concluded that poly(2-*tert*-butyl-1,3-butadiene) with high *cis*-1,4-content exhibited crystallinity with a T_m at 106 °C.[42,43] This suggests that branched, bulky 2-substituents can also induce crystallinity in an otherwise amorphous system.

Diamondoids

Diamondoids are cage alkanes with a molecular geometry that is superimposable onto the diamond lattice structure. This intriguing class of carbon allotrope has gained increased interest in the last decade. Polymantanes are a class of diamondoids that are only formed by the face fusing of adamantane ($C_{10}H_{16}$) units, the smallest of the polymantane diamondoids (Figure 1.15).[44] This separates polymantanes from what is commonly referred to as "ultra-dispersed nanodiamond" which is generally produced from either detonation or shock wave high-pressure experiments on graphitic carbon in the presence of metal powders.[45] Henceforth, we will simply refer to polymantanes as diamondoids.

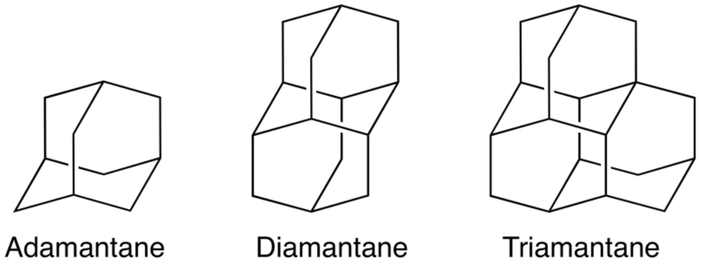

Figure 1.15: The lower order diamondoids

Adamantane was first isolated by Landa in 1933 from a petroleum distillates. In the late 1950's the first synthesis of adamantane was reported by Schleyer[46] followed by the synthesis of diamantane in 1965.[47] Synthesis of larger diamondoids was achieved in the in the 1960's and 70's,[48,49] but these methods were not amenable to the synthesis of diamondoids larger than tetramantane.[45] The synthetic roadblock to higher order diamondoids has been circumvented by the isolation of diamondoids up to undecamantane (11 units) from crude oil by chromatographic separation techniques.[50] Both the synthesis and isolation of diamondoids from crude oil has led to a surge in the research of their applications, and extensive work has been devoted to the functionalization of diamondoids, often at the tertiary, bridgehead carbon-hydrogen bonds, resulting in a range of published techniques.[45]

Diamondoids represent the low-end size limit of diamond, which exhibits extraordinary properties such a high hardness, excellent thermal stability, and high heat conductivity.[51] Research has been dedicated to correlating the evolution of bulk diamond properties as a function of particle size. Not only have the unique properties of diamondoids attracted the interest of chemists, physicists, and material scientists alike, but their availability from crude oil[51] and biocompatibility has led to applications in novel polymers, bioengineering, medicine and nanomachines.[15,44]

Diamondoids in Polymers: State of the Art

By covalently bonding them to monomers, the unique thermal stability of diamondoids has been imparted on polymer systems. Consequently, adamantane has been incorporated into a range of vinyl monomers including α-olefin, acetylene, vinyl ether, acrylate, acrylamide, and styrene moieties resulting in elevated T_g and decomposition temperatures of the resulting polymers.[17,52–61] In fact, adamantyl substituted polymers typically exhibit T_g values at least 100°C higher than their unsubstituted equivalents. The T_g of poly-(2-(1-adamantyl)-1,3-butadiene) (poly(**1**)) homopolymer was observed at 100°C, a large increase over polyisoprene (T_g = -70°C).[17]

Additionally, facile control of T_g has been observed by varying to the composition of adamantyl containing monomer in statistical copolymers.[53–55,60,61] Several approaches have been proposed for estimating the glass transition temperature for random copolymer systems; however, the Fox equation (eq. 1.8) is the most widely used method.

$$\frac{1}{T_{g,mix}} = \sum_i \frac{\omega_i}{T_{g,i}} \tag{1.8}$$

Where $T_{g,mix}$ and $T_{g,i}$ are the glass transition temperature of the mixture and the components, and ω_i is the mass fraction of component *i*. Though the Fox equation should only by applied to systems with similar solubilities it has been shown to be a useful tool and has exhibited reasonably good agreement with experimental observations of T_g dependence for diamondoid substituted statistical copolymers.[53,60,61] These results are compiled in Figure 1.16 where each point represent experimental values from the literature and the lines are corresponding predictions from eq. 1.8.

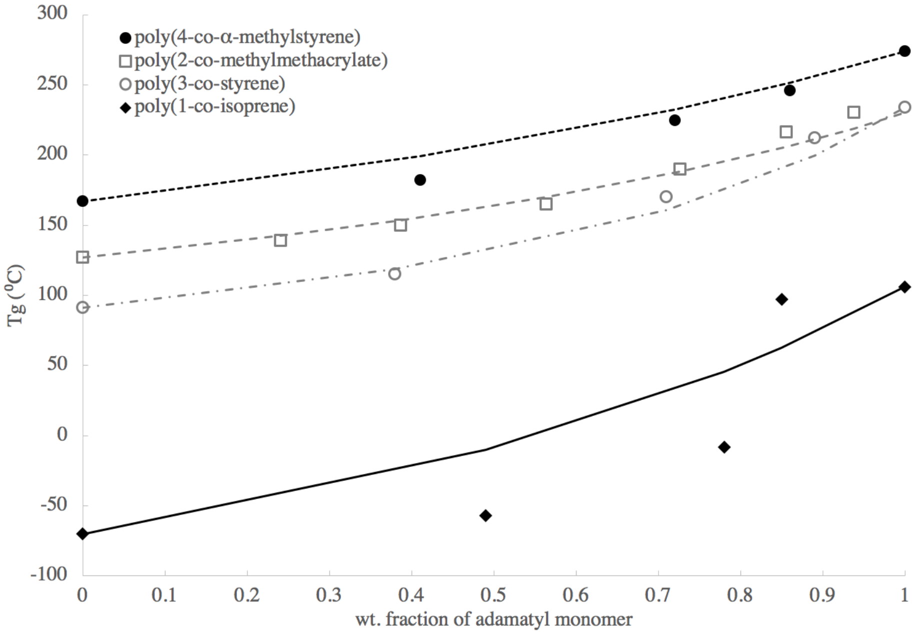

Figure 1.16: T_g variations with addition of adamantyl containing monomers. Data from refs 53,60,61

The data in Figure 1.16 shows that increasing the wt. fraction of adamantyl containing monomer results in a shift in T_g to higher temperatures, and except for poly(**1**-*ran*-isoprene), these values are in good agreement with the predictions from the Fox equation. Kobayashi et al. first confirmed their samples of poly(**1**-*ran*-isoprene) had a random distribution of comonomers, and then reasoned that deviation from predicted T_g was possibly due to a non-linear reduction in chain mobility at higher content of **1.**[53]

Although adamantane has been incorporated into a range of vinyl monomers including α-olefin, acetylene, vinyl ether, acrylate, acrylamide and styrene moieties,[17,52–61] the majority of research in adamantyl substituted polymers has been confined to polystyrene and polyacrylate derivatives, likely because they are readily polymerized by controlled radical polymerization techniques.[62,63] Poly(styrene-*block*-butadiene-*block*-styrene) (SBS) and poly(styrene-*block*-isoprene-*block*-styrene) (SIS) are widely used synthetic rubbers, however their current applications are limited by the Tg of the polystyrene segments.[64] Incorporation of adamantane to polystyrene segments of SI block copolymers via anionic polymerization of 4-(1-adamantyl)styrene and isoprene resulted in a 100°C increase in T_g, raising the potential operating temperature as high as 216°C.[61] Similarly, adamantyl containing methacrylate polymers, poly(1-adamantyl methacrylate), exhibited T_g values over 100°C higher than unsubstituted equivalents as well as lower dielectric constants, decreased moisture absorption, and higher transmittance of UV light.[56,65] Poly(methyl methacrylate) already exhibits excellent transparency and weather resistance, so these enhancements are especially relevant as they open the possibility to higher-temperature microelectronic and optoelectronic applications, where trace moisture can be detrimental.[56]

Robello reported that inclusion of adamantyl and diamantyl groups in acrylate, methacrylate, and vinyl monomers imparted some of the optical properties of diamond to the resulting polymers, which exhibited low optical dispersion and high refractive indices.[52] In fact, poly(1-vinyladamantane) exhibited the highest n_d (1.5560) of the diamondoid polymers studied, however it could only be obtained as oligomers since adamantane proved too bulky for the vinylic backbone. Desirable optical properties have since been demonstrated in copolymers of adamantyl methacrylate with methacrylate[56] and styrene,[54] adamantyl acrylate with n-butyl acrylate[57], and adamantyl vinyl ether with a host of other vinyl ethers.[58]

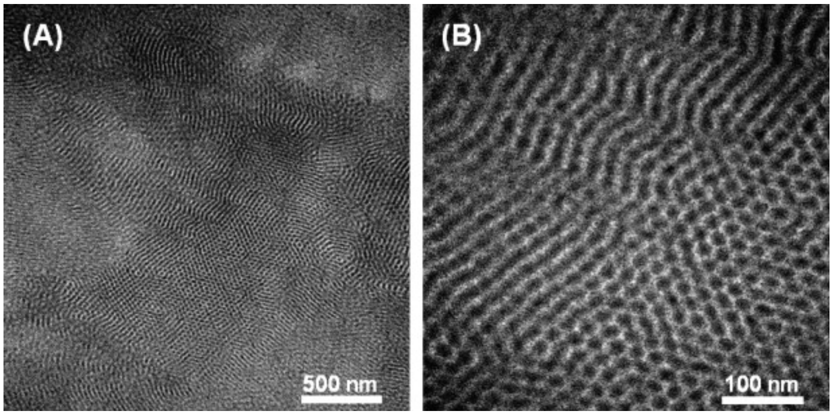

Figure 1.17: Stained TEM images of microphase separation of hydrogenated poly(isoprene-*block*-**1**-*block*-isoprene). Taken from ref. 53

Self-assembly of diamondoid containing block copolymers has also been reported, but to date has not been studied in earnest. Nakano et al. reported several instances of self-assembly in their work with adamantyl acrylates.[57] Block copolymers consisting of a pure poly(1-adamantyl acrylate) block and a block with varying content of 1-adamantyl acrylate, n-butyl acrylate and 2-hydroxyethyl acrylate demonstrated lamellar and island morphologies with various domain sizes based on the volume fraction of the blocks and the composition of the copolymer block.[57] Kobayashi observed self-assembly of the cylindrical morphology in poly(isoprene-*block*-**1**-*block*-isoprene) (40 wt% **1**) that had been subsequently hydrogenated to remove C=C bonds in the backbone (Figure 1.17).[53]

Summary of Work

Although incorporation of diamondoids into polymers has gained increased attention in the last 20 years, only two instances of diamondoid 2-substituted 1,3-butadienes have been reported.[17,53] While these preliminary reports outline the very interesting thermal properties of the poly(**1**-*ran*-isoprene) system, they do not address the effect of the adamantane 2-substituents on mechanical properties. Furthermore, the influence of adamantyl pendants on parameters like δ and T_{ODT} are unknown. The overall goal of this dissertation will be to synthesize and the poly(**1**) and poly**(1**-*ran*-isoprene) system and conduct a more exhaustive characterization of thermomechanical properties as well as initiate a preliminary investigation in self-assembly. To accomplish this, a more scalable and efficient monomer synthesis for diamondoid 2-substituted 1,3-butadienes will be developed, as contemporary syntheses have been noted as a limiting factor in their study.[66] Additionally, alternative polymerization methods to living anionic polymerization (LAP) will be explored to circumvent the prohibitively rigorous purification that it requires.

Chapter 2

This chapter will address the synthesis of 1,3-dienes with diamondoid 2-subsitutents. The relative dearth of references to polydienes with large pendant substituents, including diamondoids, is partly due to the complexity and limited scope of many contemporary synthetic methods of dienes,[67–70] which has made obtaining monomers in suitable quantities for polymerization studies difficult. Fiorito et al. highlighted the limitations of contemporary enyne cross-metathesis, cross-coupling and vinylogous Peterson elimination methods for the preparation of 2-substituted 1,3-dienes and presented an improved nickel-catalyzed Kumada vinylation.[71] Although, their method allows for improved access to a wide range of substituted diene monomers, the need for simple, mild, and scalable syntheses persists.

Here, a mild and straightforward synthesis of **1** is presented which improves upon the synthesis reported by Kobayashi et al.[17] Following the addition of vinylmagnesium bromide to adamantyl methyl ketone, the resulting tertiary allylic alcohol is dehydrated to diene using Amberlyst®-15 cationic exchange resin. Unlike heterogeneous dehydration with p-toluenesulfonic acid, this method can be conducted at room temperature and the formation of Diels-Alder side products is eliminated with the use of ethereal solvents. Inclusion of a heterogenous desiccant removed water, which deactivates Amberlyst®-15, *in-situ* allowing for a tenfold excess of substrate to be used, further enhancing the scalability of the method. Lastly, heterogeneous dehydration of a range of aliphatic, aromatic, and heteroaromatic tertiary allylic substrates was conducted to assess the broader use of the method.

Chapter 3

Experimental challenges associated with polymerizing diene monomers has also presented obstacles to the widespread study of 2-substituted 1,3-dienes. Although LAP is compatible with diene monomers, affords precise structural control and access to block copolymers, it requires rigorous purification to ensure the absence of air and electrophilic impurities.[1,21,63,72] Even with modern advancements, LAP is largely inaccessible except with specialized laboratory-scale setups.[73,74] Controlled radical polymerization (CRP) techniques are much more tolerant of electrophilic impurities, however, there are limitations in their use with dienes. Of the common CRP techniques, atom transfer radical polymerization (ATRP) cannot be used due to the chelation of isoprene with the copper catalyst.[72] Several reports of reversible addition-fragmentation termination (RAFT) polymerization have been reported[18,75–79]; however, nitroxide mediated polymerization (NMP) is the most commonly used CRP method.[20,80–83] Still, there are two obstacles facing polymerization of dienes via NMP. The first is a low polymerization rate resulting in long reaction times (typically 24h or longer) and low conversions.[20,80] The second is the susceptibility of the dienes to side reactions.[76,79,80] At temperatures required for most NMP (100-120°C), both Diels-Alder dimerization and autoinitiation of isoprene have been shown to compete with polymerization, resulting in low yields.[84]

Here NMP using the unimolecular "universal initiator" developed by Hawker et al. was applied to the polymerization of **1** and copolymerization with isoprene. It was concluded that Diels-Alder addition of monomers was the predominant product at the temperatures required for NMP. Accordingly, emulsion polymerization of **1** and mixtures of **1** and isoprene at room-temperature using a redox-pair initiator was explored. All poly(**1**) and poly(**1**-*ran*-isoprene) samples were soluble in common organic solvents and exhibited high 1,4-microstructure. A continuous increase in glass transition temperature from −63 to 172°C was observed by increasing the ratio of **1** in the comonomer feed of poly(**1**-*ran*-isoprene), and T_g values were in good agreement with the Fox equation. After complete hydrogenation to poly(1-vinyladamantane-*alt*-ethylene-*ran*-propylene-*alt*-ethylene), a continuous increase in T_g was observed from −55 to 152°C. The high solubility and improved access to poly(**1**) and poly(**1**-*ran*-isoprene) opens the door to exploration of diene polymers with enhanced high temperature properties.

Chapter 4

This chapter presents the first report of the mechanical properties of poly(**1**) and poly(**1**-*ran*-isoprene). Previously reported room temperature emulsion polymerization of poly(**1**-*ran*-isoprene) was used to produce polymer at multi-gram scale necessary for mechanical testing. Particularly, the storage and loss moduli with respect to temperature were determined by dynamic mechanical analysis (DMA) to assess the operating range for these thermoplastic elastomers and confirm the T_gs determined from DSC. Rheology was used to characterize both the rubber plateau and rubbery flow regions at varying wt% of **1**. Furthermore, rheology was used to characterize the rubbery plateau and the rubbery flow regions in poly(**1**) and several poly(**1**-*ran*-isoprene) samples. The independent contributions of backbone saturation and adamantyl pendant groups to polymer chain mobility were elucidated by rheological characterization of dynamic viscosity (η*) of poly(**1**), before and after hydrogenation, and poly(**1**-*ran*-isoprene).

Chapter 5

This chapter presents an application of a novel living anionic polymerization method for the synthesis of poly(**1**) and poly(**1**-*block*-isoprene). This method, which utilizes titration with a 4,5-methylenephenanthrene (MPT) indicator, offers an alternative to prohibitively rigorous purifications required with conventional LAP methods. In addition to identifying a suitable synthesis for block copolymers, anionic poly(**1**) could now be compared to poly(**1**) synthesized via emulsion. Kobayashi, et al. reported that poly(**1**) synthesized via LAP was almost completely insoluble above an M_n of 6,000 g/mol.[17] This is in stark contrast to poly(**1**) synthesized via emulsion, which has exhibited excellent solubility in DCM, THF, and toluene even up to 47,000 g/mol.

The central hypothesis of this exploration is that, contrary to Kobayashi et al.'s conclusions, anionic poly(**1**) is highly crystalline with a T_m that is undetectable by DSC analysis up to 270 °C. Furthermore, if short or long-chain branching are present in emulsion poly(**1**), it would inhibit crystallization and increase solubility. Powder x-ray diffraction (XRD) and DSC were used to probe for the presence of crystallinity, while the potential for branching in emulsion poly(**1**) was investigated using 1D- and 2D-NMR experiments, GPC analysis.

.

Chapter 2: Straightforward Synthesis of Diamondoid Substituted 1,3-Butadiene Monomers with Amberlyst®-15

Abstract

Heterogeneous catalysis of tertiary allylic alcohols was conducted using cationic exchange resin Amberlyst®-15 resulting in 2-substituted 1,3-dienes. Dehydration with Amberlyst®-15 presents a straightforward and scalable synthesis for 2-substituted 1,3-dienes as reactions are conducted at room temperature and require neither high-vacuum apparatus nor rigorous air-free techniques. Autopolymerization and Diels-Alder cyclization of diene product was suppressed by solvent selection. Water generated during dehydration was removed *in-situ* with the addition of a heterogeneous desiccant, which allowed tenfold molar excess of substrates to Amberlyst®-15 to be used. Extension of this method to the dehydration of 2-(4-diamantyl)-3-buten-2-ol gave diene in modest yields. In contrast, rearrangements and low yields were observed in several other aliphatic, aromatic and heteroaromatic tertiary allylic alcohols.

Introduction

Although 2-substituted 1,3-dienes are broadly useful building blocks in organic synthesis and polymer chemistry, they have proven challenging to synthesize in appreciable quantities. Consequently, the use of 2-substituted-1,3-dienes as monomers for polymerizations has been relatively limited in scope. A simple, direct, and scalable method of preparation of 2-substituted 1,3-dienes would remove a significant barrier to their study in polymer systems.

Several syntheses for 2-substituted 1,3-diene exist (Scheme 2.1). Ruthenium-catalyzed cross-metathesis between terminal alkenes and ethylene is perhaps most commonly used but requires highly flammable ethylene gas and an expensive catalyst.[67] Alternatives include Ni or Pd catalyzed Kumada and Negishi type cross coupling reactions, which involve the formation of Grignard reagents derived from chloroprene.[68] The dienyl Grignard is notoriously difficult to handle, however, limiting the scope of this method. Ni-catalyzed cross-couplings between dienyl phosphates and Grignard reagents has been employed but is limited by the scope of available Grignard reagents.[69,85,86] Vinylogous Peterson elimination of silylated allylic alcohols allows for the synthesis of dienes with variety of functionally sensitive 2-substituents.[70] An extensive synthetic route of the substrate, however, proved very limiting. Recently, Fiorito et al. presented an improved nickel-catalyzed Kumada vinylation.[71] Though this provides access to a wide range of 2-substituted dienes, it requires the use of toxic chlorophosphonates, air-free techniques, and a glove box. Indeed, a more robust and straightforward synthesis could expand the use of 2-substituted dienes for applications specifically in polymer science. It must be noted that Fokin et al. reported a preparation of diamondoid 1,3-dienes from methyl ketones via an acid catalyzed oxetane ring opening.[87] Though excellent yields were reported, high reagent excess to form the ogano-sulfur reagent makes this method poorly suited for monomer synthesis on a larger scale.

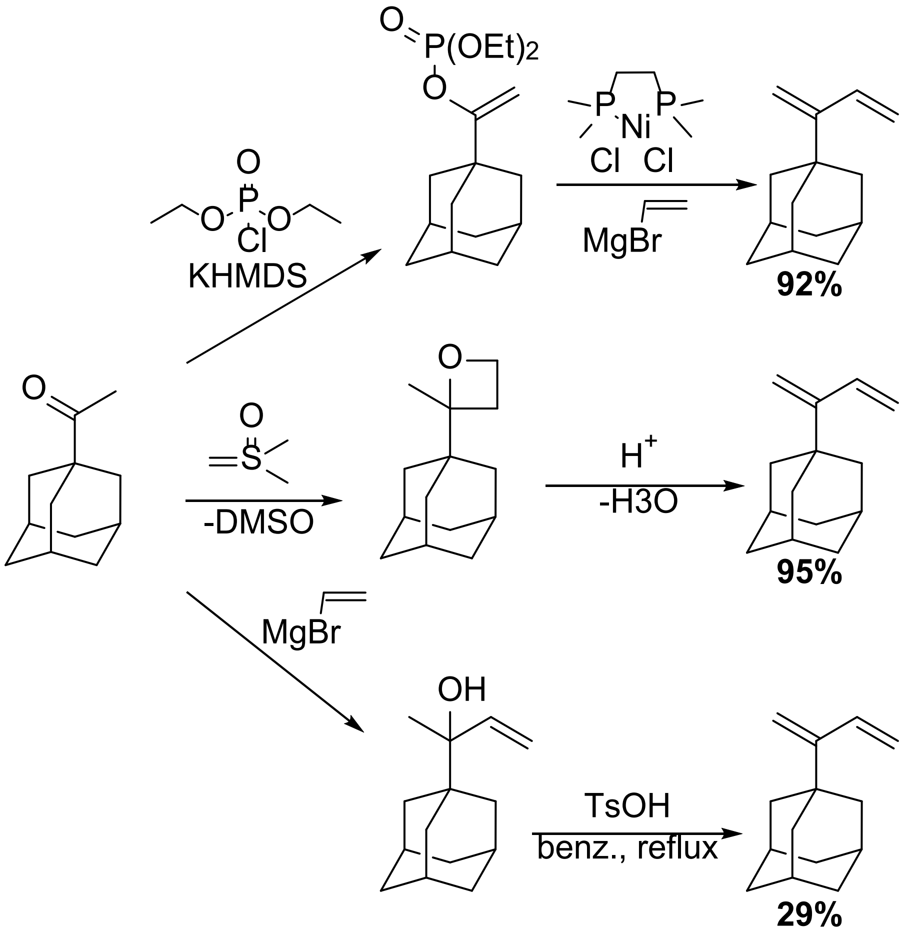

Scheme 2.1: Reported syntheses of 2-(1-adamantyl)-1,3-butadiene

Kobayashi et al. utilized a more straightforward synthesis when synthesizing poly(**1**), which involved the addition of vinylmagnesium bromide to methyl ketones and subsequent acid-catalyzed dehydration of the tertiary allylic alcohol.[17] This route is attractive for a diene monomer synthesis for several reasons. All reagents can be affordably sourced, and all steps are straightforward and can be easily conducted with limited synthesis experience. For example, Grignard addition to ketones was often a component of undergraduate organic chemistry educational lab curricula.[88] The myriad methods of tertiary alcohol dehydration are encouraging for the identification of an alternative to the dehydration reported by Kobayashi et al. in which p-toluenesulfonic acid in refluxing benzene gave **1** in 34% yield.[17] Several other examples of dehydration of 2-(1-adamantyl)-3-buten-2-ol with p-toluenesulfonic acid (TsOH) have been reported in ether[89] and at room temperature with a combination of TsOH and tetrabutylammonium perrhenate.[90] Moving forward, the primary goal was to identify a dehydration catalyst that would increase the yield of (**1**) with an emphasis on mild reaction conditions and scalability.

Tertiary alcohol dehydration generally consists of heterogenous or homogenous acid catalyzed systems, or the use of strong mineral acids or high temperatures.[91] For substrates with acid or temperature sensitive functionalities, like dienes, heterogenous acid catalysis has several distinct advantages. In comparison to their homogenous counterparts, many heterogenous systems require milder reaction conditions and exhibit increased yields. Heterogenous catalysts also greatly simplify reaction set-up and work-up.[91]

Amberlyst®-15 is a strong cationic exchange resin comprised of a porous matrix of sulfonated styrene divinyl benzene copolymer. Commercially, it is available as macroreticular beads with average pore diameter of 160 Å and a pore diameter range of 120-600 Å.[92] This structure effectively eliminates diffusion resistance within the catalyst and allows access of gaseous and liquid substrates to the acid sites; moreover, it can be used with non-swelling organic media.[91] Amberlyst®-15 has historically been used for etherification[93,94] and dehydration[95] reactions, and numerous studies have been conducted exploring the use of Amberlyst®-15 to catalyze the dimerization of olefins,[93,96–100] namely isobutene, to produce C_8 fuel additives.

In 2012, Frija and Afonso investigated the potential of Amberlyst®-15 as a mild and reusable catalyst system for the dehydration of tertiary alcohols. They concluded that dehydration with Amberlyst®-15 gave predominantly the most stable alkene product in very good yield. No polymerization products were observed, and the catalyst was tolerant of a wide range of protective functional groups (NHCBz, NHBoc, OSEM, OTBDMS, OBOM and ethylene ketals). Though Amberlyst®-15 was presented as a very promising catalyst system for tertiary alcohol dehydration, no instances of its use in dehydrating tertiary allylic alcohols to 2-substituted 1,3-dienes have been reported.

The potential for Amberlyst®-15 to provide a robust and scalable synthesis of 2-substituted 1,3-diene monomers prompted the following investigation. Our primary hypothesis is that milder reaction conditions afforded by a heterogenous catalyst will minimize or eliminate the formation of side products that are present when homogenous catalysts such as p-toluenesulfonic acid are used. This would greatly increase the yields of **1**, providing a mild monomer synthesis using commercially available reagents that does not require the use of toxic organophosphonates, specialty equipment such as high-vacuum manifolds, or air-free techniques. A secondary hypothesis, that Amberlyst$^{®}$-15 can mitigate cationic polymerization and rearrangements in acid sensitive substrates such as 2-phenyl-1,3-butadiene, will also be tested. This work will provide a preliminary assessment of the broader applicability of Amberlyst$^{®}$-15 as a general catalyst for 2-substituted 1,3-butadiene monomers via dehydration.

Experimental

Materials

All glassware was oven dried. Tetrahydrofuran (HPLC grade, Fisher), diethyl ether (Reagent grade, Fisher), and dichloromethane (HPLC grade, Fisher) were dried for a minimum 48 h using 3 Å molecular sieves (activated overnight at 300 °C, 30 mbar) and distilled immediately before use. Pentane (HPLC grade, Fisher) and toluene (HPLC grade, Macron Fine Chemicals) were used as received. Adamantyl methyl ketone (97%, AstraTech) was recrystallized from methanol prior to use. 2-methyl-3-buten-2-ol (98%, AKSci), Pinacolone (97%, Alfa Aesar), cyclohexyl methyl ketone (95% Alfa Aesar), acetophenone (Merck KGaA), 3-acetylindole (99%, AKSci), 4'-hydroxyacetophenone (98% AKSci), *tert*-butyldimethylsilyl chloride (Oakwood Chemical), di-*tert*-butyl dicarbonate (98%, Sigma-Aldrich), 4-dimethylaminopyradine (Oakwood Chemical), imidazole (>99%, Sigma-Aldrich), 2-acetonapthone (99%, Acros Organics), 2',3',4',5',6'-pentafluoroacetophenone (98%, AKSci), vinylmagnesium bromide solution (0.7 M in THF, Acros Organics), and Amberlyst$^{®}$-15(H) ion exchange resin (1.6 % moisture, Alfa Aesar) were used as received. 2,3-butanedione (98%, Alfa Aesar) was distilled immediately before use. Merck HPTLC 60 F245 aluminum backed silica gel plates were used for analytical thin layer chromatography (TLC). Silicycle SiliaFlash® P60 230-400 mesh silica was used for column chromatography. GC-MS was conducted on a ThermoScientific Trace 1300 Gas Chromatograph with an ISQ 7000 Single Quadrupole Mass Spectrometer (ZB1 30 m x 0.25 mm ID column, Phenomenex; 40 °C to 250 °C (10 min) at 5 °C/min). NMR were recorded on a Bruker AVANCE III HD 500 MHz spectrometer with Protégé cold probe.

4-acetyldiamantane

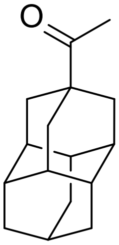

To a dry Schlenk flask was added diamantane (2.0 g, 10.6 mmol), 2,3-butanedione (10 mL, 115 mmol), and toluene (20mL). The solution was degassed by three freeze-pump-thaw cycles, brought to room temperature, and stirred for at least 1 hour to ensure that a saturated solution of diamantane was obtained. 2 mL of this saturated solution were transferred under flowing nitrogen to 17 (34 mL of solution total) borosilicate NMR tubes (L = 7", OD = 5 mm) and capped. The array of tubes was irradiated with 2 LED UV lamps (50 W, 395 – 400 nm) for at least 64 hours. Irradiated solutions were consolidated and concentrated giving a yellow oil (3.86 g). This oil was dry loaded onto silica and flash column chromatography (eluent: hexanes) gave practically pure diamantane (0.136 g, 0.7 mmol). Gradually increasing eluent to 5% ethyl acetate gave crystals which were visibly contaminated with a yellow oil. Recrystallization of this fraction from hot methanol:water gave 4-acetyldiamantane (0.218 g, 0.9 mmol). **^{1}H NMR:** ($CDCl_3$, 500 MHz) δ (ppm) = 2.11 (s, 1H), 1.87 (m, 3H), 1.81(m, 1H), 1.77 (d, 6H), 1.74 (t, 6H), 1.71(m, 3H). **^{13}C NMR:** ($CDCl_3$, 500 MHz) δ (ppm) = 45.0, 39.4, 37.9, 37.5, 36.9, 25.8, 24.8. **GC-MS (EI):** m/z (int.) = 230(6), 187(100), 159(5), 145(10), 131(16), 107(10), 105(17), 91(29), 79(27), 67(10).

1-(4-((tert-butyldimethylsilyl)oxy)phenyl)ethan-1-one

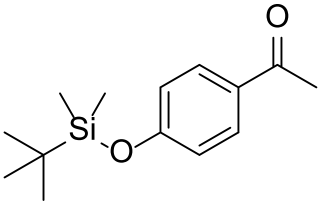

To a nitrogen purged 50 mL flask, dry dimethylformamide (15 mL) and 4'-hydroxyacetophenone (4.0 g, 29.4 mmol) were added and stirred for 10 min. Imidazole (3.0 g, 44.1 mmol) was then added and stirred for 10 minutes. The reaction was then cooled to 0 °C and *tert*-butyldimethylsilyl chloride (4.43 g, 29.4 mmol) was added slowly in three portions over 30 min. The reaction was allowed to warm to room temperature and stirred overnight. Solution was extracted with hexanes and DI water and organic layer dried with $MgSO_4$. Solvent was removed under vacuum (40 °C, 50 mbar). Residual solvent was removed by warming product to 65 °C at 0.1 mbar yielding colorless

crystals (6.70 g, 91% yield). NMR spectra agree with reported literature values.[101] **^{1}H NMR:** (CDCl$_3$, 300 MHz) δ (ppm) = 0.23 (s, 6H, Si(CH$_3$)$_2$), 0.99 (s, 9H, SiC(CH$_3$)$_3$), 2.55 (s, 3H, O=C-CH$_3$), 6.87 (d, 2H, J$_{HH}$ = 8.73 Hz, aromatic), 7.88 (d, 2H, J$_{HH}$ = 8.73 Hz, aromatic)

1-(3-(1-tert-Butoxycarbonyl)indolyl)-1-ethanone

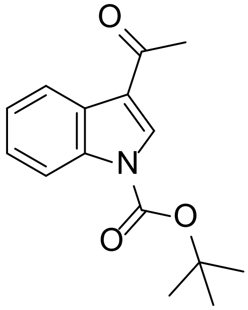

To a nitrogen purged 100 mL flask, 3-acetylindole (1.83 g 11.5 mmol) and 4-dimethylaminopyridine (0.07 g 0.57 mmol) were added and diluted with 38 mL of dry THF. Di-*tert*-butyl dicarbonate (3.0 g 13.7 mmol) was added at room temperature and reaction was stirred for 2 hours. 50mL of water was added and a white fluffy precipitate (1.94 g, 65% yield) was observed and isolated by vacuum filtration. NMR spectra agree with reported literature values.[102] **^{1}H NMR:** (CDCl$_3$, 300 MHz) δ (ppm) = 8.37 (m, 1H), 8.22 (s, 1H), 8.12 (m, 1H), 7.37 (m, 2H), 2.57 (s, 3H), 1.71 (s, 9H).

General synthesis of tertiary allylic alcohols from ketones

A 250mL Schlenk flask was cooled to 0 °C with an ice bath. Vinylmagnesium bromide solution 0.7M in THF (80 mL, 56.0 mmol, 1.2 eq.) was added via canula transfer under nitrogen. A solution of ketone (47.0 mmol, 1.0 eq.) in dry THF (20 mL) was added dropwise to the stirred vinylmagnesium bromide. The reaction was then allowed to warm to room temperature and stirred overnight. The reaction was neutralized with 15 mL of a saturated aqueous solution of ammonium chloride added dropwise at 0 °C under nitrogen resulting in the formation of a white precipitate. The organic layer was decanted from the precipitate and washed with brine. The aqueous layer was washed twice with diethyl ether and the combined organic layers were dried over MgSO$_4$. Removal of solvent under vacuum yielded allyl alcohol product which was used in subsequent dehydrations without isolation. Syntheses that deviated from this general method are reported individually.

2-adamantyl-3-buten-2-ol

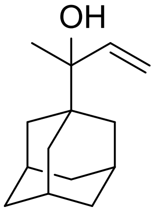

Vinylmagnesium bromide solution 0.7 M in THF (100 ml, 70.0 mmol, 1.2 eq.) was added via cannula to a 250 mL Schlenk flask cooled to 0 °C with an ice bath. Adamantyl methyl ketone (10.40 g, 58.3 mmol, 1.0 eq.) was dissolved in 35 ml of THF and the solution was added dropwise to the vinylmagnesium bromide. After addition, the reaction was slowly warmed to room temperature and stirred overnight. The reaction was then cooled to 0 °C and 10 ml of saturated NH_4Cl were added dropwise. Reaction mixture was extracted with diethyl ether three times. Combined organic layers were dried over anhydrous $MgSO_4$, filtered, and concentrated under reduced pressure yielding a pale-yellow oil (10.45 g). Product was isolated by fractional distillation of this oil in a Kugelrohr oven (75–125 °C, 1E-3 mbar) giving a white crystalline solid (6.57 g, 31.8 mmol, 55%). NMR spectra were consistent with literature values.[17] **^{1}H NMR:** (500 MHz, $CDCl_3$) δ (ppm) = 6.00 (dd, 1H) 5.17 (dd, 1H) 5.08 (dd, 1H) 1.96-2.02 (m, 3H, adamantyl 3 x CH) 1.58-1.82 (m, 12H, adamantyl 6 x CH_2), 1.31 (s, 1H) 1.19 (s, 3H); **^{13}C NMR:** (500 MHz, $CDCl_3$) δ (ppm) = 143.1, 112.5, 77.4, 38.9, 37.3, 36.5, 28.8, 22.4

2-phenyl-3-buten-2-ol

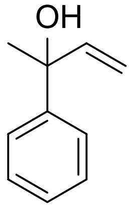

Vinylmagnesium bromide solution 0.7M in THF (50 mL, 35.0 mmol, 1.2 eq.) was added via canula transfer to a 250mL 3-neck flask cooled to 0°C with an ice bath. Acetophenone (3.45g, 28.7 mmol, 1.0 eq.) was added to 15 mL of THF and the solution was added dropwise to the vinylmagnesium bromide. The reaction was allowed to warm to room temperature, stirred overnight, and neutralized with 50 mL of 1N HCl added dropwise under cooling at 0°C. Reaction mixture was extracted with diethyl ether three times. Combined organic layers were dried over anhydrous $MgSO_4$. Removal of solvent resulted in a pale-yellow oil (4.34g), which was purified by flash column chromatography (eluent: hexanes/ethyl acetate 4:1) and then distillation (50°C, 0.1 mBar) to give product as a clear oil (2.84g, 21.8 mmol, 76%). NMR were consistent with literature values.[103,104] **^{1}H NMR:** (500 MHz, $CDCl_3$) δ (ppm) = 7.46 (d, 2H, aromatic), 7.34 (t, 2H, aromatic), 7.25 (t, 1H, aromatic), 6.15 (dd, 1H)

5.28 (d, 1H), 5.13 (d, 1H) 1.86 (s, 1H) 1.66 (s, 3H); **^{13}C NMR:** (500 MHz, $CDCl_3$) δ (ppm) = 146.4, 144.9, 128.3, 127.0, 125.2, 112.3, 74.8, 29.4

*2-(1-adamantyl)-1,3-butadiene (**1**)*

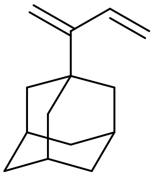

2-(1-adamantyl)-3-buten-2-ol (206 mg, 1.0 mmol), solvent (10 mL), Amberlyst®-15 (21.3 mg), and anhydrous $CaCl_2$ (100 mg) were added to a round bottom flask. Reactions were monitored with TLC (eluent: hexanes) until the disappearance of substrate was observed. Amberlyst®-15 was filtered from the reaction and then washed three times with 5 mL of solvent. Solvent was removed under reduced pressure at room temperature giving a clear oil. Diene product (150 mg, 0.8 mmol, 80%) was isolated via flash column chromatography (eluent: hexanes). NMR spectra were consistent with literature values.[17] **^{1}H NMR:** (500 MHz, CDCl3) δ (ppm) = 6.42 (dd, 1H) 5.35 (d, 1H), 5.08 (s, 1H) 4.99 (d, 1H) 4.71 (s, 1H) 1.96-2.02 (m, 3H, adamantyl 3 x CH) 1.58-1.82 (m, 12H, adamantyl 6 x CH_2); **^{13}C NMR:** δ (ppm) = 157.5, 136.7, 114.9, 107.3, 41.4, 37.1, 37.0, 28.9

2-phenyl-1,3-butadiene

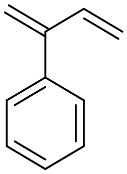

2-phenyl-3-buten-2-ol (184 mg, 1.0 mmol), solvent (10 mL), Amberlyst®-15 (21.3 mg), and anhydrous $CaCl_2$ (100 mg) were added to a round bottom flask. Reactions were monitored with TLC (eluent: hexanes/ethyl acetate 4:1) until the disappearance of substrate was observed. Amberlyst®-15 was filtered from the reaction and then washed three times with 5 mL of solvent. Solvent was removed under reduced pressure at room temperature giving a clear oil. Diene product (39.1 mg, 0.3 mmol, 30%) was isolated via flash column chromatography (eluent: hexanes 1% Et_3N). NMR spectra were consistent with literature values.[103] **^{1}H NMR:** (500 MHz, CDCl3) δ (ppm) = 7.35-7.26 (m, 5H) 6.59 (dd, 1H) 5.30 (dd, 2H) 5.22 (dd, 2H); **^{13}C NMR:** (500 MHz, CDCl3) δ 148.3, 139.8, 138.2, 128.3, 128.1, 127.5, 117.1, 116.8.

2-cyclohexyl-1,3-butadiene

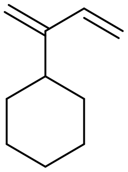

2-cyclohexyl-3-buten-2-ol (154 mg, 1.0 mmol), diethyl ether (10 mL), Amberlyst®-15 (21.3 mg), and anhydrous $CaCl_2$ (100 mg) were added to a round bottom flask. Reactions were monitored with TLC (eluent: hexanes) until disappearance of substrate was observed. Amberlyst®-15 was filtered from the reaction and then washed three times with 5 mL of solvent. Solvent was removed under reduced pressure at room temperature giving a clear oil. Diene product (74.9 mg, 0.5 mmol, 55%) was isolated via flash column chromatography (eluent: hexanes). Although a mixture of products was detected the primary component was diene. This was confirmed by the presence of vinylic proton signals in ^{1}H NMR spectra, which were consistent with literature values.[105] **^{1}H NMR:** (500 MHz, CDCl3) δ (ppm) = 6.32 (dd, 1H), 5.27 (d, 1H), 5.03 (d, 1H), 5.00 (s, 1H), 4.94 (s, 1H).

2-tert-butyl-1,3-butadiene

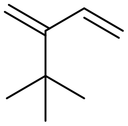

2-*tert*-butyl-3-buten-2-ol (128 mg, 1.0 mmol), diethyl ether (10 mL), Amberlyst®-15 (21.3 mg), and anhydrous $CaCl_2$ (100 mg) were added to a round bottom flask. Reactions were monitored with TLC (eluent: hexanes) until disappearance of substrate was observed. Amberlyst®-15 was filtered from the reaction and then washed three times with 5 mL of solvent. Solvent was removed by flowing nitrogen at room temperature resulting in a clear oil. Diene product (88.2 mg, 0.8 mmol. 80%) was isolated via flash column chromatography (eluent: hexanes) and solvent was removed by flowing nitrogen at room temperature. ^{1}H NMR spectra indicated the presence of diene product and was consistent with literature values.[90] **^{1}H NMR:** (500 MHz, $CDCl_3$) δ (ppm) = 6.42 (dd, 1H), 5.39 (d, 1H), 5.06 (s, 1H), 5.01 (d, 1H), 4.80 (s, 1H), 1.09 (s, 9H)

Dehydration of allylic alcohols in Runs 11-18

Tertiary allylic alcohol (0.4 mmol, 1.0 eq), solvent (4.0 mL), and Amberlyst®-15 (72.1 mg, 1.0 eq) were added to a round bottom flask and heated to 50 °C. Reactions were monitored with TLC (eluent: hexanes) until consumption of substrate was observed. Amberlyst®-15 was filtered from the reaction and washed several times with 5 mL of solvent. Solvent was removed under vacuum and remaining product was diluted in hexanes and passed through a short plug of silica. Solvent was removed from reaction product under vacuum and NMR and GC-MS samples were prepared to determine concentration and yield.

*2-(4-diamantyl)-1,3-butadiene (**2**)*

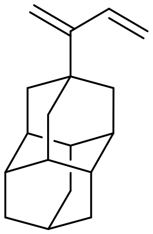

A solution of 1.0 M vinylmagnesium bromide in THF (8.0 mL, 1.2 eq.) was added to a 50 mL Schlenk flask equipped with a magnetic stir bar and cooled to 0 °C with an ice bath. 4-acetyldiamantane (1.55 g, 6.7 mmol, 1 eq.) in THF (7 mL) was added dropwise to the vinylmagnesium bromide solution under stirring and then allowed to come to room temperature overnight. The reaction was then cooled again to 0 °C with an ice bath and quenched by 1.2 mL of saturated NH_4Cl added dropwise resulting in the formation of a white precipitate. The organic layer was decanted from the precipitate and washed with brine. The aqueous layer was washed twice with THF, and the combined organic layers were dried over $MgSO_4$. Removal of solvent under vacuum yielded a mixture primarily of allyl alcohol, which was used in subsequent dehydrations without isolation. This mixture was dehydrated with Amberlyst®-15 in a 1% w/v mixture of $CaCl_2$ in diethyl ether ($[S]_0 = 0.1$, $[S]_0/[H^+] = 1.0$). After 26 hours, catalyst was filtered from the reaction. A white precipitate was then observed in the filtrate on standing for 1 hour, which adhered to the flask. Decanting of the soluble material and removal of solvent gave 0.96 g of an orange wax. Flash column chromatography of this wax (eluent: hexanes) gave pure **2** (0.421 g, 2.2 mmol, 33% yield from 4-acetyldiamantane) as a clear crystalline solid.

Results and Discussion

Synthesis of tertiary allylic alcohols

Tertiary allylic alcohols were synthesized by the addition of substituted methyl ketones to vinylmagnesium bromide solution in THF. Generally, addition of Grignard to ketones yields several products: addition, aldol-condensation, and reduction.[106,107] The addition product occurs when vinyl magnesium bromide acts as a nucleophile and adds to the carbonyl forming a tertiary allylic alcohol. Vinylmagnesium bromide may also act as a base and enolize methyl ketones. Enolized carbonyls can then react to form the self-aldol product or can be converted back to ketones on acidic workup.[106]

Because vinylmagnesium bromide lacks a transferable β-proton, no reduction product was observed in any of the Grignard additions performed. Composition of Grignard reaction products are shown in Scheme 2.2**.**

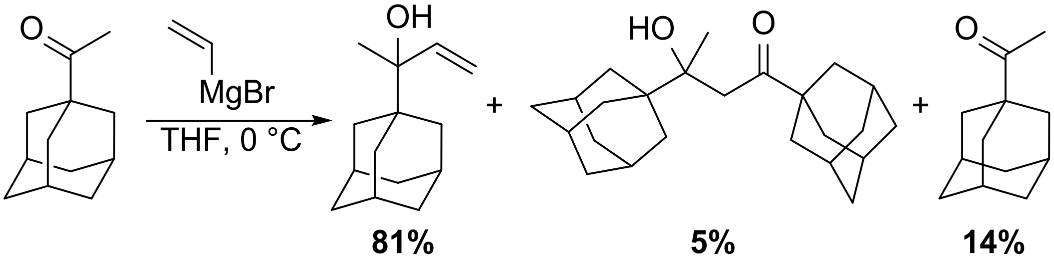

Scheme 2.2: Synthesis of 2-(1-adamantyl)-3-buten-2-ol

Preliminary Dehydration Studies

Reaction conditions were screened by dehydrating a commercially available allylic tertiary alcohol, 2-methyl-3-buten-2-ol, with Amberlyst®-15 to form isoprene. The goal of these experiments was to determine optimal conditions for the initial substrate concentration ($[S_0]$) and the ratio of substrate to Amberlyst®-15 ($[S_0]/[H^+]$). Three dehydrations of 2-methyl-3-buten-2-ol were carried out at $[S_0]/[H^+] = 1.8$, 1.0 and 0.5 and composition was monitored by analyzing the headspace with GC-MS. Dibutyl ether was used as solvent as its low vapor pressure allowed for better detection of volatile substrate and product at relatively low concentrations. All dehydrations showed near complete substrate consumption after 3 hours (Figure 2.1). However, at $[S_0]/[H^+] = 1.8$ consumption of isoprene was observed (Figure 2.2). Accordingly, subsequent dehydrations were conducted with $[S_0] = 0.1$ M and $[S_0]/[H^+] = 1.0$

Solvent Selection

Several solvents were screened for the dehydration of 2-(1-adamantyl)-3-buten-2-ol at room temperature to determine their effect on dehydration in the presence of Amberlyst®-15. 0.1 M solutions of 2-adamantyl-3-buten-2-ol in dichloromethane (DCM), pentane, diethyl ether and acetone were prepared. These solutions were then added to sealed vials containing Amberlyst®-15 such that $[S]_0/[H^+] = 1$. Reactions were stirred and monitored by GC-MS. Samples were prepared at predetermined time intervals by extracting 20 μL of the reaction with a 100 μL syringe and diluting in 1 mL of chloroform. After reaction, solutions were decanted from Amberlyst®-15 and solvent was removed.

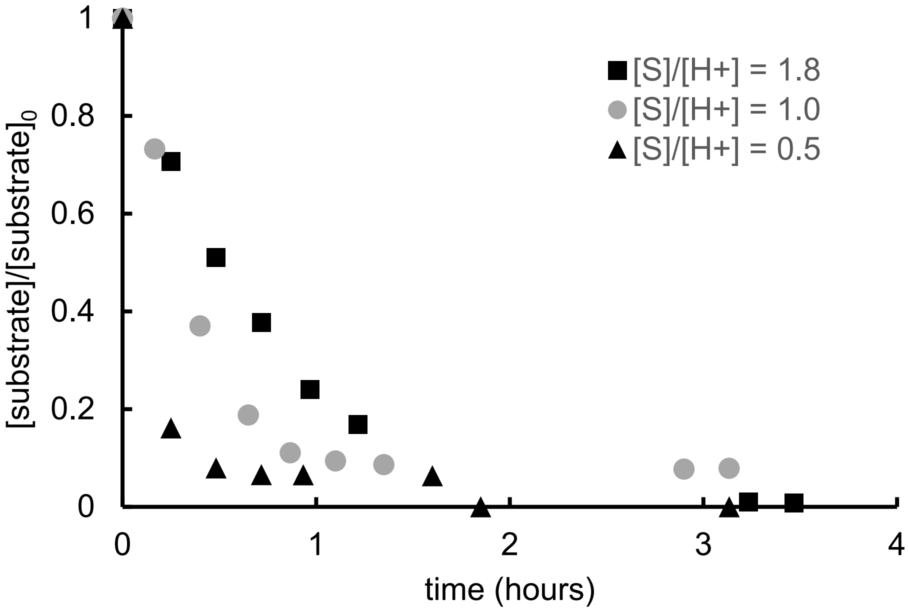

Figure 2.1: Relative concentration 2-methyl-3-buten-2-ol at various $[S]_0/[H+]$

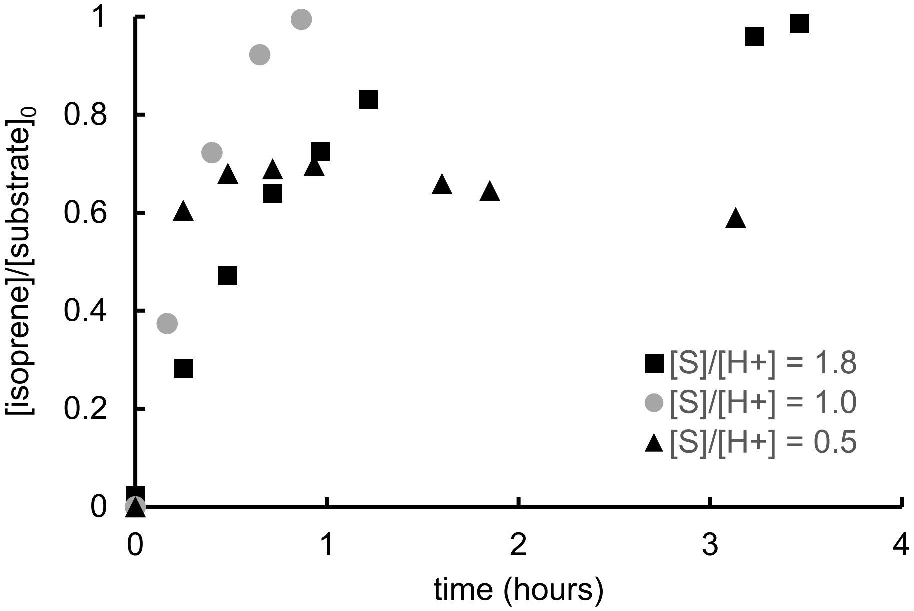

Figure 2.2: Relative isoprene concentration at various$[S]_0/[H+]$

Solvent selection had a marked effect on the rate of dehydration of 2-adamantyl-3-buten-2-ol as well as the stability of the diene product. Dehydration was observed in all solvents, however complete conversion was observed first in DCM and pentane (2.5 hours) followed by acetone (4 hours) and then diethyl ether (8 hours). Reaction of **1** was observed in dehydrations conducted in DCM and pentane, and GC-MS chromatograms detected the evolution of two peaks at 43.83 min and 49.37 min that correlated with a drop in diene concentration. These peaks have an m/z = 376, which is consistent with Diels-Alder products of **1**. ^{1}H NMR analysis of reaction products confirmed these peaks to be attributed to two separate monoterpene derivatives, **3a** and **3b** (Scheme 2.3). Product **3a** was isolated through recrystallization and a full characterization is presented in Appendix B. Crucially, no formation of side products was observed in dehydrations in acetone and diethyl ether. However, acid-catalyzed condensation of acetone to mesityl oxide was observed, which is consistent with literature,[108,109] so diethyl ether was chosen for future use.

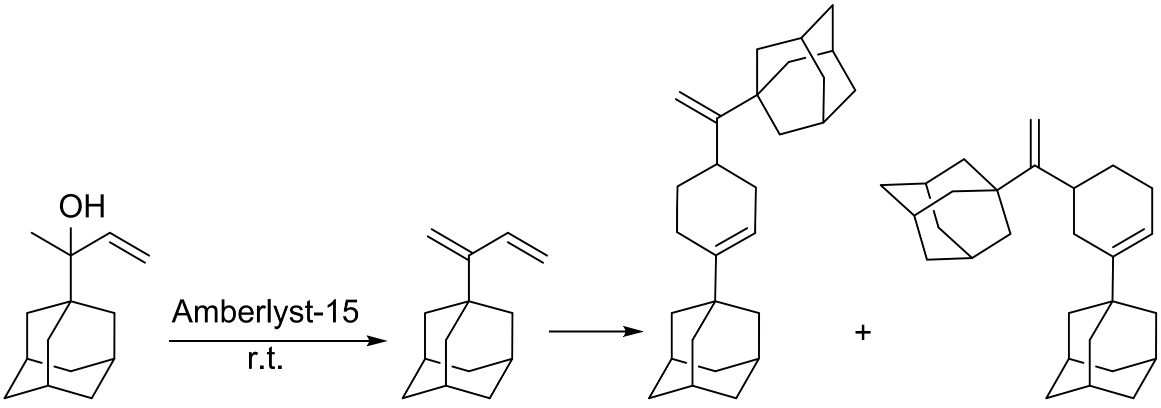

2 **1** **3a** **3b**

Scheme 2.3: Dehydration of 2-(1-adamantyl)-3-buten-2-ol and formation of terpenes

Mitigation of side products in diethyl ether prompted an investigation into the compatibility of other ethereal solvents. Tetrahydrofuran (THF), a cyclic ether, is significantly less hazardous to handle compared to diethyl ether and would be a more optimal solvent for dehydration of tertiary allylic alcohols. Acid-catalyzed ring-opening polymerization of THF has been reported with tungstophosphoric acid,[110] however its stability in the presence of Amberlyst®-15 is unknown. A 2% w/v solution of Amberlyst®-15 in THF was stirred for 24 hours at room temperature. No visible precipitate was observed nor was any residue detected upon removal of solvent. No reaction products were detected in solution with ^{1}H NMR.

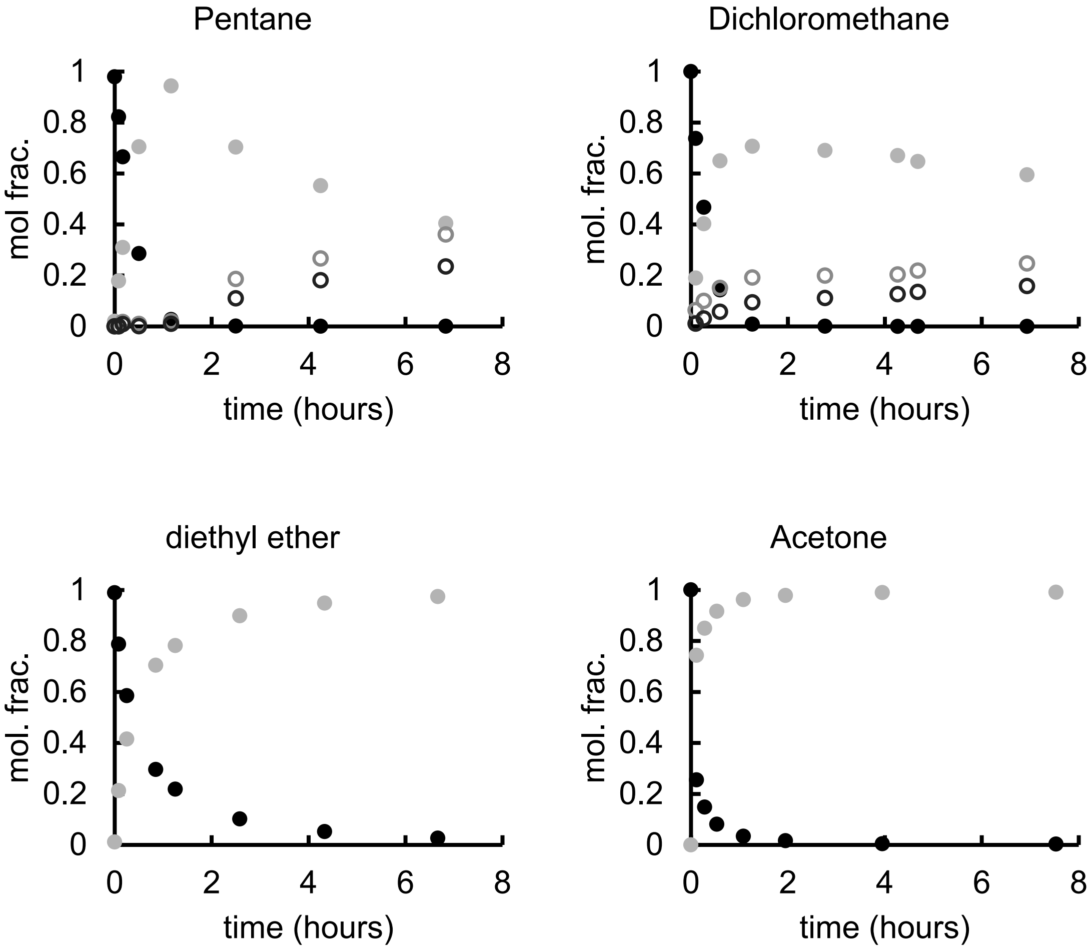

Figure 2.3: Composition of dehydrations in various solvents. **2**: ●, **1**: ●, **3a**: ○, **3**b: ○

Table 2.1: Monoterpene concentration at endpoint

Solvent	time (hr)	3a	3b
pentane	2.5	0.36	0.23
dichloromethane	2.5	0.25	0.16
diethyl ether	8.0	0	0
acetone	6.0	0	0

Mechanistic considerations elucidate the effect of solvent on monoterpene formation. The E1 reaction mechanism, through which sulfonic acids dehydrate tertiary alcohols,[111] consists of three steps (Scheme 2.4). First, hydroxyl oxygen lone pairs, which act as a Lewis base, are protonated. Then, the cleavage of the C-O bond allows loss of the of H_2O, a good leaving group, forming a tertiary carbocation intermediate. This is often the rate limiting step.[112] Last, the deprotonation of a β-carbon by a base (the H_2O leaving group) forms the alkene.

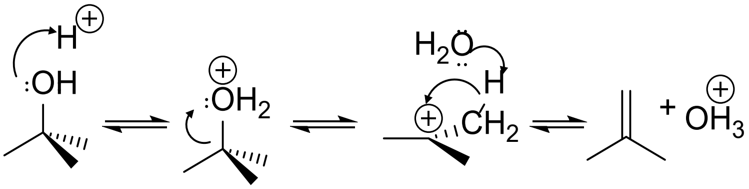

Scheme 2.4: E1 mechanism of tertiary alcohol dehydration

Honkela and Krause[99] concluded that compounds will adsorb to the sulfonic acid sites forming a more stable acidic species. They correlated the strength of adsorption to dielectric constant (ε), where compounds with higher ε like methanol (ε = 32.6) adsorb more readily than those with lower ε like methyl *tert*-butyl ether (ε = 2.6). Karinen et al.[95] confirmed that rates of isobutene etherification with various alcohols increased with decreasing polarity of alcohol, indicating that increasingly polar compounds adsorb preferentially to the active sites and inhibit proton donating ability. Adsorption of polar compounds also results in the formation of a protonated polar species. Di Giorlamo et al.[93,94] studied the effect of methanol on the dimerization and etherification of isobutene over sulfonic acid resins and, like Thornton and Gates,[113] concluded that adsorption of methanol onto the sulfonic acid site results in formation of $MeOH_2^+$, which is less acidic than the original sulfonic acid.

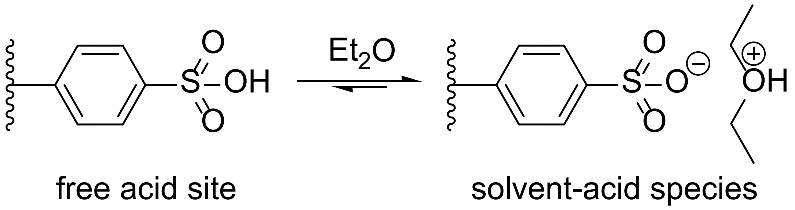

Scheme 2.5: Formation of protonated solvent species

The experimental results from dehydration of 2-(1-adamantyl)-3-buten-2-ol support the hypothesis that polar solvents capable of accepting protons lower the proton donating strength of Amberlyst®-15 by adsorbing to sulfonic acid sites and forming a less acidic species. Diethyl ether and acetone are hydrogen bond acceptors with lone pair electrons capable of accepting a proton. Once protonated, Et_2OH^+ and $(CH_3)_2OH^+$ are strong enough to initiate dehydration by protonating the allylic alcohol, but do not promote Diels-Alder cyclization of the diene product. The observed rates of dehydration of 2-adamantyl-3-buten-2-ol in diethyl ether and acetone also supports this conclusion. The relative acidity of protonated functional groups is shown in Figure 2.4. Increased reaction rate in acetone compared to diethyl ether can be attributed to increased acidity of protonated carbonyls. Stronger acids, in turn, increase the rate of alcohol protonation. Pentane and dichloromethane lack the ability to solvate a proton, so the strength of the original sulfonic acid sites is maintained, which both initiates dehydration and Diels-Alder cyclization of diene products. Additionally, rate of dehydration using pentane and DCM was identical implying that no protonated solvent species is participating in dehydration.

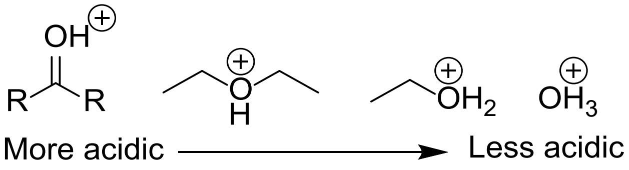

Figure 2.4: Relative acidity of protonated functional groups

Desiccant Addition

Though some polar compounds effectively modulate the strength of sulfonic acid sites,[99,113] water has been shown to deactivate Amberlyst®-15 when used in dehydrations. Dehydration of 2-(1-adamantyl)-3-buten-2-ol was conducted in diethyl ether at a constant concentration (0.1M) while $[S_0]/[H^+]$ was set to 0.5, 1.0, and 10. As $[S_0]/[H^+]$ was increased from 0.5 to 1.0, a decrease in reaction rate was observed, while at $[S_0]/[H^+] = 10$, catalyst deactivation was observed at 55% substrate conversion. These results strongly suggest that water produced during dehydration is deactivating sulfonic acid sites of Amberlyst®-15.

Heterogenous catalysis allows the unique opportunity for inclusion of a heterogenous desiccant which might otherwise react. The hypothesis that *in-situ* removal of water during dehydration by inclusion of a desiccant would allow for the use of higher $[S]_0/[H^+]$ was tested. Two identical dehydrations of a 0.1 M solution of 2-(1-adamantyl)-3-buten-2-ol in diethyl ether were conducted at $[S]_0/[H^+] = 10$: one in the presence of 4Å molecular sieve powder (10% w/v) and the other with no desiccant. Reactions were monitored by GC-MS. Complete conversion of alcohol was observed after 22 hours in the presence of 4 Å molecular sieve powder, while complete deactivation of catalyst was observed at 55% conversion in the control. Successful removal of water *in-situ* using 4 Å molecular sieve powder prompted an investigation into the efficacy of several other inexpensive heterogenous desiccants.

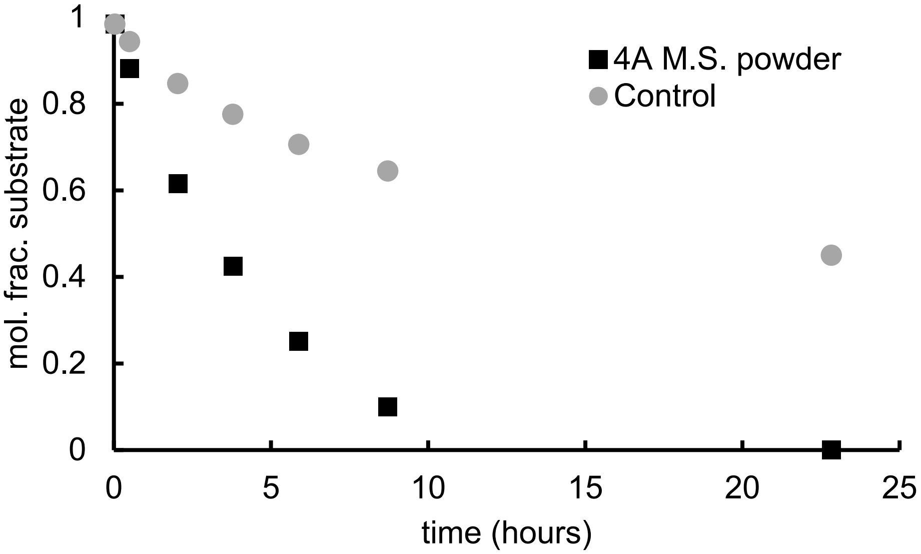

Figure 2.5: Dehydration of 2-adamantyl-3-buten-2-ol with and without desiccant

Overall, the heterogenous desiccants tested removed water from the reaction mixture and allowed for a tenfold excess of substrate to be used. $MgSO_4$ had no effect on dehydration, and catalyst deactivation was observed. After complete conversion of alcohol, determined by thin-layer chromatography, the concentrated reaction product was passed through a 1” silica plug (eluent: hexanes) yielding pure **1**. Inclusion of anhydrous $CaCl_2$ resulted fastest reaction time and was determined to be the optimal desiccant for removing water generated during dehydration.

Table 2.2: Dehydration of 2-(1-adamantyl)-1,3-butadiene in the presence of various desiccants

Desiccant	**w/v(%)**	**$[S]_0/[H^+]$**	**time (hr)**
None	0	0.5	3.5
None	0	1.0	8
None	0	10	-[a]
4A molecular sieves (powder)	10	10	22
4A molecular sieves (powder)	1	10	31
3A molecular sieves (beads)	1	10	44
$CaCl_2$ anhydrous	1	10	25
$MgSO_4$ anhydrous	1	10	-[a]

[a]Deactivation of catalyst determined after 48 hours by TLC

Broader application of Method

Dehydrations of 2-*tert*-butyl-3-buten-2-ol, 2-cyclohexyl-3-buten-2-ol, and 2-phenyl-3-buten-2-ol were conducted to understand the broader applicability Amberlyst®-15 in the synthesis 2-

substituted 1,3-butadienes. As a starting point, the optimal reaction parameters identified in the dehydration of 2-adamantyl-3-buten-2-ol were used, and results are presented in Table 2.3.

Table 2.3: Dehydration of alkyl and phenyl 2-substituted tertiary alcohols with Amberlyst®-15

Run	R=	Solvent	$[S]_0/[H^+]^a$	Time (h)	yield (%)
1	t-butyl	diethyl ether	10[c]	18	80[b]
2	cyclohexyl	diethyl ether	1	18	55[b]
3	cyclohexyl	diethyl ether	10[c]	18	37[b]
4	phenyl	diethyl ether	1	1.5	30
5[c]	phenyl	diethyl ether	10[c]	72	18
6[d]	phenyl	diethyl ether	10[c]	72	13
7	phenyl	diethyl ether	1	3	5
8	phenyl	THF	1	2.5	33
9	phenyl	DMSO	1	48	n.r.[e]
10	phenyl	pyridine	1	24	n.r.[e]
11[f]	napthyl	cyclopentyl methyl ether	10[c]	23	4[g]
12[f]	napthyl	cyclopentyl methyl ether	1	4	5[g]
13[f]	2,3,4,5,6-pentafluorophenyl	cyclopentyl methyl ether	10[c]	26	n.r.[g]
14[f]	2,3,4,5,6-pentafluorophenyl	cyclopentyl methyl ether	1	26	n.r.[g]
15[f]	4-OTBDMS-phenyl	cyclopentyl methyl ether	10[c]	24	4[g]
16[f]	4-OTBDMS-phenyl	cyclopentyl methyl ether	1	18	10[g]
17[f]	3-indole-NBoc	cyclopentyl methyl ether	10[c]	24	9[g]
18[f]	3-indole-NBoc	cyclopentyl methyl ether	1	22	5[g]
19	4-diamantyl	diethyl ether	1	24	33

[a] All reactions were conducted at $[S]_0 = 0.1M$. Molar concentration Amberlyst®-15 calculated from reported 4.7 meq./g

[b] contained a mixture of configurational isomers

[c] Reaction run in 1% w/v anhydrous $CaCl_2$

[d] Run at 0 °C

[e] No reaction observed

[f] Reaction run at 50 °C

[g] Yield estimated from GC-MS analysis of isolated material

Although yields of 2-alkyl 1,3-butadienes (figure Run 1-3) were moderate to good, products contained a mixture of configurational isomers indicating that cationic rearrangements were occurring, however no Diels-Alder addition products were detected. Isomerization was also observed by Frija et al. in dehydrations of tertiary alcohols in refluxing dichloromethane, though no solvent dependency was explored.[91] Though a rigorous identification of isomers was not performed, GC-MS analysis of Runs 2 and 3 confirmed that $[S]_0]/[H^+]$ did not have any effect on isomer composition. Dehydrations of 2-phenyl-3-buten-2-ol resulted in low yields and the formation of a hexane insoluble product, likely cationic polymerization products. Efforts to mitigate side products and increase yields were unsuccessful and included reducing temperature (Run 6) and the use of proton-accepting solvents (Runs 8 – 10). The yields of 2-phenyl-1,3-butadiene obtained with Amberlyst®-15 are comparable to those from reported reactive distillations[104] and thus do not offer any advantage except perhaps simplicity of reaction setup.

Several other aromatic and heteroaromatic substrates were synthesized from their respective methyl ketones and the unisolated mixtures were dehydrated directly with Amberlyst®-15 (Runs 11-18). Cyclopentyl methyl ether was used as solvent to allow for heating to 50 °C as initial screening in room temperature diethyl ether indicated low conversion. After dehydration, these reactions were passed through a 1" plug of silica (eluent: hexanes) and yield was estimated by GC-MS analysis of this filtered product.

Dehydration of 2-(4-diamantyl)-3-buten-2-ol first required the synthesis of 4-acetyldiamantane. This required the optimization of a UV photoacetylation of diamantane, which is covered in detail in Appendix A. Although yield of dehydration under normal conditions was low compared to the adamantyl equivalent, it was noteworthy that no rearrangement products were observed in NMR spectra. Reduced yield may also be attributed to the solid precipitate that was observed after catalyst was filtered from the reaction. Currently no characterization of this material has been performed due to its insolubility, and further optimization of dehydration parameters may successfully reduce or eliminate its formation.

Conclusions

A synthetic route for 2-substituted 1,3-dienes via the heterogeneous acid-catalyzed dehydration of allylic tertiary alcohols with Amberlyst®-15 at room temperature was identified. This method is well suited for gram-scale synthesis of **1** for use in polymerization studies. Diels-Alder cyclization of **1** was highly influenced by solvent selection and was suppressed entirely when diethyl ether was used. Catalytic amounts of Amberlyst®-15 can be utilized with the inclusion of an additional desiccant to remove water generated during dehydration.

The broader applicability of this method as a general synthesis of 2-substituted 1,3-butadienes was explored. Isomerization in dehydrations of 2-alykl-3-buten-2-ols and apparent polymerization of 2-phenyl-1,3-butadiene was observed. A series of aromatic and heteroaromatic substrates were also screened. The limited data that was obtained does not support the general utility of Amberlyst®-15 dehydration as a synthesis of 2-substituted 1,3-dienes. Further investigations into these substrates should address the following experimental flaws. Purified tertiary allylic alcohol substrates should be used to eliminate any potential side reactions between components. Additionally, solvent systems should be optimized for column chromatography of dehydrated products with TLC prior to separation. All separations in Runs 11 -18 used hexanes as the eluent. Despite hexanes being the optimal eluent for isolation of **1**, it should not have been assumed to be for the dienes products of Runs 11 – 18, which have varying degrees of polarity. Dehydration with Amberlyst®-15 was applicable to diamantyl substituted substrate and further optimization may lead to increased yield.

Overall, these results support the conclusion that heterogeneous dehydration with Amberlyst®-15 is not useful for many tertiary allylic alcohol substrates. However, it is does offer a very attractive synthesis of diamondoid 2-substituted 1,3-diene monomers. Mild conditions, simple work-up, and tenfold excess of substrate to catalyst allowed for an efficient synthesis of **1** in 100 g batches, which was required for further polymerizations studies.

Chapter 3: Poly(2-(1-adamantyl)-1,3-butadiene and Random Copolymers with Isoprene via Redox-emulsion Polymerization and their Hydrogenation

Abstract

A novel route to adamantyl substituted diene copolymers is demonstrated using emulsion polymerization, with an improved monomer synthesis. Heterogenous dehydration of 2-(1-adamantyl)-3-buten-2-ol using Amberlyst®-15 cationic exchange resin at ambient temperature gave 2-(1-adamantyl)-1,3-butadiene (**1**) in excellent yield and presents an attractive alternative monomer synthesis route. Emulsion polymerizations of **1** and mixtures of **1** and isoprene were carried out at room temperature using redox pair-type hydroperoxide initiator. All poly(**1**) and poly(**1**-*ran*-isoprene) samples were soluble in common organic solvents and exhibited high 1,4-microstructure. A continuous increase in glass transition temperature from -63 to 172 °C was observed by increasing the ratio of **1** in the comonomer feed of poly(**1**-*ran*-isoprene), and T_g values were in good agreement with the Fox equation. After complete hydrogenation to poly(1-vinyladamantane-*alt*-ethylene-*ran*-propylene-*alt*-ethylene), a continuous increase in T_g was observed from -55 to 152 °C. The high solubility and improved access to **1** opens the door to exploration of diene polymers with enhanced high temperature properties.

Introduction

For nearly a century, synthetic rubbers from dienes, particularly 1,3-butadiene and its 2-substituted variations, have been extensively used in applications including tires, adhesives and toughened plastics.[41] The need for rubbers and high performance elastomers has certainly not slowed since the World War II driven Government Rubber-Styrene (GR-S) program,[16] and as new rubber materials are developed to meet demanding modern applications, the ability to design polymer properties becomes an increasingly valuable tool. Although the targeted introduction of 2-subsitutents to 1,3-butadiene monomers presents unique challenges, it remains a promising strategy for attaining new materials with tunable glass transition temperature (T_g) and thermomechanical properties.

Marvel et al. explored the effect of bulky 2-substituents in polybutadienes shortly after the end of World War II.[114,115] Using the well-established GR-S emulsion polymerization system, homopolymers of ethyl, *n*-propyl, and *n*-amyl 2-substituted 1,3-butadienes were synthesized as well as their copolymers with butadiene and styrene. Though the alkyl side chains clearly influenced the thermal and mechanical properties of the compounded rubbers, the results were not a dramatic improvement over existing GR-S rubber. Overberger et al. followed up this work with an examination of the thermal properties of 1,3-butadienes with *tert*-butyl, *n*-heptyl, and *n*-decyl substituents at the 2-

position.[116,117] In particular, the addition of a 2-*tert*-butyl group increased T_g by ca. 80 °C, while the 2-*n*-decyl-1,3-butadiene exhibited a T_g increase of only ca. 10 °C, indicating that the addition of sterically bulky, branched chains at the 2-position of butadiene is fundamentally different to purely linear chains.

Of the branched alkanes, diamondoids are highly symmetric and polycyclic, with a molecular geometry superimposable on the diamond lattice, and the smallest diamondoid, adamantane (tricyclo[3.3.1.13,7]decane), exhibits a remarkably high melting point above 220 °C.[44] When incorporated as a pendant group in a range of olefins,[17,52,54–59,118,119] adamantane has imparted unique thermal and oxidative stability, low surface energy, high density and hydrophobicity, high-refractive index and UV-transparency to polymers.[17,52,55] Tunable T_gs have been observed by statistical copolymerizations varying the proportions of adamantyl-modified monomers with their parent monomers.[54,55,60,118] Intriguingly, poly(1-vinyladamantane) oligomers have recently been utilized as a template for nanodiamond synthesis,[120] even though the polymerization of 1-vinyladamantane is notoriously challenging.[52,121]

Relatively recently, living anionic polymerization (LAP) of 2-(1-adamantyl)-1,3-butadiene (**1**) was conducted by Kobayashi et al., and poly(**1**) exhibited a T_g of 100 °C, a remarkable 170 °C increase over the T_g of polyisoprene.[17] Increasing the fraction of **1** in poly(**1**-*ran*-isoprene) raised T_g from -70 to 100 °C with a discontinuity above 80 wt% **1**. When fully hydrogenated a continuous increase in T_g with increasing composition of **1** was observed, although T_g values deviated from those predicted by the Fox equation.[122] Despite its potential, no instances of poly(**1**) or poly(**1**-*ran*-isoprene) have been reported following the initial work of Kobayashi et al., perhaps due to perceived difficulties with the monomer synthesis and the sensitive anionic polymerization technique.

As noted earlier, the observed T_g range of poly(**1**-*ran*-isoprene) is significantly higher than any other reported 2-alkylbutadiene and highlights the effect of side chain geometry on thermal properties and motivates this study. For comparison, poly(*n*-decyl-1,3-butadiene), with a linear C_{10} 2-substituent, exhibited a T_g at -53 °C. Thus, the poly(**1**-*ran*-isoprene) system presents itself to entirely new applications. Unsaturation in the poly(1,3)-diene backbone also allows for chemical, enzymatic, and bacterial degradation[72] and presents opportunities for additional modifications including grafting,[80] crosslinking, addition of solubility modifiers,[123] and blending or covulcanization with other butadiene rubbers.[40] With these possibilities at hand, this report documents a new exploration of poly(**1**-*ran*-isoprene).

Revisiting the earlier GR-S approach, emulsion polymerization has been employed for the synthesis of 2-alkylbutadienes and offers distinct advantages for the synthesis of poly(**1**) and poly(**1**-

ran-isoprene). In particular, redox pair type initiators[124,125] consisting of hydroperoxides have allowed for room temperature emulsion polymerization. This is significant because although controlled radical polymerization techniques such as RAFT[18,75–79] and NMP[20,80–83] have been successfully applied to conjugated diene systems, Diels-Alder cyclization of the diene monomer into terpenes competes with polymerization at the necessary temperatures.[76]

Room temperature emulsion polymerization was employed for the synthesis of poly(**1**) and poly(**1**-*ran*-isoprene). Mild-conditions provided straightforward access to a more comprehensive dataset of copolymers which allowed for an in-depth study of the thermal properties of the poly(**1**-*ran*-isoprene) system. The relationship between adamantyl composition and T_g for both poly(**1**-*ran*-isoprene) and its fully hydrogenated derivative poly(1-vinyladamantane-*alt*-ethylene-*ran*-propylene-*alt*-ethylene) was determined using differential scanning calorimetry (DSC) analysis.

Methods and Materials

Materials

All glassware was oven dried. Tetrahydrofuran (HPLC grade, Fisher), diethyl ether (Reagent grade, Fisher), dichloromethane (HPLC grade, Fisher) were dried for a minimum 48 h using 3 Å molecular sieves (activated overnight at 300 °C, 30 mbar) and distilled immediately before use. Pentane (HPLC grade, Fisher) and toluene (HPLC grade, Macron Fine Chemicals) were used as received. Adamantyl methyl ketone (97%, AstraTech), vinylmagnesium bromide solution (0.7M in THF, Acros Organics) and Amberlyst®-15(H), ion exchange resin (1.6% moisture, Alfa Aesar) was used as received. Isoprene (98%, Alfa Aesar) was distilled from CaH_2 immediately before use. *Tert*-dodecylmercaptan (>98%, TCI), sodium dodecyl sulfate (98%, Aldrich), *tert*-butyl hydroperoxide (70% in water, TCI), tetraethylene pentamine (TCI) and p-toluenesulfonyl hydrazide (97%, Acros Organics) were used as received. Emulsion polymerizations were performed in 18 mΩ deionized water. Merck HPTLC 60 F245 aluminum backed silica gel plates were used for analytical thin layer chromatography (TLC).

Characterization

FTIR spectra were obtained on a ThermoScientific iS-10 FTIR spectrometer fitted with a Smart Orbit diamond ATR cell. NMR spectra were recorded on a Bruker AVANCE III HD 500 MHz spectrometer with Protégé cold probe. GC-MS was conducted on a ThermoScientific Trace 1300 Gas Chromatograph with an ISQ 7000 Single Quadrupole Mass Spectrometer (ZB1 30 m x 0.25 mm ID column, Phenomenex; 40 °C to 250 °C (10 min) at 5 °C/min). Number and weight averaged molecular weights (M_n and M_w) of polymers were determined by right angle/low angle laser light scattering size exclusion chromatography (RALLS/LALLS-SEC) in conjunction with differential viscometry using a Viscotek (Houston, TX) 270 Dual Detector equipped with a Waters Chromatography (Milford, MA) Model 510 HPLC pump, Waters Chromatography (Milford, MA) 410 Differential Refractometer, and a Jordi-Gel DVB Mixed Bed column (250 mm x 10 mm ID) THF (HPLC grade, Fisher). A triple detection method was used (RI, LS and viscosity) was used and calibrated to a narrow polystyrene standard (M_w = 98,938 g/mol, Viscotek) in THF at a flow of 0.5 mL/min. Certain low molecular weight samples were analyzed with a universal polystyrene calibration curve (M_w = 953, 1300, 2200 and 13,780 g/mol) using the RI detector. Differential scanning calorimetry was performed on a TA Instruments (New Castle, DE) Q200 equipped with refrigerated cooling. A heat-cool-heat cycle was performed from -80 to 200 °C at a rate of 10 °C/min. T_g is reported as midpoint temperature of the transition.

*2-(1-adamantyl)-3-buten-2-ol (**2**)*

Vinylmagnesium bromide solution 0.7M in THF (100 mL, 70.0 mmol, 1.2 eq.) was added via cannula to a 250 mL Schlenk flask cooled to 0 °C with an ice bath. Adamantyl methyl ketone (10.40 g, 58.3 mmol, 1.0eq.) was dissolved in 35 mL of THF and the solution was added dropwise to the vinylmagnesium bromide. After addition, the reaction was slowly warmed to room temperature and stirred overnight. The reaction was then cooled to 0 °C, and 10 mL of saturated NH_4Cl was added dropwise. Reaction mixture was extracted with diethyl ether three times. Combined organic layers were dried over anhydrous $MgSO_4$, filtered, and concentrated under reduced pressure giving a pale-yellow oil (10.45 g). Pure **2** was isolated by fractional distillation of this oil in a Kugelrohr oven (75-125 °C, 1E-3 mbar) giving a white crystalline solid (6.57 g, 31.8 mmol, 55%). NMR spectra were consistent with literature values.[10]

*2-(1-adamantyl)-1,3-butadiene (**1**)*

2 (6.57 g, 31.8 mmol), diethyl ether (300 mL), and Amberlyst®-15 (6.78 g, 31.8 mmol) were added to a 500 mL three-neck flask fitted with a thermometer and magnetic stir bar. Reaction was monitored by TLC (eluent: hexanes) until the disappearance of **2** was observed. Amberlyst®-15 was filtered and then washed three times with 50 mL of diethyl ether. Solvent was removed under reduced pressure at room temperature giving **1** as clear oil (5.83 g, 30.9 mmol) in 97% yield. This oil was stored at -8 °C and distilled (50 °C, 1E-3 mbar) immediately before use in polymerization. NMR spectra were consistent with literature values.[10]

Emulsion Polymerization

The following is representative a typical emulsion copolymerization. Sodium dodecyl sulfate (SDS) (0.120 g, 0.4 mmol) was added to a 20 mL scintillation vial fitted with a PTFE-lined screw-cap septa and a magnetic stir bar. Deionized water was degassed by sparging with argon for 1 h, added to the vial (70 mM solution), and SDS was dissolved by gentle heating. **1** (0.443 g, 2.3 mmol) was added via syringe under flowing argon followed by isoprene (0.295 g, 4.3 mmol). The comonomer solution stirred for 30 min resulting a milky white emulsion. TDM (2.3 mg, 0.01 mmol) and t-BHP (3.0 mg, 0.02 mmol) were added to the emulsion and stirred for 30 min. A 0.1 M solution of TEPA in degassed DI water (0.221 mL) was added to initiate polymerization. After 48 h the reaction was quenched by addition of a 1 mg/mL solution of hydroquinone in methanol in 0.04:1 ratio to the reaction emulsion. The polymer was coagulated by addition of threefold excess acetone. The acetone was decanted, and the polymer was washed several times with acetone. The coagulated material was then dissolved in THF and precipitated into cold pentane. Polymer was filtered, dissolved in THF and concentrated under reduced pressure (0.530 g, 73%). Polymers were characterized by ^{1}H and ^{13}C NMR and all peaks were consistent with reported assignments.[17,53] ^{1}H and ^{13}C NMR spectra and assignments are included in Appendix B.

Hydrogenation

Polymer (0.10 g), butylated hydroxytoluene (ca. 5 mg, 0.02 mmol), p-toluenesulfonyl hydrazide (1.0 g, 5.4 mmol), and toluene (5 mL) were added to a 15 mL heavy wall glass pressure vessel and sealed. The reaction vessel was then placed in a 135 °C oil bath for 12 h resulting in a yellowish solution. Reactions were filtered, toluene was removed under vacuum (25 mbar, 50 °C), and the remaining solid material was washed several times with 70:30 methanol:water followed by several washes of methanol. The washed polymer was dried, dissolved in $CHCl_3$ (1 mL) and precipitated into cold methanol (100 mL). Filtered polymer was dried to constant weight under vacuum (0.08 g, 80%).

Results and Discussion

Monomer Synthesis

The investigation into poly(**1**-*ran*-isoprene) began by revisiting the monomer synthesis route used by Kobayashi et al., specifically the dehydration portion. (While not considered here, promising syntheses of **1** from methyl ketone have been reported via acid-catalyzed oxetane ring opening,[87] as well as an improved Nickel-catalyzed Kumada vinylation.[71]) Examples of dehydration of 2-(1-adamantyl)-3-buten-2-ol (**2**) with p-toluenesulfonic acid (TsOH) in refluxing benzene[17] and ether[89] and at room temperature with a combination of TsOH and tetrabutylammonium perrhenate[90] have also been reported. Amberlyst®-15 is a strong cationic exchange resin utilizing sulfonic acid sites that has been applied to heterogeneous acid catalysis including alkene oligomerizations, dehydrations and esterifications.[126] Frija and Afonso demonstrated the dehydration of a range of tertiary alcohols with Amberlyst®-15 at room temperature with excellent yields,[91] however no instances of tertiary allylic alcohol dehydration with Amberlyst®-15 have been reported to our knowledge. As shown in Scheme 3.1, Amberlyst®-15 was employed for the dehydration of **2**, as heterogeneous catalysis is advantageous for its simplified setup, workup, and mild reaction conditions,[45] all which facilitate synthesis of **1** at gram-scale.

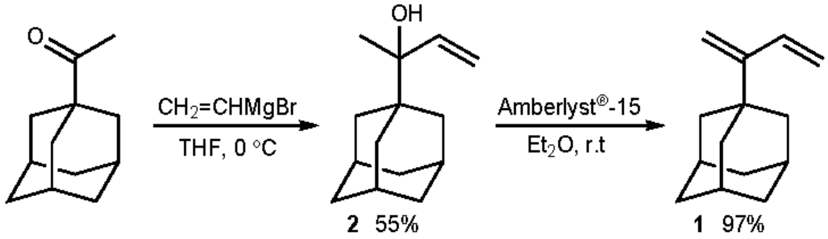

Scheme 3.1: Synthesis of **1**

Selection of solvent had a marked effect on the rate of dehydration of **2,** as well as the solution stability of **1** once formed. Diels-Alder cyclization of **1** was observed in dehydrations conducted in dichloromethane and pentane. No monoterpene products were observed in dehydrations carried out in diethyl ether or acetone. However, acid-catalyzed condensation of acetone to mesityl oxide was observed, consistent with literature.[108,109] Thus, diethyl ether was used in subsequent dehydrations.

The role of solvent on the formation of cyclization products can be explained by the effect of polar compounds on the catalytic activity of cationic exchange resins. Polar compounds exhibit stronger adsorption to sulfonic acid active sites.[95,99] Di Girolamo et al.[93,94] studied the effect of methanol on the dimerization and etherification of isobutene over sulfonic acid resins and, like Thornton and Gates,[113] concluded that adsorption of methanol onto the sulfonic acid sites results in the formation of $MeOH_2^+$, which is considerably less acidic that the original sulfonic acid site. Polar solvents like diethyl ether and acetone can solvate a proton, lowering the effective proton donating strength of the catalyst. The resulting acidic species (e.g. Et_2OH^+) initiates dehydration but does not promote Diels-Alder cyclization of the resulting diene. Our results support the hypothesis that pentane and dichloromethane poorly solvate protons, so the acidity of the active sites is strong enough to promote cyclization.

Gram-scale dehydration of **2** using Amberlyst®-15 in ambient conditions gave **1** in nearly quantitative yields. These results confirmed that dehydration of **2** with Amberlyst®-15 presents an attractive, straightforward, and scalable alternative synthesis route for **1**.

Nitroxide Mediated Polymerization

Controlled radical polymerization (CRP) techniques such as reversible addition-fragmentation chain-transfer (RAFT)[18,75–79] and nitroxide mediated polymerization (NMP)[20,80–83] have been successfully applied to conjugated diene systems and rely on establishing a dynamic equilibrium between a low concentration of active propagating chains and a predominant number of dormant chains that are unable to propagate or terminate.

In NMP, propagating radical chains are reversibly terminated by nitroxide radicals forming thermally labile alkoxyamines. Polymerization is stopped when the reaction is brought to a low enough temperature. However, because termination by the nitroxide radical is thermally reversible, polymers synthesized using NMP can be reinitiated after isolation and characterization. Polymers synthesized by NMP are essentially macroinitiators, which can be reinitiated by returning to a sufficiently high temperature (approx. 120 °C). Not only does NMP allow for the synthesis of statistical copolymers, but heating of NMP macroinitiators in the presence of a different monomer allows for the formation of well-defined block copolymers.[20]

NMP Initiation can be classified as either unimolecular or bimolecular. Unimolecular initiators contain both the radical initiating species and nitroxide mediator in one molecule. Hawker et al. developed a unimolecular NMP initiator also known as the "Universal Alkoxyamine" or TIPAL.[127] Mechanistically, bimolecular initiation is identical to unimolecular; the only difference is that a separate radical initiator and nitroxide mediator are used. Contreras-Lopez et al. investigated the use of several bimolecular initiating systems for the polymerization of isoprene in an effort to decrease costs and increase overall scalabity.[80] Until then, all reported polymerizations of diene monomers using NMP used a unimolecular initiator.[20,80,82,83] They found the bimolecular process to be poorly suited for polyisoprene polymerization, even with the inclusion of known rate accelerating additives.[80]

Though NMP with unimolecular TIPAL initiator presents a straightforward polymerization of **1**, CRP of dienes has presented several unique challenges. Low reactivity of propagating diene radicals[78] results in a low rate of polymerization leading to long reaction times (>24h) and low conversions.[20,80] At temperatures required for typical RAFT and NMP techniques (100 – 120 °C) propagation competes with autoinitiation and Diels-Alder cyclization of diene monomers and decreases yields.[76,79,80,84] Despite these obstacles, the potential of NMP with TIPAL initiator to provide a singular synthesis route for poly(**1**), poly(**1**-*ran*-isoprene), and block copolymers merited a preliminary investigation.

Table 3.1: NMP copolymerization with TIPAL[a]

	Content (wt%) of **1**					
Run	Target	Obsd.[b]	Yield (%)	M_n (kg/mol)[c]	PDI[e]	T_g
NMP_0	0	0	23	24	<1.1	-57
NMP_1	38	31	17	22	<1.1	-31
NMP_2	50	51	16	15[d]	<1.1	-11
NMP_3	70	77	13	11[d]	<1.1	50
NMP_4	100	100	7	7.5[d]	<1.1	107

[a] All reactions were conducted at 130 °C, 30 wt% monomer in toluene, [M]:[I] = 1000

[b] Determined by ^{1}H NMR

[c] Molecular weight obtained by SEC triple-detection method

[d] Number average molecular weight (M_n) obtained by SEC using a standard calibration using polystyrene standards in THF

[e] Polydispersity index

Results from copolymerization of **1** with isoprene are presented in Table 3.1. Observed **1** content in Runs NMP_1 – NMP_4 agreed well with targeted values. Yields of all poly(**1**) and poly(**1**-*ran*-isoprene) runs were lower than the polyisoprene control experiment (Run NMP_0) and decreased with increased amount of **1** (Runs NMP_1 – NMP_4). Analysis of polymerization product with ^{1}H NMR indicated that the majority of **1** was being converted to monoterpene products. M_n values for Runs NMP_1 – NMP_4 are considerably lower that would be expected at [M]:[I] = 1000, which can be explained by the reaction of monomers to monoterpenes during polymerization. Though poor control of M_n was observed, all polymers that were isolated exhibited very low PDI (<1.1).

Overall, NMP of **1** with TIPAL does not present a practical synthetic route for poly(**1**) and poly(**1**-*ran*-isoprene). Diels-Alder cyclization of **1** at temperatures necessary for polymerization wastes an excessive amount of monomer and greatly limits the ability to obtain polymers in quantities necessary for comprehensive thermal and mechanical characterization. Moving forward, it was concluded that low or ambient temperature polymerization would be crucial.

Emulsion Polymerization and Hydrogenation

Emulsion polymerization, as seen in Scheme 3.2, describes a heterogeneous process employed for radical chain polymerizations that relies on the formation of surfactant stabilized monomer-rich micelles in water.[21] Polymerization occurs within these micelles, which due to their small size, typically 2-10 nm, only permit a single active radical species to exist.[21] This compartmentalization, or segregation of propagating radicals, reduces the rate of termination reactions and allows for higher conversions and increased molecular weights compared to homogenous polymerization systems.[21]

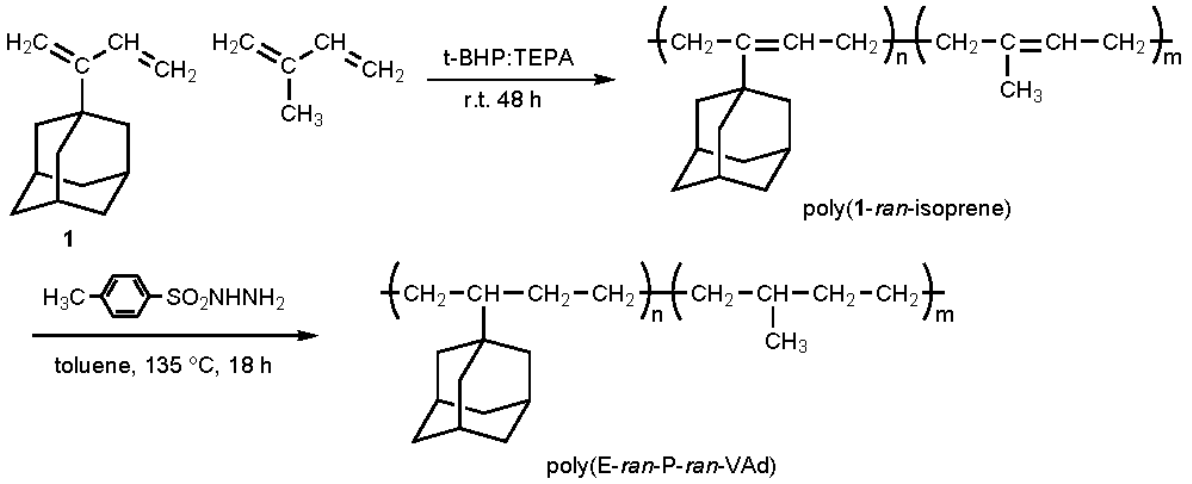

Scheme 3.2: Copolymerization of **1** and isoprene and subsequent dehydration

Following the procedure of Gramlich et al.,[76] emulsion polymerization of **1** was conducted at 25 °C using *tert*-butyl hydroperoxide/tetraethylene pentamine (t-BHP/TEPA) as the redox pair initiator (I) in a 1:1 ratio. Sodium dodecyl sulfate (SDS) was used as the surfactant. A chain transfer agent (CTA), *tert*-dodecyl mercaptan was also included at [CTA]:[I] = 0.5 to influence molecular weight of formed polymers. After 48 h, polymerizations were quenched by adding a 1 mg/mL hydroquinone solution in methanol at a 0.04:1 ratio to the reaction emulsion.

Table 3.2: Emulsion polymerization of **1**^{a}

Run	[M]	[M]:[I]^b	x_1^{c}	Yield (%)	M_n (kg/mol)	PDI
1	1.35	50	0.41	31	5.8^d	1.39
2	0.75	20	0.52	28	8.8^d	1.50
3	0.75	240	0.35	28	35	1.24
4^e	0.75	310	0.12	8	14	1.77

^{a}[SDS] = 70 mM unless otherwise stated. [CTA]:[I] = 0.5.
^{b}Monomer to initiator ratio.
^{c}Conversion of **1** determined gravimetrically
^{d}Number average molecular weight (M_n) obtained by SEC using a standard calibration using polystyrene standards in THF.
^{e}[SDS] = 140 mM

Increasing [M]:[I] (Run 2 and 3) resulted in lower monomer conversion but higher M_n values. A decrease in the average number of radicals per micelle is expected with an increase in [M]:[I] leading to a slower polymerization rate and lower monomer conversion. Furthermore, as [M]:[CTA] decreases at higher [M]:[I], polymer chains are able to propagate longer before undergoing chain transfer resulting in the observed increase in M_n. No polymerization was observed in emulsions that excluded CTA. The rate and degree of polymerization is primarily influenced by the number of active polymer micelles, which is dependent on surfactant concentration.[1,21] Surfactant concentration was increased in Run 4 as an attempt to increase conversion, however the result was a decrease in both conversion and M_n. Though overall monomer conversions were relatively low for all homopolymerizations after 48 h, quantitative recovery of unreacted monomer was possible by extraction of the concentrated coagulant with hexanes. No Diels-Alder cyclization products were detected in recovered monomer.

Emulsion polymerization was then applied to the synthesis of poly(**1**-*ran*-isoprene). Comonomer mixtures with predetermined content of **1** were polymerized at room temperature using the t-BHP/TEPA initiator system. To account for the density disparity of comonomers ($\rho_{isoprene} = 0.681$, $\rho_1 \sim 1$), [M] was adjusted so that the total volume of monomer was 15 vol% for all polymerizations. Poly(**1**-*ran*-isoprene) was obtained in good yields, and reported values represent isolated polymer following precipitation in cold pentane, which was necessary to remove residual **1** present in the copolymers. While the runs here are unoptimized, higher molecular weights were successfully targeted by increasing [M]:[I], as evident in Runs 6 - 8 and 12 - 14. Conversion of monomer was not determined for copolymerizations.

Table 3.3: Random copolymerization of 1 with isoprene[a]

	Content (wt%) of **1**						
Run	Target	Obsd.[b]	[M]:[I][c]	[CTA]:[I][d]	Yield (%)	M_n (kg/mol)	PDI
5	0	0	60	0.7	81	25	2.81
6	20	13	70	0.6	58	20	2.33
7	20	15	220	0.5	75	43	4.26
8	20	10	450	0.7	33	52	2.30
9	30	37	390	0.7	27	140	1.35
10	40	49	60	0.7	39	37	1.09
11	40	33	490	0.8	29	120	1.23
12	60	68	60	0.6	56	53	1.43
13	60	63	240	0.8	64	71	1.76
14	60	62	330	0.7	73	120	1.54
15	80	68	460	0.9	17	42	1.81
16	85	87	170	1.7	62	24	1.63
17	90	86	460	1.1	35	67	1.35

[a] [SDS] = 70 mM.
[b] Determined by ^{1}H NMR.
[c] Monomer to initiator ratio
[d] Chain transfer agent to initiator ratio

Composition of **1** in copolymer samples was determined by comparison of olefinic proton signals in ^{1}H NMR to those in the alkyl range (1.5 - 2.5 ppm). A derivation of this method can be found in Appendix B. The conditions of these polymerizations preclude a meaningful determination of reactivity ratio, although overall the fraction of **1** in copolymers agreed well with the targeted content. All copolymers exhibited a single T_g indicating that they are neither blocky nor contain long homo sequences of comonomer, and additional DSC analysis of physical mixtures presented in Appendix B confirms the immiscibility of the monomers.

Table 3.4: Polymer microstructure and thermal properties

					Microstructure[a] (%)					
	Content (wt%) of **1**				1,4-				T_g/°C	
Run	Target	Obsd.[a]	M_n[b] (kg/mol)	PDI	cis-	trans-	3,4-	1,2-	Before[c]	After[d]
5	0	0	25	2.81	89		6	5	-63	-55
6	20	13	20	2.33	90		6	4	-47	-31
7	20	15	43	4.26	90		6	4	-48	-41
8	20	10	52	2.30	90		6	4	-56	-24
9	30	37	140	1.35	90		5	4	-22	-26
10	40	49	37	1.09	91		6	3	-4	-1
11	40	33	120	1.23	90		6	4	-33	-16
12	60	68	53	1.43	91		7	2	34	29
13	60	63	71	1.76	91		7	2	22	27
14	60	62	120	1.54	92		6	2	26	27
15	80	68	42	1.81	92		6	2	39	30
16	85	87	24	1.63	92		7	1	95	72
17	90	86	67	1.35	92		7	1	91	74
1	100	100	5.8[e]	1.39	88	5	7	0	139	125
2	100	100	8.8[e]	1.50	88	5	7	0	115	109
3	100	100	35	1.24	88	5	7	0	172	152
4	100	100	14	1.77	83	6	6	5	111	95

[a] Determined by ^1H NMR.
[b] Molecular weight obtained by SEC-triple detection in THF.
[c] Before hydrogenation.
[d] After hydrogenation.
[e] Molecular weight obtained by SEC using a standard calibration using polystyrene standards in THF.

Microstructure of poly(**1**) and poly(**1**-*ran*-isoprene) was also determined by ^1H NMR analysis of olefinic protons (see Appendix B). Assignments determined by HSQC-NMR are in agreement with those reported by Kobayashi et al.[17] and are as follows: *cis*-1,4- (5.13 ppm), *trans*-1,4- (5.05 ppm), 3,4- (4.82 and 4.77 ppm). Samples of poly(**1**) synthesized at an [SDS] of 70 mM possessed an identical microstructure consisting of high *cis*-1,4 content and complete absence of 1,2-addition product. An increase in [SDS] in Run 4 to 140 mM resulted in an increase in both 3,4- and 1,2-content.

Copolymerization with isoprene did not have a marked effect on the microstructure with all poly(**1**-*ran*-isoprene) samples exhibiting high overall 1,4- content, though a determination of *cis*- and *trans*-conformation was not made.

Notably, Kobayashi et al. reported poly(**1**) synthesized via living anionic polymerization was insoluble in organic solvents after precipitation in methanol.[17] They attributed increased solubility of poly(**1**) with a decrease in 1,4-microstructure and hypothesized that the stiff and planar C=C-Ad units in the backbone might interfere with polymer chain movement and lower solubility. The products isolated here, however, generally show very good solubility, e.g. solubility of poly(**1**) with M_n = 35 kg/mol and 93% overall 1,4-microstructure was completely soluble in THF, $CHCl_3$ and toluene. Though an explanation for this solubility in emulsion polymerized poly(**1**) is beyond the scope of this work, the solubility of poly(**1**) of moderate molecular weight in organic solvents is significant as it expands the potential applications for this novel polymer system.

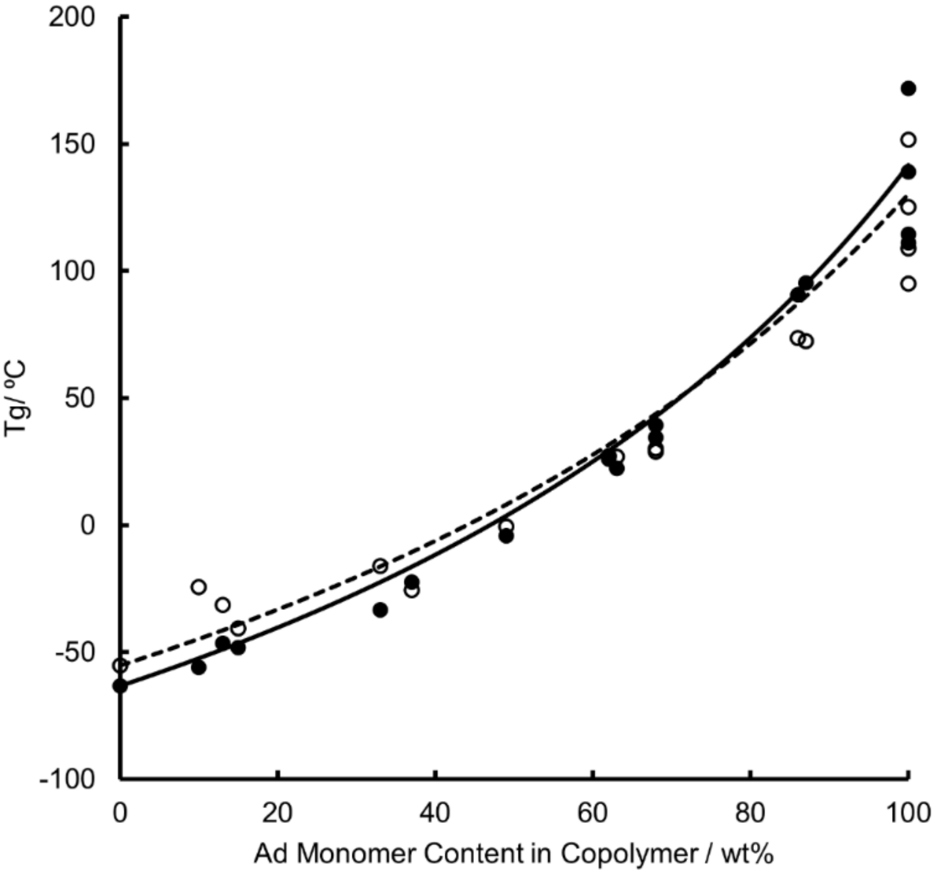

Figure 3.1: Relationship between T_g and the weight composition of adamantyl containing monomer with Fox prediction lines. ● and solid line: poly(**1**-*ran*-isoprene). ○ and dashed line: poly(1-vinyladamantane-*alt*-ethylene-*ran*-propylene-*alt*-ethylene)

The T_gs of all samples were determined by DSC. A single thermal transition was observed, indicating that copolymers did not contain blocky segments of either monomer. Figure 3.1 shows the relationship between T_g and the wt% **1** for poly(**1**-*ran*-isoprene) as well as the corresponding hydrogenated polymers poly(1-vinyladamantane-*alt*-ethylene-*ran*-propylene-*alt*-ethylene). A continuous increase in T_g was observed as wt% **1** increased in good agreement with predicted values derived from the Fox equation.[122]

In contrast, Kobayashi et al.[53] reported a significant deviation in T_g from the Fox equation for poly(**1**-*ran*-isoprene) samples with high 1,4-content obtained via LAP. With M_n varying from 6.0 to 21 kg/mol, a steep, discontinuous increase in T_g around 80 wt% **1** was observed and attributed to a reduction in chain mobility due to the prevalence of short segments poly(**1**). This explanation is not consistent with the data presented here where a continuous increase in T_g with composition is observed for both predominantly 1,4-poly(**1**-*ran*-isoprene) and poly(1-vinyladamantane-*alt*-ethylene-*ran*-propylene-*alt*-ethylene). It should be noted that better agreement to the Fox equation could also be due to a larger dataset compared to that presented by Kobayashi et al.[17] whose analysis was based upon 3 copolymer samples.

Though no obvious dependence of T_g on M_n was observed for this set of copolymers, the T_gs of poly(**1**) varied significantly from 111 to 172 °C. The glass transition temperature is largely influenced by overall chain stiffness, which for polydienes is a function of both molecular weight and microstructure. Of the homopolymers presented, Run 4 shows an increase in 1,2- and 3,4-microstructure, resulting in fewer C=C units in the backbone and presumably increased flexibility.[128] This explains the observed T_g reduction in Run 4. Microstructure is identical, however, in Runs 1–3 and cannot explain T_g variation.

As a definitive correlation between M_n and T_g for poly(**1**) was not observed in Runs 1–4, nor was one reported by Kobayashi, et al.,[17] the available published and unpublished results are presented in Appendix B. The polydispersity index (M_w/M_n, PDI) has been shown to have a dramatic influence many features of polymers including phase behavior,[129,130] rheology[131] and processing instabilities.[132] Though recent simulation studies[133] do not support a strong dependence of T_g on PDI, a linear relationship between PDI and T_g is observed in Runs 1–4. Persistence of the trend after the samples were fully saturated suggest that it cannot be attributed solely to increased backbone rigidity.

Conclusions

Copolymers incorporating the adamantane substituted diene (**1**) are readily synthesized through emulsion techniques, exhibiting a dramatic range of glass transition temperatures. Heterogeneous dehydration of **2** with Amberlyst®-15 in diethyl ether provides an attractive and straightforward synthetic route for **1**. Nitroxide mediated polymerization resulted primarily in the formation of monoterpene products and was deemed unsuitable for synthesis of poly(**1**). Emulsion polymerization using a room temperature redox pair initiator was demonstrated as a viable technique for the polymerization of **1**. Inclusion of a chain transfer agent was necessary for polymerization and higher molecular weight polymers could be targeted by increasing [M]:[I]. Microstructure of both poly(**1**) and poly(**1**-*ran*-isoprene) consisted of high 1,4-content. An increase in 3,4- and 1,2-addition was observed with an increase in surfactant concentration. T_gs of poly(**1**-*ran*-isoprene) and poly(1-vinyladamantane-*alt*-ethylene-*ran*-propylene-*alt*-ethylene) increased continuously with wt% **1** and were in good agreement with predicted values from the Fox equation. Overall, the T_g of poly(**1**-*ran*-isoprene) could be controlled by varying the wt% of **1** from -63 to 172 °C, a remarkable 235 °C range, while poly(1-vinyladamantane-*alt*-ethylene-*ran*-propylene-*alt*-ethylene) exhibited T_gs from -53 to 152 °C. The identification of a straightforward monomer synthesis and room temperature emulsion polymerization conditions for poly(**1**) and poly(**1**-*ran*-isoprene) will allow for a more comprehensive characterization of mechanical properties in the near future.

Chapter 4: Mechanical Characterization of poly(1) and poly(1-*ran*-isoprene)

Abstract

The first mechanical characterization of poly(**1**) and poly(**1**-*ran*-isoprene) is reported. Dynamic mechanical analysis using a 3-point bend geometry and rheology provided a complete characterization of the viscoelastic behavior with respect to temperature. Poly(**1**) exhibited a rubbery plateau between 170 – 180 °C, while poly(**1**-*ran*-isoprene) with 88 wt% **1** extended this plateau from 120 – 180 °C. Shear-thinning behavior was observed in all samples. Decreasing **1** content from 100 to 88 wt% decreased viscous modulus (G") while having no effect on storage modulus (G'). Rheology of poly(**1**), before and after saturation, and poly(**1**-*ran*-isoprene) was used to elucidate the independent contributions of backbone saturation and adamantyl pendants to the overall chain mobility. Determination of dynamic viscosity with rheology led to the conclusion that chain mobility is more sensitive to the amount of adamantyl pendant than to backbone saturation.

Introduction

Due to their desirable elastomeric properties, synthetic rubbers have been extensively used in tires, adhesives, and toughened plastics for over a century.[41] As rubber materials are developed to meet demanding modern applications, the ability to design polymer properties becomes increasingly valuable tool. Along with microstructure, the addition of pendant 2-subsitutents has a considerable effect on the elastomeric properties of synthetic polydienes; this is especially evident when comparing *cis*-1,4-polybutadiene with a to *cis*-1,4-polyisoprene.[41] The low T_g of *cis*-1,4-polybutadiene (-94 °C) provides exceptional flexibility and excellent strong deformation tolerance.[41] In fact, polybutadiene is perhaps the most flexible synthetic rubber. Inclusion of methyl 2-subsitutents in *cis*-1,4-polyisoprene results in an increase in T_g (-64 to -70 °C) and reduced elasticity but enhanced strength.[41,115] Marvel et al. demonstrated[115] that increasing the length of linear 2-substituents from ethyl to pentyl in compounded rubbers reduced the 300% modulus from $5.8E^6$ to $2.9E^6$ Pa, while increasing the elongation at break from 400% to 740%. Poly(2-isopropyl-1,3-butadiene), a lightly branched substituent, further reduced the 300% modulus to $2.3E^6$ Pa and increased elongation at break to 850%. Though the inclusion of larger targeted 2-subsituents presents unique synthetic challenges it remains a promising strategy for producing new elastomeric materials.

Using the well-established GR-S emulsion polymerization system Marvel et al. explored the effect of bulky alkyl 2-substituents in polybutadienes shortly after the end of World War II.[3,4] Though several copolymers of 2-alkyl-1,3-butadienes (5 wt%) with butadiene exhibited desirable low temperature mechanical properties compared to conventional GR-S, the results were not a deemed significant for further study. Overberger et al. followed up this work with an examination of the effect on T_g of several linear and branched alkyl 2-substituents.[5,6] In particular, the addition of a 2-*tert*-butyl group increased T_g by ca. 80 °C, while the 2-*n*-decyl-1,3-butadiene exhibited a T_g increase of only ca. 10 °C, indicating that the addition of a sterically bulky, branched species at the 2- position of butadiene is fundamentally different to purely linear chains. In fact, Marconi et al. noted that poly(2-*tert*-butyl-1,3-butadiene) with high *cis*-1,4- content was semicrystalline with a T_m = 106 °C. Unfortunately, no mechanical properties were reported.

Of the branched alkanes, diamondoids are highly symmetric and polycyclic, with a molecular geometry superimposable on the diamond lattice, and the smallest diamondoid, adamantane (tricyclo[3.3.1.13,7]decane), exhibits a remarkably high melting point above 270 °C.[44] When incorporated as a pendant group in a range of olefins, adamantane has imparted unique thermal and oxidative stability, low surface energy, high density and hydrophobicity, high refractive index and UV-transparency to polymers.[17,52,54–59,118,119,134] Tunable T_gs have been observed by statistical copolymerizations varying the proportions of adamantyl-modified monomers with their parent monomers.[54,55,118,119] Beyond these considerations, poly(1-vinyladamantane) oligomers have recently been utilized as a template for nanodiamond synthesis,[120] even though the polymerization of 1-vinyladamantane is notoriously challenging.[52,120] For example, poly(1-vinyladamantane) with M_n = 2400 g/mol (N = 15) was obtained only with extremely reactive cationic initiators.[120]

Recently, we reported a straightforward synthesis route for poly(2-(1-adamantyl)-1,3-butadiene) as well as a room-temperature redox-pair initiated emulsion polymerization. Random copolymers of **1** and isoprene exhibited a continuous increase in T_g from -63 to 172 °C as the wt% of **1** was increased. Contrary to reports of poly(**1**) synthesized via anionic polymerization, all emulsion-polymerized poly(**1**) homopolymers were quite soluble in organic solvents (toluene, $CHCl_3$, and THF).

Encouraged by the overall processability of the emulsion-polymerized poly(**1**) system, we report here the first mechanical characterization of poly(**1**) and poly(**1**-*ran*-isoprene). Previously reported room-temperature emulsion polymerization of poly(**1**-*ran*-isoprene) was used to produce polymer at multi-gram scale necessary for mechanical testing. Particularly, the storage and loss moduli with respect to temperature were determined by dynamic mechanical analysis (DMA) to assess the operating range for these thermoplastic elastomers and confirm the T_gs determined from DSC. Rheology was used to characterize both the rubbery plateau and rubbery flow regions at varying wt%

of **1** in poly(**1**) and several poly(**1**-*ran*-isoprene) samples. The independent contributions of backbone saturation and adamantyl pendant groups to polymer chain mobility were elucidated by rheological characterization of dynamic viscosity (η*) of poly(**1**), before and after hydrogenation, and poly(**1**-*ran*-isoprene).

Methods and Materials

Materials

All glassware was oven dried. Isoprene (98%, Alfa Aesar) was distilled from CaH_2 immediately before use. *Tert*-dodecylmercaptan (>98%, TCI), sodium dodecyl sulfate (98%, Aldrich), *tert*-butyl hydroperoxide (70% in water, TCI), tetraethylene pentamine (TCI) and p-toluenesulfonyl hydrazide (97%, Acros Organics) were used as received. Emulsion polymerizations were performed in 18 mΩ deionized water.

Emulsion Polymerization

Water (150 mL), sodium dodecyl sulfate (SDS) (3.54 g, 12.3 mmol), **1** (6.95 g, 36.9 mmol), isoprene (12.9 g, 7.03 mL, 0.10 mol), tDM (68.0 mg, 0.3 mmol), and t-BHP (58.9 mg, 0.5 mmol) were added to a Schleck flask with a magnetic stir bar and capped with a rubber septum. The contents of the flask were then degassed with three freeze-pump-thaw cycles, brought to room temperature, and stirred until dissolution of SDS was observed. A 0.1 M solution of TEPA in degassed DI water (6.54 mL) was added to initiate polymerization. After 96 h the reaction was quenched by addition of a 1 mg/mL solution of hydroquinone in methanol in a 0.04:1 ratio to the reaction emulsion. The polymer was coagulated by addition of threefold excess acetone. The acetone was decanted, and the polymer was washed several times with acetone. The coagulated material was then dissolved in THF and precipitated into cold pentane. Polymer was filtered, dissolved in THF and concentrated under reduced pressure (18.9 g, 95%). Polymers were characterized by ^1H and ^{13}C NMR and all peaks were consistent with reported assignments.[17,53]

Hydrogenation

Polymer (0.10 g), butylated hydroxytoluene (ca. 5 mg, 0.02 mmol), p-toluenesulfonyl hydrazide (1.0 g, 5.4 mmol) and toluene (5 mL) were added to a 15 mL heavy wall glass pressure vessel and sealed. The reaction vessel was then placed in a 135 °C oil bath for 12 h resulting in a yellowish solution. Reactions were diltered, toluene was removed under vacuum (25 mbar, 50 °C), and the remaining solid material was washed several times with 70:30 methanol:water followed by several washes of methanol. The washed polymer was dried, dissolved in $CHCl_3$ (1 mL) and precipitated into cold methanol (100 mL). Filtered polymer was dried to constant weight under vacuum (0.08 g, 80%).

Characterization

FTIR spectra were obtained on a ThermoScientific iS-10 FTIR spectrometer fitted with a Smart Orbit diamond ATR cell. NMR spectra were recorded on a Bruker AVANCE III HD 500 MHz spectrometer with Protégé cold probe. Number and weight averaged molecular weights (M_n and M_w) of polymers were determined by right angle/low angle laser light scattering size exclusion chromatography (RALLS/LALLS-SEC) in conjunction with differential viscometry using a Viscotek (Houston, TX) 270 Dual Detector equipped with a Waters Chromatography (Milford, MA) Model 510 HPLC pump, Waters Chromatography (Milford, MA) 410 Differential Refractometer, and a Jordi-Gel DVB Mixed Bed column (250 mm x 10 mm ID) in THF (HPLC grade, Fisher). A triple detection method was used (RI, LS and viscosity) and calibrated to a narrow polystyrene standard (M_w = 98,938 g/mol, Viscotek) in THF at a flow of 0.5 mL/min. Certain low molecular weight samples were analyzed with a linear regression polystyrene calibration curve (M_w = 953, 1300, 2200 and 13,780 g/mol) using the RI detector. Differential scanning calorimetry was performed on a TA Instruments (New Castle, DE) Q200 equipped with refrigerated cooling. A heat-cool-heat cycle was performed from -80 to 200 °C at a rate of 10 °C/min. T_g is reported as midpoint temperature of the transition. DMA was performed on a Perkin Elmer (Waltham, MA) DMA 7 instrument in a 3-point bend geometry from −40 °C to 200 °C at a heating rate of 3 °C/min using a static force of 150 mN and a dynamic force of 100 mN at 1 Hz. Dynamic rheological measurements (viscous modulus (G”), elastic modulus (G’) and complex viscosity (η*))) were acquired on a Bohlin CVO 100 N rheometer (East Brunswick, NJ) with smooth parallel plates (D = 25 mm). Rheological measurements were determined with a plate gap of between 800 and 1000 μm, 0.5% strain, and a frequency range of 0.01 Hz to 100 Hz at 220 °C.

Results and Discussion

Emulsion polymerization

The sensitivity of emulsion polymerizations to termination by oxygen is well known.[21] In the previous report, all reaction components (i.e. surfactant, chain transfer agent, and initiator) were added sequentially via syringe to degassed water. Repeated transfers increase the possibility of introducing even small amounts of oxygen to the reaction. To minimize the potential for introduction of oxygen, all components, except tetraethylene pentamine, were combined prior to degassing with at least 3 freeze-pump-thaw cycles, and reaction times were extended to 96 hours.

Results from emulsion polymerization are presented in Table 4.1. Overall, all polymerizations that utilized the modified procedure (Runs 1, 5 and 8) gave polymer in high yields. Yield of poly(**1**) was increased to 70% (Run 8) from 25% and 42% using the modified method of addition, and yield in Run 1 was nearly quantitative. Higher M_n values were obtained by increasing [M]:[I]. All polymers exhibited high *cis*-1,4- content. T_g of poly(**1**-*ran*-isoprene) samples from DSC agreed well with predicted values derived from the Fox equation. Variability in T_g in poly(**1**) was observed, though no correlation with M_n was apparent.

Table 4.1: Emulsion polymerized poly(**1**) and poly(**1**-*ran*-isoprene)[a]

							Microstructure[b] (%)					
	Content (wt%) of **1**						1,4-				T_g/°C	
Run	Target	Obsd.[b]	[M]:[I][d]	Yield (%)	M_n[e] (kg/mol)	PDI	cis-	trans-	3,4-	1,2-	DSC	DMA
1	35	41	350	95	157	3.21	90		6	4	-17	-20
2[c]	60	68	60	56	53	1.43	91		7	2	34	18
3[c]	60	63	240	64	71	1.76	91		7	2	22	12
4[c]	60	62	330	73	120	1.54	92		6	2	26	13
5	85	88	250	66	33	1.81	92		7	1	104	91
6[a]	100	100	125	25	22	1.42	90	2	8	0	164	-[f]
7[a]	100	100	250	42	18	2.71	90	2	8	0	158	162
8	100	100	210	70	47	1.47	90	2	8	0	170	149

[a] [SDS] = 70 mM unless, [CTA]:[I] = 0.5.
[b] Determined by ^{1}H NMR
[c] Polymerized by emulsion procedure presented in Chapter 3
[d] Monomer to initiator ratio.
[e] Molecular weight obtained by SEC-triple detection in THF
[f] DMA not performed

*Mechanical characterization of poly(**1**) and poly(**1**-ran-isoprene)*

Dynamic mechanical analysis using a 3-point bend geometry was performed to determine the elastic modulus (E') in the glassy state and verify the T_gs as determined by DSC. The T_gs determined by the onset of E' (Figure 4.1) were consistently lower than when determined by DSC. This may be attributed to the thermal history of the DMA samples, which were hot pressed prior to sampling. The elastic modulus was only slightly affected by the wt% of **1** in the copolymer and varied from $2.2E^9$ to $3.0E^9$ Pa. M_n had no effect on the E' over a range of 71 to 120 kg/mol as evident from Runs 3 and 4.

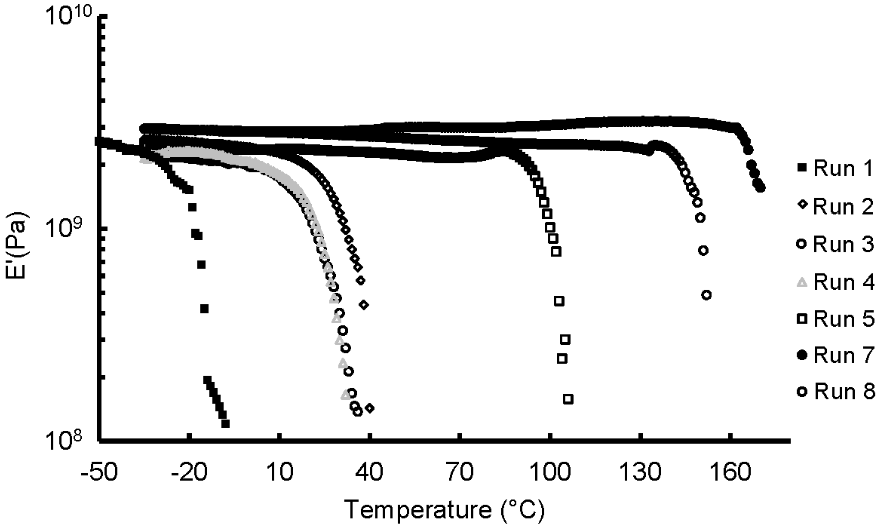

Figure 4.1: Storage modulus (E') of poly(**1**) and poly(**1**-*ran*-isprene) at varying wt% **1**

Rheology was conducted on two poly(**1**-*ran*-isoprene) samples (Runs 1 and 5) and poly(**1**) (Run 8). Figure 4.2 presents storage and loss modulus with respect to temperature at various wt% of **1**. Because temperature was lowered below the T_gs observed in DSC and DMA, rheology provided a complete picture of the viscoelastic behavior.

The temperature at which G' and G" are equal is termed the crossover temperature (T_C), and above this temperature the polymer exists in the rubbery flow region. Poly(**1**) (Figure 4.2) exhibits a T_g of 170 °C and T_C at 180 °C indicating a very small rubbery plateau. Decreasing the wt% of **1** to 88% (Run 5) resulted in a rubbery plateau region that spanned around 60 °C from 120 – 180 °C (Figure 4.2). Comparison of Runs 5 and 8 also reveals that although lowering content of **1** in poly(**1**-*ran*-isoprene) decreases T_g, T_C for both samples is 180 °C.

Run 1 exhibited a rubbery plateau that extended at least until 220 °C (Figure 4.2). This may be due to the presence of chain entanglements, inadvertent crosslinking, or long-chain branching. Long-chain branching is prevalent in emulsion polymerizations, especially at high conversions,[135] and would also explain the increase in PDI.[136] To ensure that no crosslinking was present, the polymer was stirred for one month in a 10% w/v solution of THF and was filtered to remove any insoluble material, which is referred to as gel. At least 60% of the total mass of Run 1 was found to be soluble by this method. Rheology was then conducted on the soluble Run 1 material. Interestingly, G' and G" of the soluble sample of Run 1 were essentially identical to the original unflitered sample. Furthermore, no transition to the rubbery flow was observed up to 220 °C.

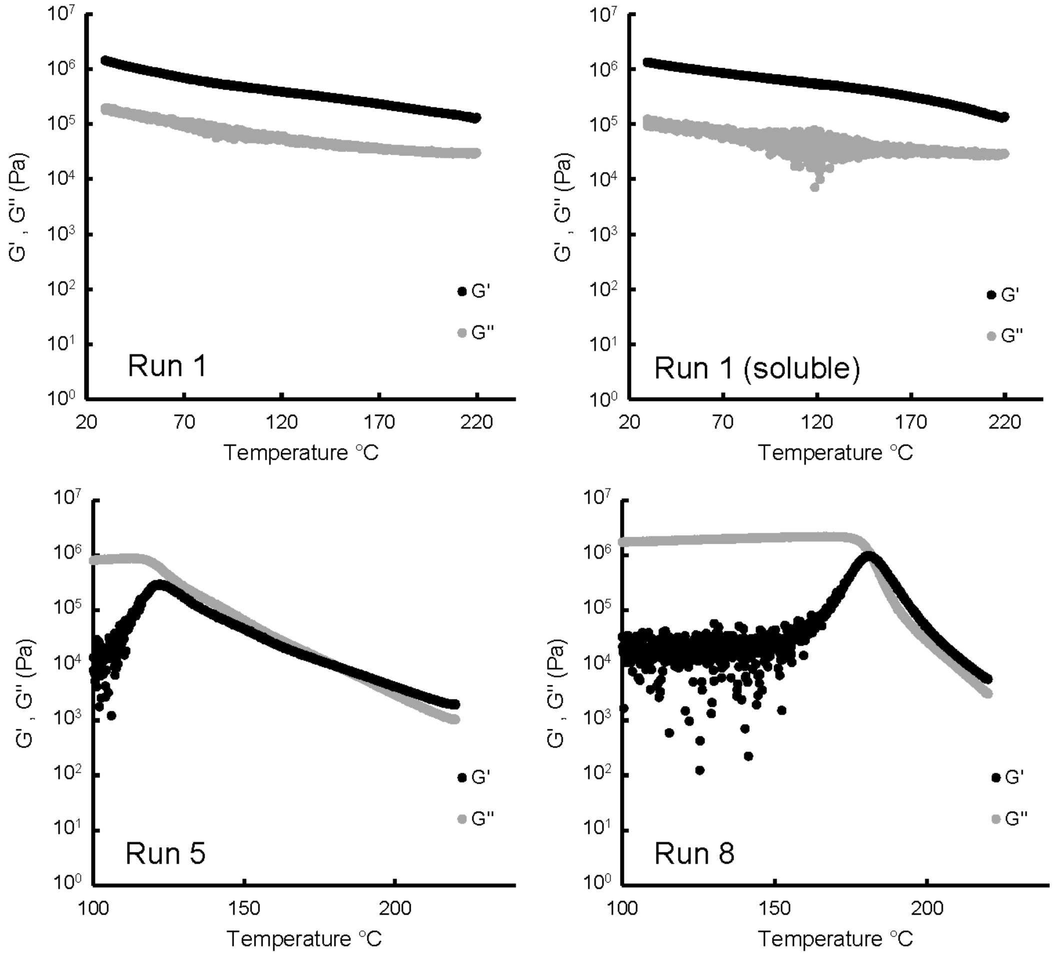

Figure 4.2: Storage (G’) and loss (G”) modulus versus temperature

Figure 4.3 (top, middle) presents G’ and G” of Runs 1, 5 and 8 with respect to angular frequency (ω). G’ and G” both increased with increased frequency, however, Runs 5 and 8 suggest that G” is more dependent on the wt% of **1** than G’. Both moduli for Run 1 are higher than Runs 5 and 8 despite the decreased wt% of **1**. This is attributed to the sample not exhibiting rubbery flow at the sampling temperature (220 °C). Consequently, a direct comparison of Run 1 to Runs 5 and 8 does not offer insight into the flow properties of poly(**1**-*ran*-isoprene) with respect to content of **1**. Complete dissolution of Run 1 increased the G’ with respect to angular frequency (ω), while G” was mostly unchanged. It is possible that complete dissolution of the polymer chains allows for the formation of more chain entanglements compared to the coagulation from emulsion.

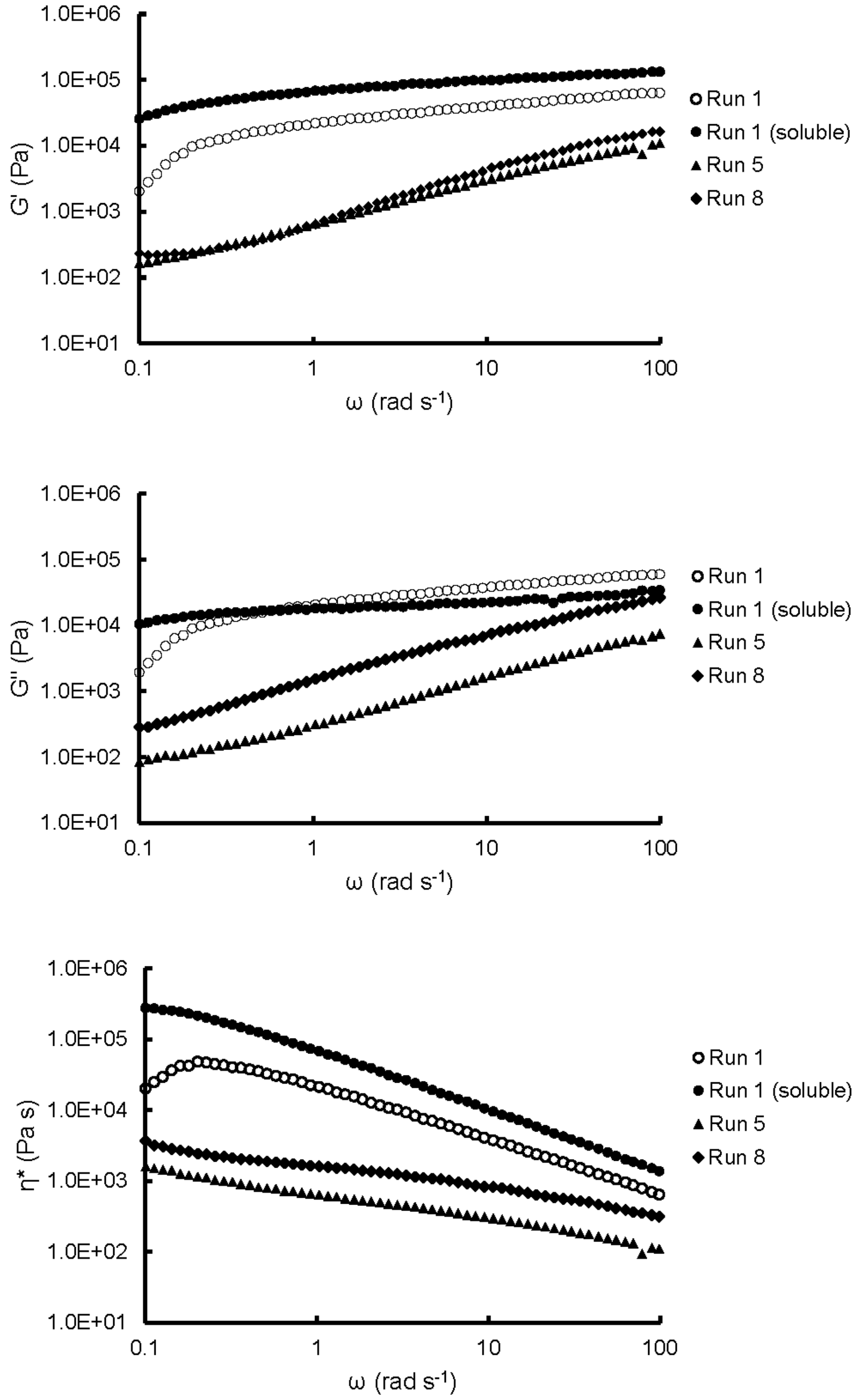

Figure 4.3: Top: angular frequency (ω) versus storage modulus (G’) at 220 °C. Middle: angular frequency (ω) versus loss modulus (G”) at 220 °C**.** Bottom: angular frequency (ω) versus dynamic viscosity (η*) at 220 °C

Figure 4.3 (bottom) presents dynamic viscosity (η*) with respect to angular frequency for Runs 1, 5, and 8. η* decreases at higher angular frequencies for all samples indicating shear thinning behavior. Shear thinning is the most common type of non-Newtonian flow behavior and is the result of micro-structural rearrangements occurring in the plane of the applied shear.[25] In polymer melts, this is attributed to the disentangling of polymer chains and the alignment with the flow, which results in decreased molecular interactions and a decrease in η*. The increase in η* with increasing wt% of **1** (Runs 5 and 8) confirms that the adamantyl pendant reduces the ability of the polymer chains to flow.

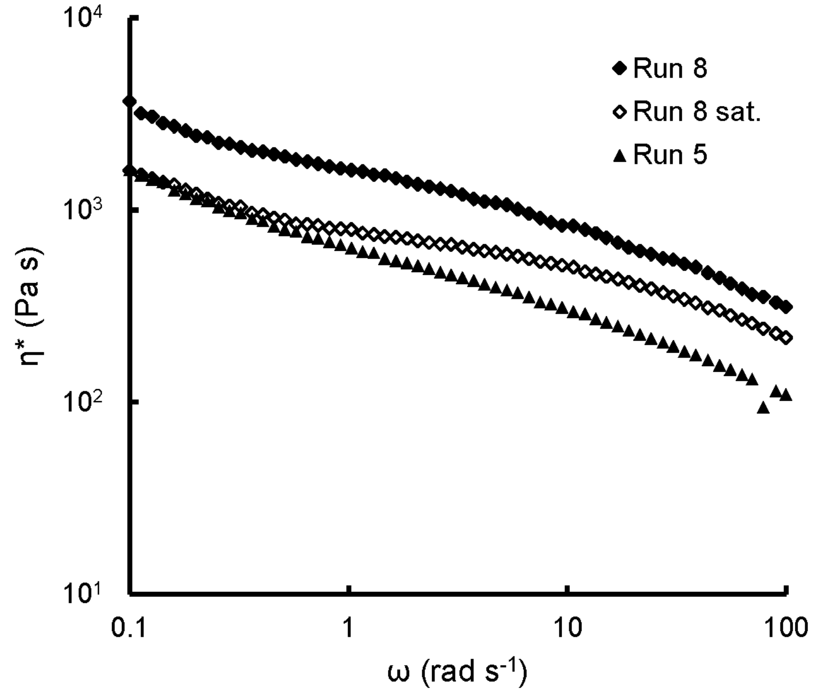

Figure 4.4: Dynamic viscosity (η*) versus angular velocity (ω) of poly(**1**) (Run 8) before and after hydrogenation as well as poly(**1**-*ran*-isoprene) (Run 5) at 220 °C

A portion of Run 8 was fully saturated, and rheology was performed to elucidate the effect of backbone saturation on overall chain mobility of poly(**1**). Figure 4.4 presents the dependence of dynamic viscosity (η*) on the angular frequency (ω) of poly(**1**), before and after hydrogenation, and Run 5 at 220 °C. As expected, poly(**1**) exhibited the highest dynamic viscosity. This can be attributed the presence of a rigid unsaturation in the backbone as well as the bulky adamantyl pendants which inhibit polymer mobility. Accordingly, saturation of the backbone increases polymer chain mobility decreasing the overall dynamic viscosity.

Kobayashi et al. reported a discontinuity in the relationship between the wt% **1** and the T_gs of poly(**1**-*ran*-isoprene) synthesized via LAP.[118] They attributed this to the prevalence of short sequences of poly(**1**) within the copolymer when the content of **1** exceed 80 wt%. Likewise, the continuous relationship between content of **1** and T_g after full saturation of the backbone was reasoned to be a result of increased chain mobility. Though a direct comparison is not made here between emulsion and anionic poly(**1**) and poly(**1**-*ran*-isoprene), the dynamic viscosity data in Figure 4.3 does not completely support this explanation. Run 5, containing 88 wt% **1**, exhibited lower dynamic viscosity than fully hydrogenated Run 8, especially at higher shear rates. This implies that a reduction in adamantyl pendants by only 12 wt% imparts more chain mobility than the complete saturation of the backbone.

Conclusions

A modified emulsion procedure afforded poly(**1**) and poly(**1**-*ran*-isoprene) in excellent yields and allowed for the first investigation of their mechanical properties. Dynamic mechanical analysis using a 3-point bend geometry revealed the elastic and storage moduli in the glassy state as well as T_g. Rheology of poly(**1**) and poly(**1**-*ran*-isoprene) was conducted and provided a complete picture of viscoelastic behavior with respect to the content of **1**. Though increasing the wt% of **1** in poly(**1**-*ran*-isoprene) increases T_g, it appears to have little to no effect on the temperature at which the polymer enters the rubbery flow region. The rubbery plateau, indicative of the operating range, was between 170 - 180 °C for poly(**1**) and 120 - 180 °C for poly(**1**-*ran*-isoprene) with 88 wt% **1**. Currently, poly(**1**-*ran*-isoprene) with 41 wt% **1** exhibits no transition to the rubbery flow region up to 220 °C. This was originally attributed to branching or crosslinking, however characterization of a soluble sample exhibited nearly identical rehological behavior. Rheology of poly(**1**) before and after hydrogenation revealed that dynamic viscosity, a measure of overall chain mobility, is more sensitive to the amount of bulky adamantyl pendants than to backbone rigidity due to unsaturation.

Chapter 5: Anionic Polymerization of poly(2-(1-adamantyl)-1,3-butadiene)

Abstract

A novel living anionic polymerization technique involving titration with 4,5-methylenephenanthrene was used for the synthesis of poly(**1**) and poly(**1**-*block*-isoprene). The insolubility of anionic poly(**1**) was investigated by a direct comparison to emulsion polymerized poly(**1**). XRD and DSC analysis supports the hypothesis that anionic poly(**1**) is highly crystalline with a T_m exceeding 270 °C. NMR analysis showed an increase in distinct tertiary and secondary carbon environments in emulsion poly(**1**), which is consistent with the presence of branching. A branching analysis using GPC strongly suggests that branching occurs in emulsion polymerization of **1** at high conversion.

Introduction

The ability of block copolymers (BCPs) to self-assemble into distinct morphologies with resolutions ranging from a few nanometers to tens of nanometers has garnered significant attention, especially in the microelectronics industry.[137,138] As current top-down photolithographic methods are strained to meet the demands of sub-10 nm domains,[139] directed self-assembly has emerged as a promising next-generation lithographic technique for high-volume manufacturing of sub-10 nm features by the International Technology Roadmap for Semiconductors (ITRS).[140]

Although the domain shape and size of self-assembled BCP morphology is dictated by the overall chain length (***N***) and the volume fraction of the blocks (f_i), the driving force for self-assembly is the chemical incompatibility between each block. This incompatibility is quantified by a term that combines all enthalpic and noncombinatorial entropic factors into an effective interaction parameter, χ. Mean-field theory predicts that symmetric diblock copolymers (i.e. $f_i = 0.5$) with χN values greater that 10.5 will undergo self-assembly into ordered morphologies.[140] This means that at constant χ, a minimum value of ***N*** exists below which the morphology is disordered. BCPs with highly incompatible segments, termed "high χ" polymers have generated significant interest as they allow for BCPs with lower ***N*** values to induce self-assembly leading to smaller feature sizes.[140]

Currently, there are no reported values of solubility parameter (δ) for adamantyl substituted monomers, however, the semiempirical framework of Small and Hoy estimates δ to be 12.8 $\text{MPa}^{1/2}$ and 16.8 $\text{MPa}^{1/2}$, respectively. For reference, solubility of poly(tetrafluoroethylene) is reported[1] as 12.7 $\text{MPa}^{1/2}$. Kobayashi et al. reported[118] self-assembly in hydrogenated poly(isoprene-*block*-**1**-*block*-isoprene) (40 wt% poly**1**), which suggests that incorporation of adamantane pendant groups has a significant effect on δ. If semiempirical predictions are accurate, poly(**1**) may constitute a new "high χ" polymer.

In order to initiate an investigation into self-assembly of poly(**1**), a suitable block copolymerization method must be identified. Although living anionic polymerization (LAP) provides exceptional control of M_n and PDI and allows for block copolymerization, conventional methods are still largely inaccessible except with specialized equipment (e.g. break seal glassware) and rigorous purification of the reaction vessel, monomers, and solvent.[74] Controlled radical polymerization (CRP) techniques such as reversible addition-fragmentation chain-transfer (RAFT)[18,75–79] and nitroxide mediated polymerization (NMP)[20,80–83] have been successfully applied to conjugated diene systems and are significantly more tolerant to protic impurities. Unfortunately, our previous work also determined NMP was unsuitable for polymerization of **1** due to the previously noted Diels-Alder cyclization of monomers at the necessary temperature.

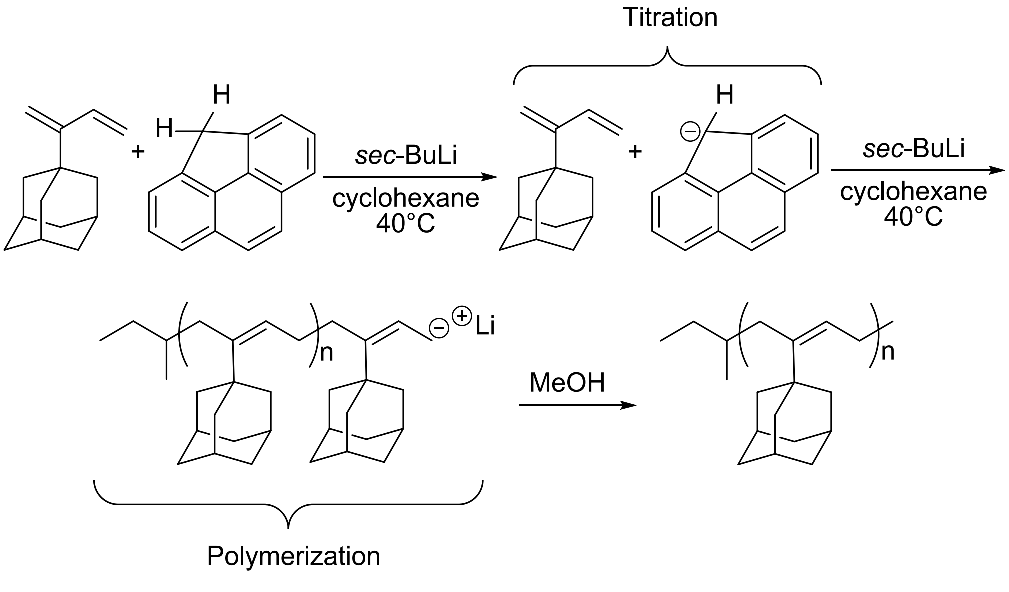

Scheme 5.1: Anionic polymerization of 1 using 4,5-methylenephenanthrene indicator

Fortuitously, Sänger et al. reported a simplified procedure for the anionic polymerization of styrene and dienes in which all purification steps are carried out in the reaction vessel by titration with *sec*-Butyllithium (*sec*-BuLi) using 4,5-methylenephenanthrene (MPT) as an indicator.[141] Since the rate of reaction of *sec*-BuLi with protic impurities and oxygen is much faster than with MPT or monomer, these impurities are selectively neutralized by the *sec*-BuLi first. When the reaction mixture is free of impurities, MPT is deprotonated resulting in a colored carbanion. An adaptation of this method, as shown in Scheme 5.1, was applied for the synthesis of poly(**1**) and poly(**1**-*block*-isoprene).

In addition to identifying a suitable synthesis for block copolymers, anionic poly(**1**) could now be compared to poly(**1**) synthesized via emulsion. Kobayashi et al. reported that poly(**1**) synthesized via living anionic polymerization was almost completely insoluble above an M_n of 6,000 g/mol.[17] This is in stark contrast to poly(**1**) synthesized via emulsion, which has exhibited excellent solubility in DCM, THF, and toluene even up to 47 kg/mol. To better understand this phenomenon, the potential for branching was investigated using 1D- and 2D-NMR experiments, as well as GPC analysis.

The central hypothesis of this exploration is that, contrary to Kobayashi et al.'s conclusions, anionic poly(**1**) is semicrystalline with a T_m that is undetectable by DSC analysis. Furthermore, if short or long-chain branching is present in emulsion poly(**1**), it would inhibit crystallization and increase solubility. Powder x-ray diffraction (XRD) and DSC were used to probe for the presence of crystallinity, while a combination of NMR and GPC was used to verify the presence of branching in emulsion poly(**1**).

Experimental

Materials

All glassware oven dried before use. Cyclohexane (Macron Chemicals) was distilled under Argon immediately before use. Isoprene (Alfa Aesar) was distilled from CaH_2 immediately before using. Styrene (Alfa Aesar) and **1** were distilled immediately before use. sec-butyllithium 1.0 M in cyclohexane (Sigma Aldrich) and 4,5-methylenephenanthrene (MPT) (Sigma Aldrich) were used as received.

Characterization

NMR spectra were recorded on a Bruker AVANCE III HD 500 MHz spectrometer with Protégé cold probe. Number and weight averaged molecular weights (M_n and M_w) of polymers were determined by right angle/low angle laser light scattering size exclusion chromatography (RALLS/LALLS-SEC) in conjunction with differential viscometry using a Viscotek (Houston, TX) 270 Dual Detector equipped with a Waters Chromatography (Milford, MA) Model 510 HPLC pump, Waters Chromatography (Milford, MA) 410 Differential Refractometer, and a Jordi-Gel DVB Mixed Bed column (250 mm x 10 mm ID) in THF (HPLC grade, Fisher). A triple detection method was used (RI, LS and viscosity) was used and calibrated to a narrow polystyrene standard (M_w = 98,938 g/mol, Viscotek) in THF at a flow of 0.5 mL/min. Certain low molecular weight samples were analyzed with a linear regression polystyrene calibration curve (M_w = 953, 1300, 2200 and 13,780 g/mol) using the RI detector. Differential scanning calorimetry was performed on a TA Instruments (New Castle, DE) Q200 equipped with refrigerated cooling. A heat-cool-heat cycle was performed from -80 to 200 °C at a rate of 10 °C/min. T_g is reported as midpoint temperature of the transition. Dynamic rheological measurements (viscous modulus (G"), elastic modulus (G') and complex viscosity (η*))) were acquired on a Bohlin CVO 100 N rheometer (East Brunswick, NJ) with smooth parallel plates (D = 25 mm). Rheological measurements were determined with a plate gap of between 800 and 1000 µm, 0.5% strain, and a frequency range of 0.01 Hz to 100 Hz at 220 °C. XRD was taken on a Siemens (Munich, Germany) Diffraktometer D5000 with a Cu source. Scans were performed from 5 to 30° 2θ at a rate of 0.5° 2θ per step.

Anionic polymerization of 1

MPT (7.0 mg, 0.04 mmol), cyclohexane (10 mL), and **1** (1.0 g, 5.3 mmol) were added to a 20 mL scintillation flask fitted with magnetic stir bar and a headspace sampling cap and heated to 40 °C. The solution was titrated with *sec*-butyllithium using a 100 µL gas-tight syringe until a pale-yellow color was observed indicating the absence of impurities. The calculated amount of *sec*-butyllithium for compensation of MPT and initiation was then added quickly resulting in a deep-orange color change. The reaction was stirred for 3 hours and then then quenched with 0.1 mL of degassed methanol. Polymer was obtained in quantitative yield.

*Synthesis of poly(**1**-block-isoprene)*

MPT (7.0 mg, 0.04 mmol), cyclohexane (70 mL), and **1** (2.8 g, 14.9 mmol) were added to a 100 mL Schlenk flask fitted with magnetic stir bar. The solution was titrated with *sec*-butyllithium using a 100 µL gas-tight syringe until a pale-yellow color was observed indicating the absence of impurities. The solution was heated to 40 °C and the calculated amount of *sec*-butyllithium for compensation of MPT and initiation was then added quickly resulting in a deep-orange color change. The reaction was stirred for 3 hours, and isoprene was added. Reaction was stirred for 3 more hours at 40 °C and then quenched with degassed methanol. Quenched solution was transferred to a 250 mL round bottom flash and solvent was removed. Remaining solids were dissolved in refluxing toluene and hot filtered first through a cellulose filter and then a 0.7 µm glass filter, and solvent was removed.

Results and Discussion

Anionic Polymerization with MPT indicator

Anionic homopolymerizations of **1** were conducted by first adding MPT indicator, cyclohexane, and **1** to 20 mL scintillation vials with a sealable headspace sampling cap to minimize the introduction of impurities. Titration was then performed by adding *sec*-BuLi dropwise to the stirred solution. A pale-yellow color was observed at titration endpoint in polymerizations of **1** as pictured in

Figure 5.1a. After the titration endpoint was reached, the reactions were heated to 40 °C and *sec*-BuLi was added to account for the remaining unreacted indicator as well as the initiation of **1** resulting in a deep-orange color change (Figure 5.1b). The intensity of color change increased with decreasing [M]:[I] and was persistent throughout the reaction. Quenching with degassed methanol resulted in a slightly opaque colorless solution (Figure 5.1c).

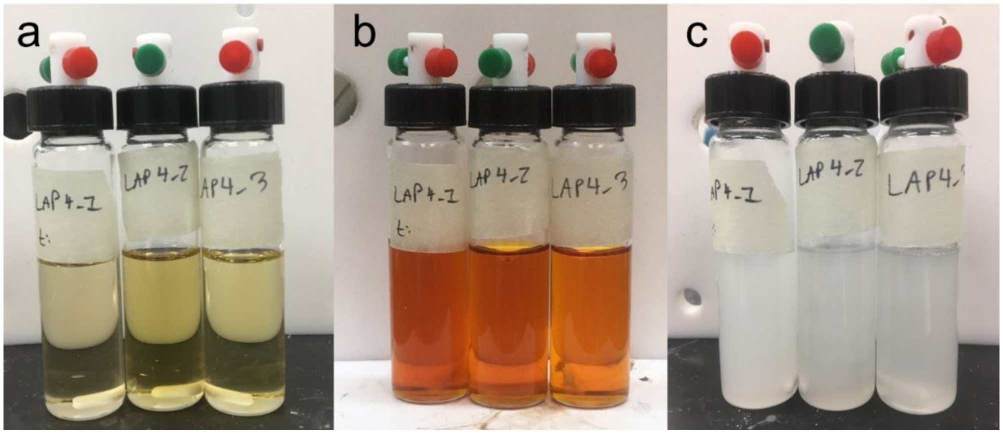

Figure 5.1: Stages of the anionic polymerization of **1** with MPT indicator: a) at titration endpoint b) during polymerization c) after quenching with degassed methanol

Interestingly, when the quenched polymerizations were left unagitated for 12 hours the entire reaction mixture solidified into a loose gel, pictured in Figure 5.2. This is particularly notable since the polymer represents less than 10% of the total reaction volume. Although this behavior was not explicitly reported by Kobayashi et al., they did report gradual appearance of a white precipitate from the quenched polymerizations.[17] Removal of solvent gave **1** as a white powder in quantitative yields. Results are presented in Table 5.1.

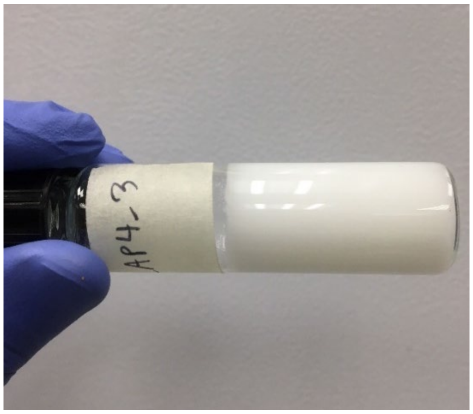

Figure 5.2: Solidification of quenched anionic polymerization of 1 (Entry 3)

Block copolymerizations of **1** with isoprene and styrene were conducted in Schlenk flasks. As with homopolymerizations, block copolymerizations were conducted by titrating a solution of **1** and MPT in cyclohexane with *sec*-BuLi until a pale-yellow color persisted. **1** was selected as the first block in all copolymerizations so that any poly(**1**), which is assumed to be completely insoluble, that was formed by undesired termination by impurities present in the second monomer addition could be removed by filtration. A solution of second monomer and MPT in cyclohexane was then titrated and added directly the polymerization initiating the polymerization of the second block.

Isolation of poly(**1**-*block*-isoprene) samples required sequential filtration of polymers in refluxing toluene, which appeared to remove a significant amount of insoluble poly(**1**). After filtration, the soluble material was precipitated with acetone to remove any possible poly(isoprene) that may have initiated during titration. Results are presented in Table 5.1

Table 5.1: Anionic polymerization and block copolymerization of **1**

			block copolymer (homopolymer)		
	Monomer (polymerization time, h)		M_n (kg/mol)		
Entry	1st	2nd	Target[a]	GPC[b,d]	PDI[d]
1	**1**(3)	none	(20)[c]	(20)	(1.38)
2	**1**(3)	none	(10)	(1.9)	(10.6)[e]
3	**1**(3)	none	(5.6)	(16)	(1.29)
4	**1**(3)	none	(3.8)	(10)	(2.12)
5	**1**(3)	none	(1.9)	(2.4)	(15.1)[e]
6	**1** (3)	isoprene (3)	1.6 (1.0)	4.7(1.0)	1.20(1.32)
7	**1** (3)	Isoprene (3)	7.9 (4.7)	14(3.2)	1.30(1.37)
8	**1** (3)	isoprene (3)	16 (9.4)	13(5.1)	1.41(1.37)

[a] Determined by [M]:[I]
[b] Molecular weight obtained by SEC using a standard calibration using polystyrene standards in THF
[c] Molecular weight obtained by SEC triple-detection method
[d] Determined after hydrogenation
[e] Bimodal molecular weight distribution overserved

Although LAP with MPT indicator did ultimately produce poly(**1**) with reasonably narrow PDI (Run 1), poor control of M_n and PDI was generally observed. Bimodal molecular weight distribution was observed in Runs 2 and 5. This is attributed to over titration of monomer resulting in unintended initiation. Of the five homopolymerizations conducted, Runs 1 and 3 exhibited the best control of M_n and PDI and were used for comparison to emulsion poly(**1**).

Unlike emulsion polymerized poly(**1**), but consistent with Kobayashi's findings, nearly all poly(**1**) samples prepared by anionic polymerization were completely insoluble in THF, dichloromethane, and toluene even when heated to reflux. A portion of Run 5, the lowest molecular weight poly(**1**) sample, was found to be sparingly soluble in toluene. It is possible that this sample represents the lower M_n portion of the bimodal distribution. All poly(**1**) samples (Runs 1-5) were completely soluble after hydrogenation to poly(1-vinyladamantane-*alt*-ethylene) and allowed for characterization by NMR and GPC.

*Solubility behavior of LAP and emulsion poly(**1**)*

Glaring differences in the solubilities of poly(**1**) synthesized via emulsion and anionic polymerization have enormous implications for potential applications of the polymer system and merited a more thorough investigation. Initially, DSC was performed on anionic poly(**1**) runs 1 and 3 before and after hydrogenation (Figure 5.3). Interestingly, no distinct T_g was observed in any of the unsaturated anionic poly(**1**), even when considering the 2nd derivative of the heat flow. Upon complete hydrogenation, however, all samples were both readily soluble in organic solvents (e.g. $CHCl_3$, toluene, and THF) and had distinct T_gs. No crystalline melting endotherms were observed for any of the samples which is consistent with Kobayashi et al.'s findings.

The absence of a discernable T_gs in the anionic poly(**1**) samples led to the hypothesis that anionic poly(**1**) was highly crystalline with a T_m exceeding 270 °C, which explains the observed insolubility. Though Kobayashi reported that crystallinity was absent in their anionic poly(**1**), this conclusion was based upon a DSC analysis that showed no endotherm up to 270 °C. It is worth noting that DSC thermograms are not included in their publication or in supplementary information. Marconi et al.[42] reported that poly(2-*tert*-butyl-1,3-butadiene) with high *cis*-1,4- content exhibited crystallinity with a T_m of 106 °C and a T_g of 20 °C, demonstrating the ability for bulky branched 2-substituents to induce crystallinity. Considering that the T_g of emulsion poly(**1**) is as high as 172 °C, it is quite plausible that the T_m for such a system would exceed 270 °C and thus be undetectable with the DSC experiments conducted by Kobayashi et al.

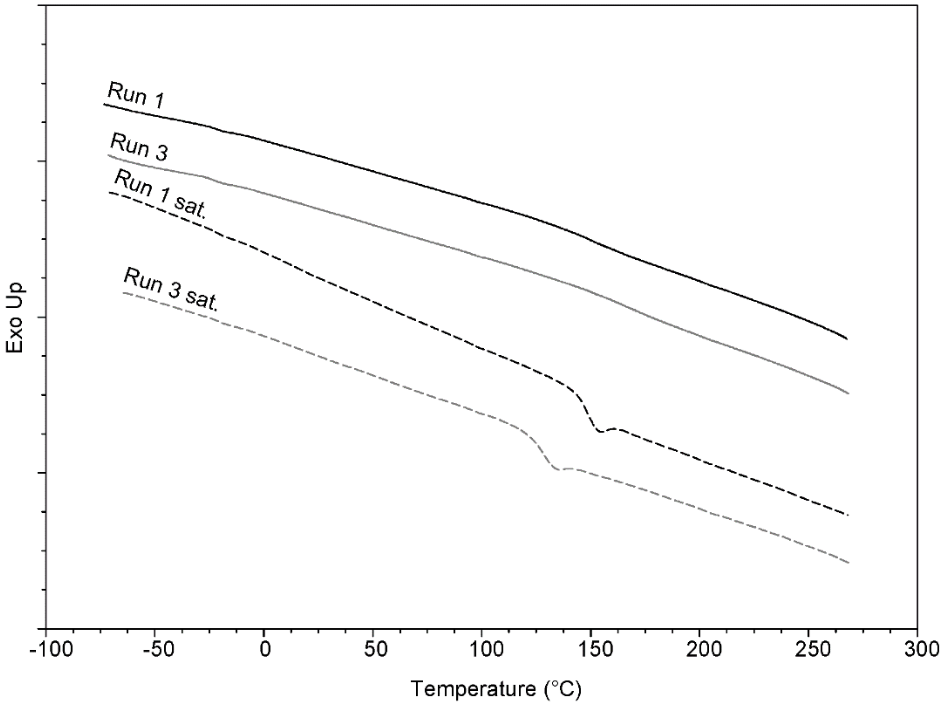

Figure 5.3: DSC overlay of anionic poly(**1**) before and after hydrogenation

Powder x-ray diffraction (XRD) experiments were conducted on anionic and emulsion poly(**1**) and their hydrogenated equivalents and results are presented in Figure 5.4. XRD is advantageous because it directly detects crystallinity and does not require heating the sample through the melt transition, which is not feasible for these anionic poly(**1**) samples. Diffraction peaks at $2\theta = 12.1°$ and 16.5° were observed in anionic poly(**1**) Run 1. These peaks are not observed after hydrogenation nor were they observed in emulsion poly(**1**) Run 8 before and after hydrogenation.

The absence of a distinct T_g as well as the presence of a distinct scattering pattern in the XRD spectrum support the hypothesis that anionic poly(**1**) is highly crystalline with a T_m exceeding 270 °C, and insolubility of anionic poly(**1**) can now be attributed to crystalline domains. The disappearance of scattering peaks and the appearance of a distinct T_g indicate that hydrogenation inhibits crystallinity and also explains the increased solubility of saturated poly(**1**) Runs 1 and 3. The presence of a distinct T_g and absence of x-ray diffraction peaks also indicates that, despite unsaturation, emulsion poly(**1**) does not contain crystalline domains. The complete solubility of saturated emulsion poly(**1**), even with M_n as high as 47 kg/mol, indicates that solubility is dictated by the presence of insoluble crystalline domains and not increased backbone rigidity as was originally concluded by Kobayashi et al.[17]

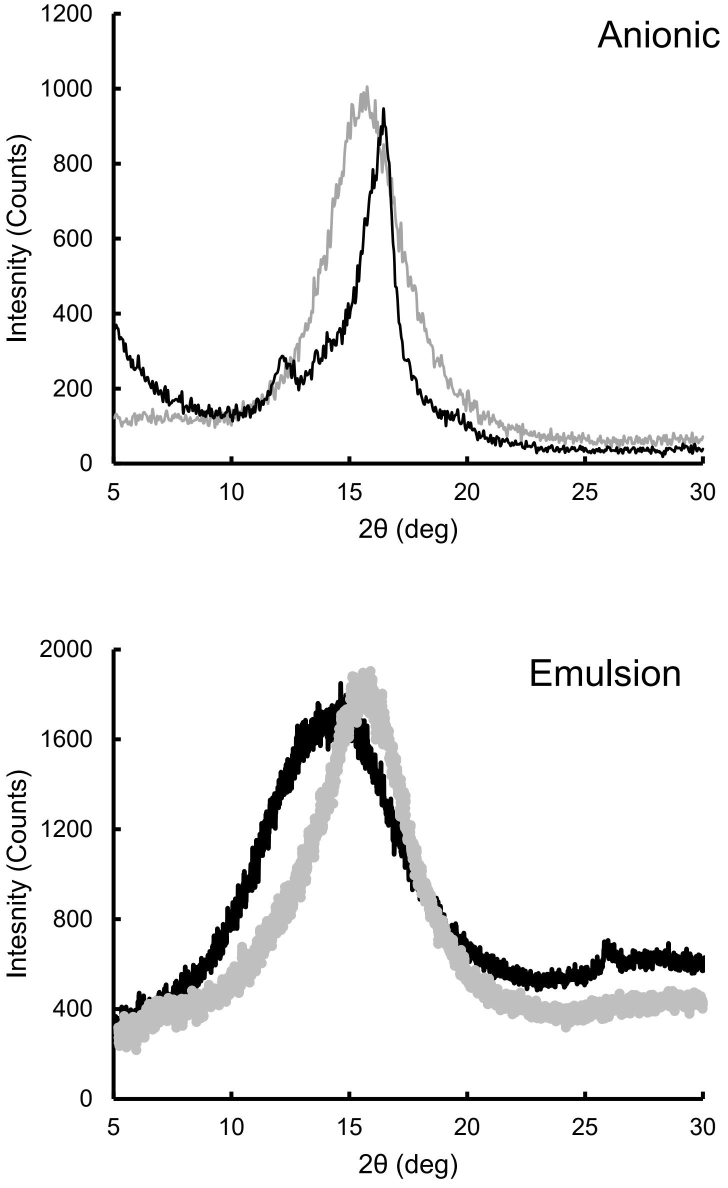

Figure 5.4: Powder x-ray diffraction patterns of anionic and emulsion poly(**1**) before (black) and after (grey) hydrogenation

*Branching in emulsion poly(**1**)*

To develop a hypothesis as to why emulsion polymerized poly(**1**) is completely amorphous while anionic poly(**1**) is highly crystalline, the mechanisms of each polymerization must be considered. The mechanism of free radical polymerization, whether homogenous or in emulsion, includes multiple termination and chain transfer steps outlined in Figure 5.5. Chain transfer refers to the process by which a propagating chain radical abstracts a molecule (usually a proton) from either a monomer or solvent molecule, an added chain transfer agent, or a polymer chain, thereby terminating the propagating chain and transferring an active radical to that species. Chain transfer to polymer leads to branching and is usually more significant in emulsion polymerizations than in homogenous free-radical polyerizations.[136] Chain transfer to polymer can proceed either intramolecularly, leading to short branches, or intermolecularly which results in long branches. Figure 5.5 presents a visual representation of inter- and intramolecular chain transfer to polymer in polyethylene. Unlike radical polymerization, living anionic polymerizations do not undergo a termination or chain transfer.[24,142] Consequently, branching is not observed in living anionic polymerizations of olefins.

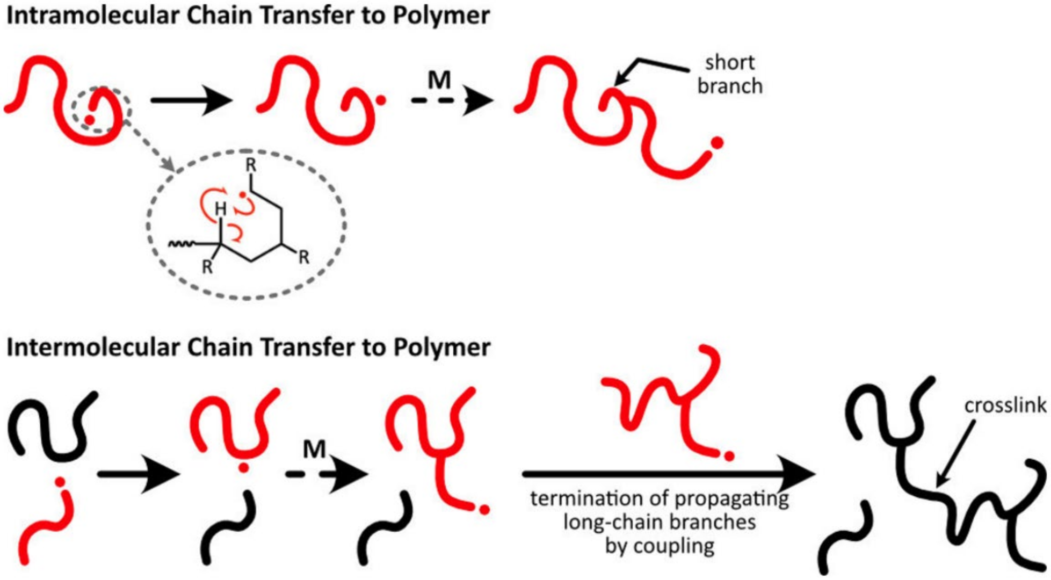
Intramolecular Chain Transfer to Polymer
M
short branch
H
R
R
R
Intermolecular Chain Transfer to Polymer
M
termination of propagating long-chain branches by coupling
crosslink

Figure 5.5: Visual representation of intramolecular and intermolecular chain transfer to polymer in polyethylene (from ref 136)

Short-chain branching disrupts local polymer conformations and has a significant effect on polymer properties. This is especially true in crystalline polymers as branching prevents the formation of highly ordered lamellae. Because intramolecular chain transfer does not affect the number of polymer chains, it has little effect of on M_n.

Generally, intermolecular chain transfer to polymer is less frequent, however it becomes more prevalent as conversion increases.[136] The resulting long-chain branches have a very significant effect polymer relaxation behavior and thus the physical properties of amorphous polymers above the T_g.[136] Because the number of chains does not change, M_n is largely unaffected by long-chain branching. However, the original propagating chain is prematurely terminated upon transfer leading to higher PDI values.

Considering the prevalence of chain transfer to polymer in emulsion,[136] we hypothesized that branching is present in emulsion poly(**1**) which inhibits the formation of crystallinity. Not only would this explain the enhanced solubility over anionic poly(**1**), but varying degrees of short- and long-chain branching in emulsion poly(**1**) may be influencing the observed fluctuations in T_g reported in Chapter 3.

To investigate this hypothesis ^{13}C, DEPT 135, and HSQC NMR experiments were performed on fully saturated samples of emulsion poly(**1**) (Run 8) and anionic poly(**1**) (Run 1) to determine if different carbon environments consistent with branching are present. Because chain transfer is not present in the anionic polymerization mechanism, it was assumed that the anionic poly(**1**) was representative of a completely linear polymer. ^1H and ^{13}C NMR of hydrogenated Run 1 agreed well with the reported spectrum from Kobayashi.[17] Compared to Run 1, the ^{13}C NMR spectra of hydrogenated emulsion Run 8 showed an increase CH environments from δ = 49 to 51 ppm and CH_2 environments from δ = 29 to 32 ppm (Figure 5.6). These assignments were confirmed with DEPT 135 (Figure 5.7).

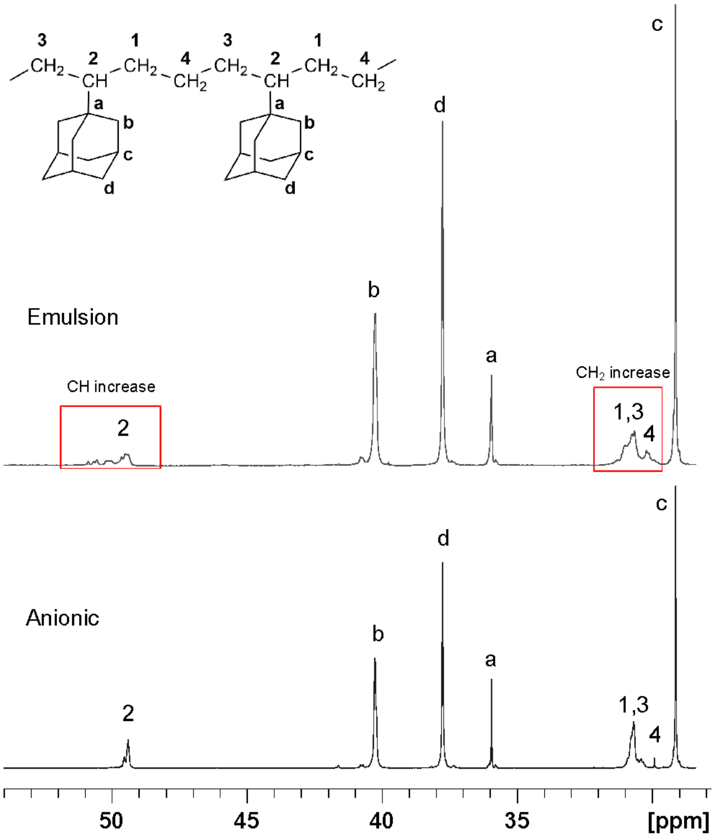

Figure 5.6 ^{13}C NMR comparison of emulsion and anionic poly(**1**)

To confirm that both emulsion and anionic poly(**1**) had comparable microstructures, and that carbon environments were not attributed to large differences in 3,4- or 1,2- content in either samples, ^{1}H NMR of unsaturated polymers were compared. Although all samples of anionic poly(**1**) were insoluble after quenching in MeOH, a portion of Run 5 was found to be partially soluble in toluene-D8. ^{1}H NMR confirmed that microstructure of anionic poly(**1**) was nearly identical to emulsion poly(**1**): 85% *cis*-1,4-, 9% *trans*-1,4-, 0% 1,2-, 6% 3,4-.

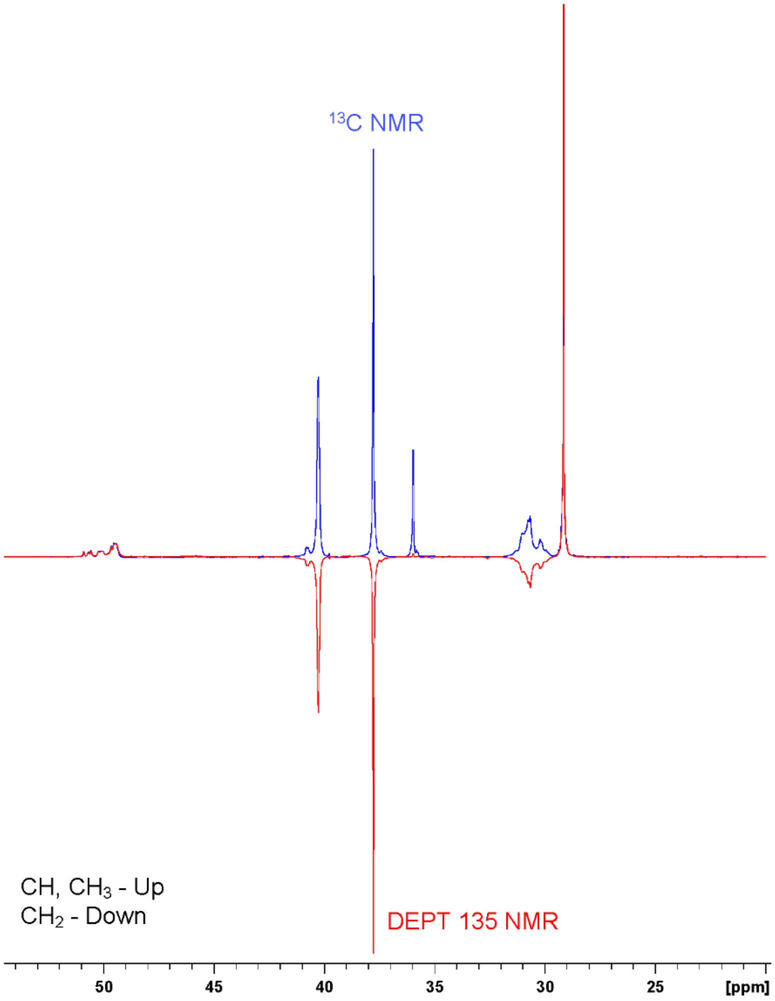

Figure 5.7: ^{13}C and DEPT 135 NMR of hydrogenated poly(**1**) (Run 8)

Whether chain transfer occurs at the C1, C3, or C4 position, the net effect is the formation of new CH carbon environments (Scheme 5.2 blue) as well as the shifting of its neighboring CH and CH_2 environments (Scheme 5.2 red). Although a rigorous assignment of CH and CH_2 peaks was not feasible here, the overall increase in these environments is consistent with branching in emulsion poly(**1**).

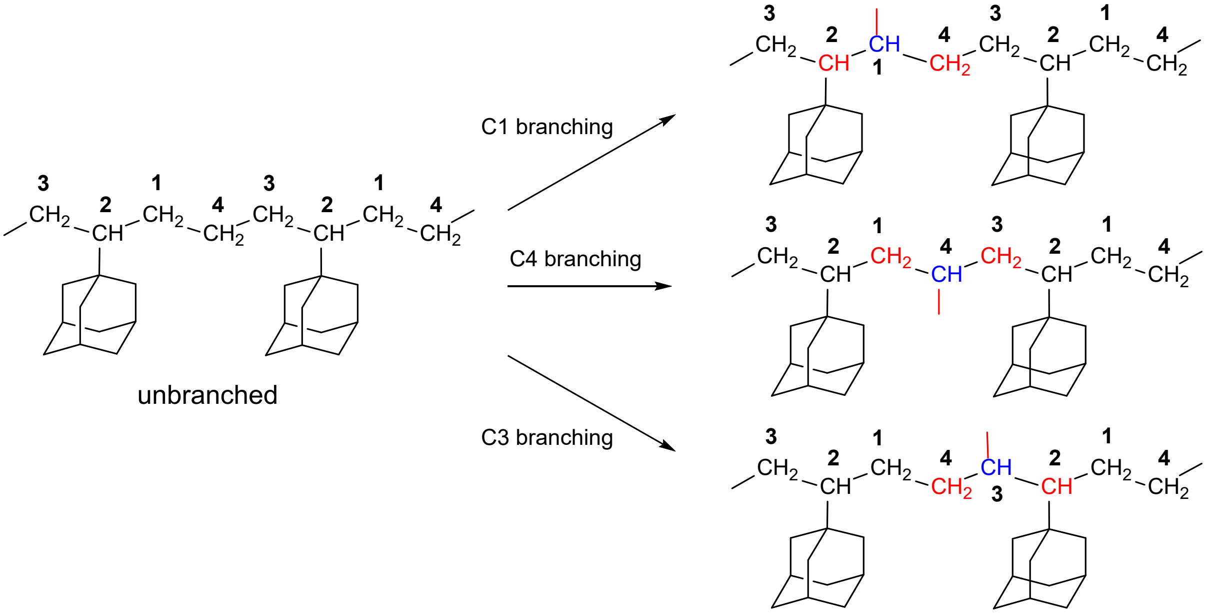

Scheme 5.2: Carbon environments of emulsion poly(**1**) before and after branching

GPC Branching Analysis

An analysis of branching was performed on a hydrogenated sample of anionic poly(**1**) (Run 1) and emulsion poly(**1**) Run 8. For completely linear polymer samples, the dependence of intrinsic viscosity ([η]) of molecular weight (M) can be represented by the Mark-Houwink equation (eq. 5.1).

$$[\eta] = KM^{a} \qquad (5.1)$$

Where *K* and *a* are the Mark-Houwink parameters and are dependent on the polymer-solvent system used. Therefore, a log-log plot of *M* versus [η] will be linear.

[η] is a measurement of the molecular density of the polymer chains in dilute solution. The tighter polymer chains fold or coil in solution translates to a higher molecular density and the lower the intrinsic viscosity. Branching increases the molecular density of the polymer in dilute solution, which lowers [η]. This means that a linear polymer chain may have a higher [η] than a branched polymer chain of the same molecular weight. Viscometers used in GPC analysis are very sensitive to these changes in [η] which manifest as nonlinearity in the log-log Mark-Houwink plot.

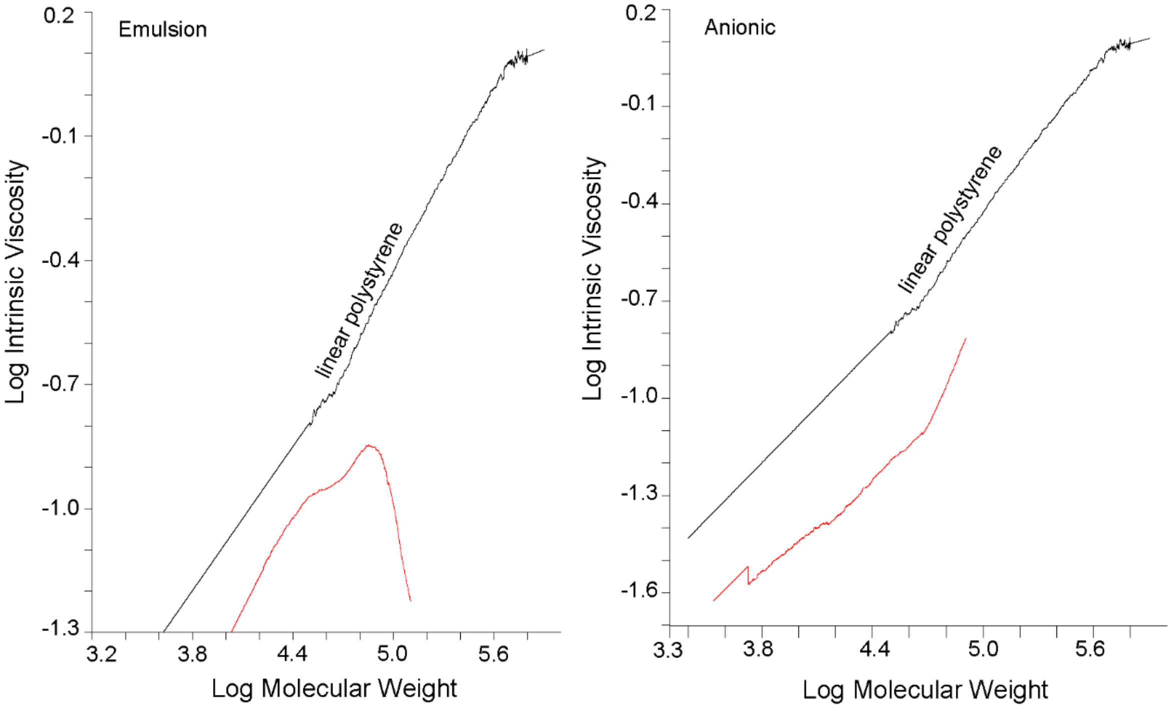

Figure 5.8: Mark-Houwink plots of hydrogenated poly(**1**) (red) and linear polystyrene standard (black). Left: emulsion Run 8, right: anionic Run 1

The OmniSEC software package was used for a branching analysis of hydrogenated emulsion (Run 8) and anionic (Run 1) poly(**1**), and the Mark-Houwink plots are presented in Figure 5.8. A linear polystyrene sample with a broad PDI (2.3) was used as linear reference in the software and is depicted as the black lines. The plot of emulsion poly(**1**) (Figure 5.8 left) clearly shows a deviation in [η] from the Mark-Houwink equation when molecular weight exceeds 25 kg/mol. This suggests that branching at higher conversion is occurring during emulsion polymerization of **1**. The linearity of anionic poly(**1**) chains was confirmed by the linear relationship of M and [η] on the Mark-Houwink plot (Figure 5.8 right).

Conclusions

A novel living anionic polymerization including titration of impurities with 4,5-methylenephenanthrene was employed for the synthesis of poly(**1**) and poly(**1**-*block*-isoprene). Good control of M_n and low PDIs were achieved for one sample of poly(**1**) and all poly(**1**-*block*-isoprene) polymerizations. However, general control on M_n was poor, and bimodal distributions were observed. The insolubility of poly(**1**) from anionic polymerization was investigated by direct comparison to soluble emulsion polymerized poly(**1**). No T_gs were detected in anionic poly(**1**) up to 270 °C using DSC but were clearly present after hydrogenation. Distinct x-ray diffraction peaks were detected in anionic poly(**1**), which were not present following hydrogenation or in emulsion poly(**1**). NMR analysis revealed that hydrogenated emulsion poly(**1**) contained more distinct secondary and tertiary carbon environments which is consistent with the presence of branching. GPC branching analysis indicated that branching is present at molecular weights greater than 25 kg/mol indicating that branching is occurring at higher conversion.

From the DSC and XRD results it was concluded that anionic poly(**1**) is highly crystalline with a T_m higher than 270 °C. Insolubility is attributed to this crystallinity. Crystallinity is completely inhibited by both saturation and branching and explains the solubility of emulsion poly(**1**) and anion poly(**1**) after hydrogenation.

Chapter 6: Conclusions and Future Work

Summary

This dissertation was successful in its objective of improving the access of 2-(1-adamantyl)-1,3-butadiene at a scale suitable for its use as a monomer. Identification of room-temperature emulsion polymerization provides a robust, high-throughput, and scalable route for poly(**1**) and poly(**1**-*ran*-isoprene. The ability to synthesize a robust sample set of polymers allowed for the first mechanical characterization of poly(**1**) and poly(**1**-*ran*-isoprene) and elucidated the dependence of T_g and viscoelasticity on the content of **1** in poly(**1**-*ran*-isoprene). The effect of adamantyl pendants on the overall polymer chain mobility was documented and contributes to the scarce fundamental knowledge of bulky 2-subsituted polydiene polymers. Overall, this work not only facilitates future studies into diamondoid 2-substituted 1,3-butadienes but has also identified interesting properties that motivate doing so.

Broader Impacts and Future Work

*Compounding of poly(**1**-ran-isoprene) rubber*

A preliminary investigation of the effect of **1** content on the viscoelasticity in poly(**1**-*ran*-isoprene) was presented and highlights the potential for the system as a new thermoplastic elastomer system. Future work is still needed to fully characterize the relationships between M_n, PDI, and degree of branching and viscoelasticity. The improved monomer synthesis and developed emulsion polymerization procedures will facilitate these ongoing studies.

Blending and covulcanization of poly(**1**) and poly(**1**-*ran* isoprene) with other rubbers such as natural rubber (NR), styrene-butadiene rubber (SBR), and butadiene rubber (BR) presents a very interesting area of study for these polymers. Although unblended polyisoprene rubbers are suitable for applications such as tire carcasses and off-road tires, their inadequate tensile strength, elongation at break, and tear resistance preclude their use in more demanding applications such as heavy-duty truck and aircraft tires.[41] Blending of polybutadiene and isoprene rubbers with NR and SBR has allowed for more mechanically robust materials, however, NR is still necessary and constitutes up to 40% of a tire's rubber.[143]

Blending and covulcanization of *trans*-polyisoprene with NR, SBR, and BR has also resulted in outstanding dynamic mechanical properties, especially the rolling resistance, heat buildup, and wet skid resistance.[40] Qi et al. highlighted the potential for bulky phenyl and adamantyl substituents to increase these dynamic mechanical properties, perhaps even mitigating the need for NR, which is highly susceptible to supply chain disruptions.[41] The improved access to **1** and scalable emulsion polymerization methods reported in this dissertation allow for a comprehensive investigation into the the effect of blending and covulcanization of poly(**1**) and poly(**1**-*ran*-isoprene) with NR, SBR, and BR on dynamic mechanical properties.

Self-assembly of poly(1) containing block copolymers

Block copolymerization of **1** with isoprene was demonstrated in this dissertation. Although good control of M_n was not observed, three samples of poly(**1**-*block*-isoprene) were obtained with moderately low PDI. These samples can be used to make a preliminary determination of the effective χ-parameter (χ_{eff}), which can be accomplished by either rheometry or small-angle x-ray scattering (SAXS) experiments.

The degree of segregation in a block copolymer system is dictated by χN. Using mean-field theory, χN for a block copolymer can be estimated at the order-disorder transition (T_{ODT}) using the theoretical phase map[144] in Figure 6.1. For example, polystyrene-*block*-polyisoprene with a polystyrene volume fraction of 0.5 (f_{PS} = 0.5) would have a χN value of 10.5 at T_{ODT}. Because the degree of polymerization (N) is known, χ_{eff} can be obtained at T_{ODT} for the block copolymer system.

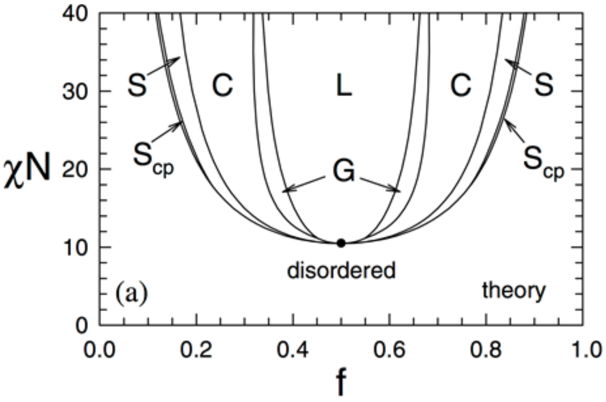

Figure 6.1: Theoretical Phase Map taken from ref 123

The transition from ordered to disordered morphology is accompanied by a sharp drop in shear storage modulus (G'), meaning that T_{ODT} can be determined by rheology.[137] Temperature sweep rheometry experiments are used to measure G' as a function of temperature, and the temperature at which a precipitous drop in G' is observed is determined to be the T_{ODT}. Although rheological experiments can provide a preliminary determination of χ_{eff}, the technique requires approximately 500 mg of polymer per experiment, which can be limiting in the short-term. Furthermore, it does not provide any information about morphology or domain size, which will require SAXS experiments.

Optical polymers

The utility of optical plastics is largely determined by refractive index (n_d), dispersion, transmittance in the visible light region, and moisture absorption. Dispersion is a measure of the variance of refractive index with respect to wavelength and is often quantified by Abbe number (ν_D), which is approximately inversely proportional to optical dispersion. Low dispersion (high ν_D) is especially desirable in the visible light region as it minimizes chromatic aberration.[52] Polymers possessing both high n_d and ν_D have received much attention due to their applications as lenses, prisms, and waveguides, especially since their weight, processability and impact resistance is far superior to conventional inorganic glasses.[145]

Robello reported that inclusion of adamantyl and diamantyl groups in acrylate, methacrylate, and vinyl monomers imparted some of the optical properties of diamond to the resulting polymers, which exhibited low optical dispersion and high refractive indices.[52] In fact, poly(1-vinyladamantane) (poly(VAd)) exhibited the highest n_d (1.5560) of the diamondoid polymers studied. Low ν_D values were attributed to low degree of polymerization of poly(VAd), which could only be obtained as oligomers. Although Spohn et al. have demonstrated polymerization of poly(VAd) up to 15 repeat units with extremely strong cationic initiating systems,[120] adamantane is generally considered to be too bulky for the vinylic backbone.

By extending the length of the polymer backbone, we demonstrated that poly(**1**) with up to 250 repeat units (47 kg/mol) can be obtained via emulsion polymerization. When fully hydrogenated, this would represent a close analog to high molecular weight poly(VAd). Light induced electronic transitions in polymers are responsible for absorptions in the UV region. According to molecular orbital theory, the energy requirement for a transition from $\sigma \rightarrow \sigma^*$ is significantly higher than for nonbonding or π electrons and occurs at wavelengths as low as 135nm.[145] Consequently, compounds with only σ bonds are transparent in the UV region. Removal of π bonds in higher molecular weight poly(**1)** via hydrogenation should, therefore, result in a chemical and oxidative resistant polymer with UV-transparency, low water absorption, high refractive index, and low optical dispersion. These properties would lend it to applications as optical fibers, lenses, and photoresists. Incorporation of higher order diamondoid pendants may further increase these effects.

Although the synthesis of 2-(4-diamantyl)-1,3-butadiene starting from diamantane was detailed in this dissertation, its polymerization has not yet been carried out. A future investigation into the optical properties should include polymerization studies of 2-(4-diamantyl)-1,3-butadiene. Variable Angle

Spectroscopic Ellipsometry (VASE) can then be used to quantify the refractive index and optical dispersion of hydrogenated poly(**1**) and poly(2-(4-diamantyl)-1,3-butadiene).

Chapter 7: References

1. J.M.G. Cowie; Arrighi, V. *Polymers: Chemistry and Physics of Modern Materials, Third Edition*; CRC Press, **2007**.
2. Morawetz, H. *Polymers: The Origins and Growth of a Science*; Courier Corporation, **2002**.
3. Andrady, A. L.; Neal, M. A. *Philosophical Transactions of the Royal Society B: Biological Sciences* **2009**, *364*, 1977.
4. Jambeck, J. R.; Geyer, R.; Wilcox, C.; Siegler, T. R.; Perryman, M.; Andrady, A.; Narayan, R.; Law, K. L. *Science* **2015**, *347*, 768.
5. Bläsing, M.; Amelung, W. *Science of The Total Environment* **2018**, *612*, 422.
6. McCrum, N. G.; Buckley, C. P.; Bucknall, C. B.; Bucknall, C. B. *Principles of Polymer Engineering*; Oxford University Press, **1997**.
7. Hosler, D.; Burkett, S. L.; Tarkanian, M. J. *Science* **1999**, *284*, 1988.
8. Jr, C. E. C. *Seymour/Carraher's Polymer Chemistry : Sixth Edition*; CRC Press, **2003**.
9. Ciesielski, A. *An Introduction to Rubber Technology*; iSmithers Rapra Publishing, **1999**.
10. Davis, W.; Schultes, R. *The Lost Amazon: The Photographic Journey of Richard Evans Schultes*; Chronicle Books, **2004**.
11. Dean, W. *Brazil and the Struggle for Rubber: A Study in Environmental History*; Cambridge University Press, **1987**.
12. Tully, J. *Journal of World History* **2009**, *20*, 559.
13. Goodman, A.; Schilder, H.; Aldrich, W. *Oral Surgery, Oral Medicine, Oral Pathology and Oral Radiology* **1974**, *37*, 954.
14. Prakash, D. R.; Gopikrishna, D. V.; Kandaswamy, D. D. 5.
15. Lee, D.-K.; Kim, S. V.; Limansubroto, A. N.; Yen, A.; Soundia, A.; Wang, C.-Y.; Shi, W.; Hong, C.; Tetradis, S.; Kim, Y.; Park, N.-H.; Kang, M. K.; Ho, D. *ACS Nano* **2015**, *9*, 11490.
16. Bisio, A.; Herbert, V. D. *Synthetic Rubber: A Project That Had to Succeed*; Praeger: Westport, Conn, **1985**.
17. Kobayashi, S.; Kataoka, H.; Ishizone, T. *Macromolecules* **2009**, *42*, 5017.
18. Germack, D. S.; Wooley, K. L. *J. Polym. Sci. A Polym. Chem.* **2007**, *45*, 4100.
19. Bonnet, F.; Visseaux, M.; Pereira, A.; Barbier-Baudry, D. *Macromolecules* **2005**, *38*, 3162.
20. Benoit, D.; Harth, E.; Fox, P.; Waymouth, R. M.; Hawker, C. J. *Macromolecules* **2000**, *33*, 363.
21. Odian, G.; Odian, U. G. *Principles of Polymerization*; John Wiley & Sons, **2004**.
22. Sperling, L. H. *Introduction to Physical Polymer Science*; John Wiley & Sons, **2005**.
23. Carothers, W. H. *J. Am. Chem. Soc.* **1929**, *51*, 2548.
24. Flory, P. J. *Principles of Polymer Chemistry*; Cornell University Press, **1953**.
25. Menard, K. P. *Dynamic Mechanical Analysis: A Practical Introduction, Second Edition*; 2nd ed.; CRC Press: Boca Raton, **2008**.
26. Paul, D. R. In *Multicomponent Polymer Materials*; Paul, D. R.; Sperling, L. H., Eds.; American Chemical Society: Washington, DC, **1985**; Vol. 211, pp 3.
27. Kohno, Y.; Saita, S.; Men, Y.; Yuan, J.; Ohno, H. *Polymer Chemistry* **2015**, *6*, 2163.
28. Li, M.; Ober, C. K. *Materials Today* **2006**, *9*, 30.
29. Matsen, M. W. *Journal of Physics: Condensed Matter* **2002**, *14*, R21.
30. Matsen, M. W.; Schick, M. *Phys. Rev. Lett.* **1994**, *72*, 2660.
31. Eng, A. H.; Tanaka, K.; Tanaka, Y. *Rubber Chemistry and Technology* **1994**, *67*, 159.
32. Burfield, D. R.; Lim, K. L. *Macromolecules* **1983**, *16*, 1170.
33. Cornish, K. *Natural Product Reports* **2001**, *18*, 182.
34. Kent, E. G.; Swinney, F. B. *I&EC Product Research and Development* **1966**, *5*, 134.
35. Hadjichristidis, N.; Zhongde, X.; Fetters, L. J.; Roovers, J. *J. Polym. Sci. Polym. Phys. Ed.* **1982**, *20*, 743.

36. Adams, H. E.; Stearns, R. S.; Smith, W. A.; Binder, J. L. *Industrial and Engineering Chemistry*. **1958,** *50,* 1507.
37. Tobolsky, A. V.; Rogers, C. E. *Journal of Polymer Science* **1959**, *40*, 73.
38. Tobolsky, A. V.; Rogers, C. E. *Journal of Polymer Science* **1959**, *38*, 205.
39. Halasa, A. F.; Hsu, W.-L. 9.
40. Song, J.-S.; Huang, B.-C.; Yu, D.-S. *Journal of Applied Polymer Science* **2001**, *82*, 81.
41. Qi, Y.; Liu, Z.; Liu, S.; Cui, L.; Dai, Q.; He, J.; Dong, W.; Bai, C. *Catalysts* **2019**, *9*, 97.
42. Marconi, W.; Mazzei, A.; Cucinella, S.; Cesari, M. *Journal of Polymer Science Part A: General Papers* **1964**, *2*, 4261.
43. Marconi, W.; Mazzei, A.; Cucinella, S.; Cesari, M.; Pauluzzi, E. *Journal of Polymer Science Part A: General Papers* **1965**, *3*, 123.
44. Gunawan, M. A.; Poinsot, D.; Domenichini, B.; Schreiner, P. R.; Fokin, A. A.; Hierso, J.-C. In *Chemistry of Organo-Hybrids*; Charleux, B.; Copéret, C.; Lacôte, E., Eds.; John Wiley & Sons, Inc.: Hoboken, NJ, USA, **2015**; pp 69.
45. Charleux, B.; Coperet, C.; Lacote, E. *Chemistry of Organo-hybrids: Synthesis and Characterization of Functional Nano-Objects*; John Wiley & Sons, **2015**.
46. von R. Schleyer, P. *J. Am. Chem. Soc.* **1957**, *79*, 3292.
47. Cupas, C.; von R. Schleyer, P.; Trecker, D. J. *J. Am. Chem. Soc.* **1965**, *87*, 917.
48. Burns, W.; B. Mitchell, T. R.; Anthony McKervey, M.; J. Rooney, J.; Ferguson, G.; Roberts, P. *Journal of the Chemical Society, Chemical Communications* **1976**, *0*, 893.
49. Williams, V. Z.; von Ragué Schleyer, P.; Gleicher, G. J.; Rodewald, L. B. *J. Am. Chem. Soc.* **1966**, *88*, 3862.
50. Dahl, J. E. P.; Moldowan, J. M.; Wei, Z.; Lipton, P. A.; Denisevich, P.; Gat, R.; Liu, S.; Schreiner, P. R.; Carlson, R. M. K. *Angewandte Chemie International Edition* **2010**, *49*, 9881.
51. Clay, W. A.; Dahl, J. E. P.; Carlson, R. M. K.; Melosh, N. A.; Shen, Z.-X. *Rep. Prog. Phys.* **2015**, *78*, 016501.
52. Robello, D. R. *Journal of Applied Polymer Science* **2013**, *127*, 96.
53. Kobayashi, S.; Kataoka, H.; Ishizone, T.; Kato, T.; Ono, T.; Kobukata, S.; Arimoto, K.; Ogi, H. *Reactive and Functional Polymers* **2009**, *69*, 409.
54. Koike, K.; Araki, T.; Koike, Y. *Polymer International* **2015**, *64*, 188.
55. Matsumoto, A.; Tanaka, S.; Otsu, T. *Macromolecules* **1991**, *24*, 4017.
56. Tsai, C.-W.; Wang, J.-C.; Li, F.-N.; Chang, Y.-C.; Wu, K.-H. *Materials Express* **2016**, *6*, 220.
57. Nakano, Y.; Sato, E.; Matsumoto, A. *Journal of Polymer Science Part A: Polymer Chemistry* **2014**, *52*, 2899.
58. Namikoshi, T.; Hashimoto, T.; Makino, Y.; Imaeda, T.; Urushisaki, M.; Sakaguchi, T. *Polym. Bull.* **2014**, *71*, 1389.
59. Kobayashi, S.; Kataoka, H.; Ishizone, T. *J. Phys.: Conf. Ser.* **2009**, *184*, 012017.
60. Kobayashi, S.; Kataoka, H.; Goseki, R.; Ishizone, T. *Macromol. Chem. Phys.* **2018**, *219*, n/a.
61. Kobayashi, S.; Matsuzawa, T.; Matsuoka, S.; Tajima, H.; Ishizone, T. *Macromolecules* 2006, 39, 5979.
62. Nicolas, J.; Guillaneuf, Y.; Lefay, C.; Bertin, D.; Gigmes, D.; Charleux, B. *Progress in Polymer Science* **2013**, *38*, 63.
63. Matyjaszewski, K.; Spanswick, J. *Materials Today* **2005**, *8*, 26.
64. Hsieh, H. L.; Quirk, R. P. *Anionic Polymerization : Principles and Practical Applications*; Plastics Engineering; CRC Press: New York, **1996**.
65. Fuchise, K.; Sone, M.; Miura, Y.; Sakai, R.; Narumi, A.; Sato, S.-I.; Satoh, T.; Kakuchi, T. *Polym J* **2010**, *42*, 626.
66. Fiorito, D.; Folliet, S.; Liu, Y.; Mazet, C. *ACS Catal.* **2018**, *8*, 1392.
67. Diver, S. T.; Giessert, A. J. *Chem. Rev.* **2004**, *104*, 1317.

68. Nunomoto, S.; Kawakami, Y.; Yamashita, Y. *BCSJ* **1981**, *54*, 2831.
69. Sahlberg, C.; Quader, A.; Claesson, A. *Tetrahedron Letters* **1983**, *24*, 5137.
70. Li, H.; Fiorito, D.; Mazet, C. *ACS Catal.* **2017**, *7*, 1554.
71. Fiorito, D.; Folliet, S.; Liu, Y.; Mazet, C. *ACS Catal.* **2018**, *8*, 1392.
72. Harrisson, S.; Couvreur, P.; Nicolas, J. *Macromolecules* **2011**, *44*, 9230.
73. Ndoni, S.; Papadakis, C. M.; Bates, F. S.; Almdal, K. *Review of Scientific Instruments* **1995**, *66*, 1090.
74. K, K.; W, L.; D, C.; T, C. *Korea Polym. J.* **1999**, *7*, 321.
75. Germack, D. S.; Harrisson, S.; Brown, G. O.; Wooley, K. L. *Journal of Polymer Science Part A: Polymer Chemistry* **2006**, *44*, 5218.
76. M. Gramlich, W.; Theryo, G.; A. Hillmyer, M. *Polymer Chemistry* **2012**, *3*, 1510.
77. Jitchum, V.; Perrier, S. *Macromolecules* **2007**, *40*, 1408.
78. Moad, G. *Polymer International* **2017**, *66*, 26.
79. Contreras-López, D.; Fuentes-Ramírez, R.; Albores-Velasco, M.; de los Santos-Villarreal, G.; Saldívar-Guerra, E. *Journal of Polymer Science Part A: Polymer Chemistry* **2018**, *56*, 2463.
80. Contreras-López David; Albores-Velasco Martha; Saldívar-Guerra Enrique *Journal of Applied Polymer Science* **2017**, *134*, 45108.
81. Detrembleur, C.; Sciannamea, V.; Koulic, C.; Claes, M.; Hoebeke, M.; Jérôme, R. *Macromolecules* **2002**, *35*, 7214.
82. Wegrzyn, J. K.; Stephan, T.; Lau, R.; Grubbs, R. B. *J. Polym. Sci. A Polym. Chem.* **2005**, *43*, 2977.
83. Harrisson, S.; Couvreur, P.; Nicolas, J. *Macromol. Rapid Commun.* **2012**, *33*, 805.
84. Hong, S.-C. *Elastomers and Composites* **2009**, *44*, 55.
85. Karlström, A. Sofia. E.; Itami, K.; Bäckvall, J.-E. *J. Org. Chem.* **1999**, *64*, 1745.
86. Karlström, A. S. E.; Rönn, M.; Thorarensen, A.; Bäckvall, J.-E. *J. Org. Chem.* **1998**, *63*, 2517.
87. Fokin, A. A.; Butova, E. D.; Chernish, L. V.; Fokina, N. A.; Dahl, J. E. P.; Carlson, R. M. K.; Schreiner, P. R. *Org. Lett.* **2007**, *9*, 2541.
88. Nelson, D. J.; DiFrancesco, R.; Petters, D. *J. Chem. Educ.* **1977**, *54*, 648.
89. Sasaki, T.; Shimizu, K.; Ohno, M. *Chemical & Pharmaceutical Bulletin* **1984**, *32*, 1433.
90. Cheung, F. K.; Hayes, A. M.; Morris, D. J.; Wills, M. *Org. Biomol. Chem.* **2007**, *5*, 1093.
91. Frija, L. M. T.; Afonso, C. A. M. *Tetrahedron* **2012**, *68*, 7414.
92. Kun, K. A.; Kunin, R. *J. polym. sci., C Polym. symp.* **1967**, *16*, 1457.
93. Di Girolamo, M.; Lami, M.; Marchionna, M.; Pescarollo, E.; Tagliabue, L.; Ancillotti, F. *Ind. Eng. Chem. Res.* **1997**, *36*, 4452.
94. Di Girolamo, M.; Tagliabue, L. *Catalysis Today* **1999**, *52*, 307.
95. Karinen, R. S.; Linnekoski, J. A.; Krause, A. O. I. *Catalysis Letters* **2001**, *76*, 81.
96. Rehfinger, A.; Hoffmann, U. *Chem. Eng. Technol.* **1990**, *13*, 150.
97. Izquierdo, J. F.; Vila, M.; Tejero, J.; Cunill, F.; Iborra, M. *Applied Catalysis A: General* **1993**, *106*, 155.
98. Honkela, M. L.; Krause, A. O. I. *Ind. Eng. Chem. Res.* **2004**, *43*, 3251.
99. Honkela, M. L.; Krause, A. O. I. *Catalysis Letters* **2003**, *87*, 113.
100. Hauge, K.; Bergene, E.; Chen, D.; Fredriksen, G. R.; Holmen, A. *Catalysis Today* **2005**, *100*, 463.
101. Schubert, K.; Saumweber, R.; Görls, H.; Weigand, W. *Zeitschrift für anorganische und allgemeine Chemie* **2003**, *629*, 2091.
102. Danheiser, R. L.; Brisbois, R. G.; Kowalczyk, J. J.; Miller, R. F. *J. Am. Chem. Soc.* **1990**, *112*, 3093.
103. Suzuki, T.; Tsuji, Y.; Takegami, Y.; Harwood, H. J. *Macromolecules* **1979**, *12*, 234.
104. Zhu, S.; Lu, X.; Luo, Y.; Zhang, W.; Jiang, H.; Yan, M.; Zeng, W. *Org. Lett.* **2013**, *15*, 1440.

105. Wu, J. Y.; Moreau, B.; Ritter, T. *J. Am. Chem. Soc.* **2009**, *131*, 12915.
106. Hatano, M.; Ito, O.; Suzuki, S.; Ishihara, K. *J. Org. Chem.* **2010**, *75*, 5008.
107. Zong, H.; Huang, H.; Liu, J.; Bian, G.; Song, L. *J. Org. Chem.* **2012**, *77*, 4645.
108. Klein, F. G.; Banchero, J. T. *Ind. Eng. Chem.* **1956**, *48*, 1278.
109. Panov, A. G.; Fripiat, J. J. *Journal of Catalysis* **1998**, *178*, 188.
110. Aouissi, A.; Al-Deyab, S. S.; Al-Shahri, H. *Molecules* **2010**, *15*, 1398.
111. Carey, F. A.; Sundberg, R. J. *Advanced Organic Chemistry: Part A: Structure and Mechanisms*; Part A: Structure and Mechanisms; 5th ed.; Springer US, **2007**.
112. Vollhardt, K. P. C.; Schore, N. E. *Organic Chemistry; Palgrave version: Structure and Function*; Macmillan International Higher Education, **2014**.
113. Thornton, R.; Gates, B. C. *Journal of Catalysis* **1974**, *34*, 275.
114. Marvel, C. S.; Williams, J. L. R. *J. Am. Chem. Soc.* **1948**, *70*, 3842.
115. Marvel, C. S.; Williams, J. L. R.; Baumgarten, H. E. *J. Polym. Sci.* **1949**, *4*, 583.
116. Overberger, C. G.; Arond, L. H.; Wiley, R. H.; Garrett, R. R. *J. Polym. Sci.* **1951**, *7*, 431.
117. Overberger, C. G.; Fischman, A.; Roberts, C. W.; Arond, L. H.; Lal, J. *J. Am. Chem. Soc.* **1951**, *73*, 2540.
118. Kobayashi, S.; Kataoka, H.; Ishizone, T.; Kato, T.; Ono, T.; Kobukata, S.; Arimoto, K.; Ogi, H. *Reactive and Functional Polymers* **2009**, *69*, 409.
119. Kobayashi, S.; Kataoka, H.; Goseki, R.; Ishizone, T. *Macromolecular Chemistry and Physics* **2018**, *219*, 1700450.
120. Spohn, M.; Alkahtani, M. H. A.; Leiter, R.; Qi, H.; Kaiser, U.; Hemmer, P.; Ziener, U. *ACS Appl. Nano Mater.* **2018**, *1*, 6073.
121. Sinkel, C.; Agarwal, S.; Fokina, N. A.; Schreiner, P. R. *Journal of Applied Polymer Science* **2009**, *114*, 2109.
122. FOX, T. G. *Bull. Am. Phys. Soc.* **1956**, *1*, 123.
123. Ren, Y.; Lodge, T. P.; Hillmyer, M. A. *Macromolecules* **2002**, *35*, 3889.
124. Cheong, I. W.; Fellows, C. M.; Gilbert, R. G. *Polymer* **2004**, *45*, 769.
125. Wicklatz, J. E.; Kennedy, T. J.; Reynolds, W. B. *Journal of Polymer Science* **1951**, *6*, 45.
126. Gelbard, G. *Ind. Eng. Chem. Res.* **2005**, *44*, 8468.
127. Benoit, D.; Chaplinski, V.; Braslau, R.; Hawker, C. J. *J. Am. Chem. Soc.* **1999**, *121*, 3904.
128. Widmaier, J. M.; Meyer, G. C. *Macromolecules* **1981**, *14*, 450.
129. Lynd, N. A.; Meuler, A. J.; Hillmyer, M. A. *Progress in Polymer Science* **2008**, *33*, 875.
130. Lynd, N. A.; Hillmyer, M. A.; Matsen, M. W. *Macromolecules* **2008**, *41*, 4531.
131. Minoshima, W.; White, J. L.; Spruiell, J. E. *Polymer Engineering & Science* **1980**, *20*, 1166.
132. Hatzikiriakos, S. G. *Progress in Polymer Science* **2012**, *37*, 624.
133. Li, S.-J.; Xie, S.-J.; Li, Y.-C.; Qian, H.-J.; Lu, Z.-Y. *Phys. Rev. E* **2016**, *93*, 012613.
134. Kobayashi, S.; Matsuzawa, T.; Matsuoka, S.; Tajima, H.; Ishizone, T. *Macromolecules* **2006**, *39*, 5979.
135. Minari, R. J.; Rodriguez, V. I.; Estenoz, D. A.; Vega, J. R.; Meira, G. R.; Gugliotta, L. M. *Journal of Applied Polymer Science* **2010**, *116*, 590.
136. Lovell, P. A.; Schork, F. J. *Biomacromolecules* **2020**, *21*, 4396.
137. Kennemur, J. G.; Hillmyer, M. A.; Bates, F. S. *Macromolecules* **2012**, *45*, 7228.
138. Gottlieb, S.; Rösner, B.; Evangelio, L.; Fernández-Regúlez, M.; Nogales, A.; García-Gutiérrez, M. C.; Keller, T. F.; Fraxedas, J.; Ezquerra, T. A.; David, C.; Perez-Murano, F. *Mol. Syst. Des. Eng.* **2019**, *4*, 175.
139. Herr, D. J. C. *Journal of Materials Research; Warrendale* **2011**, *26*, 122.
140. Sinturel, C.; Bates, F. S.; Hillmyer, M. A. *ACS Macro Lett.* **2015**, *4*, 1044.
141. Sänger, J.; Tefehne, C.; Lay, R.; Gronski, W. *Polymer Bulletin* **1996**, *36*, 19.
142. Webster, O. W. *Science* **1991**, *251*, 887.

143. Hobhouse, H. *Seeds of Wealth: Five Plants that Made Men Rich*; Counterpoint Press, **2005**.
144. Leibler, L. *Macromolecules* **1980**, *13*, 1602.
145. Harmon, J. P. In *Optical Polymers*; Harmon, J. P.; Noren, G. K., Eds.; American Chemical Society: Washington, DC, **2001**; Vol. 795, pp 1.
146. Gund, T. M.; Nomura, M.; Schleyer, P. v. R. *J. Org. Chem.* **1974**, *39*, 2987.
147. Khusnutdinov, R. I.; Shchadneva, N. A.; Mukhametshina, L. F. *Russ J Org Chem* **2010**, *46*, 820.
148. Kishi, A.; Kato, S.; Sakaguchi, S.; Ishii, Y. *Chem. Commun.* **1999**, 1421.
149. Tabushi, I.; Kojo, S.; Schleyer, P. v. R.; Gund, T. M. *J. Chem. Soc., Chem. Commun.* **1974**, 591.
150. Schreiner, P. R.; Fokina, N. A.; Tkachenko, B. A.; Hausmann, H.; Serafin, M.; Dahl, J. E. P.; Liu, S.; Carlson, R. M. K.; Fokin, A. A. *J. Org. Chem.* **2006**, *71*, 6709.
151. Fokin, A. A.; Gunchenko, P. A.; Novikovsky, A. A.; Shubina, T. E.; Chernyaev, B. V.; Dahl, J. E. P.; Carlson, R. M. K.; Yurchenko, A. G.; Schreiner, P. R. *European Journal of Organic Chemistry* **2009**, *2009*, 5153.
152. Lukes, P.; Clupek, M.; Babicky, V.; Sunka, P. *Plasma Sources Sci. Technol.* **2008**, *17*, 024012.

Appendix A - Chapter 2 Supporting Information

UV Photoacetylation of Diamantane

Functionalization of diamondoids is well documented and often focuses on the tertiary bridgehead carbons.[44] Although several multi-step acetylations of adamantane have been reported,[146–148] a single-step method was sought for the synthesis of 4-acetyldiamantane. Direct photoacetylation of diamondoids up to pentamantane with diacetyl and UV irradiation has been reported[149–151] and was the preferred method for synthesis of 4-acetyldiamantane and the subsequent production of 2-(4-diamantyl)-1,3-butadiene.

Complete results of the photoacetylation of diamantane are presented in Table 7.1. Two UV reactor setups were employed. The first consisted of a circular array of 16 x 75W, high-pressure mercury lamps and the other of 2 50W LED UV lamps. All reactions were conducted in Pyrex borosilicate glass vessels, degassed by several freeze-pump-thaw cycles, and backfilled with argon.

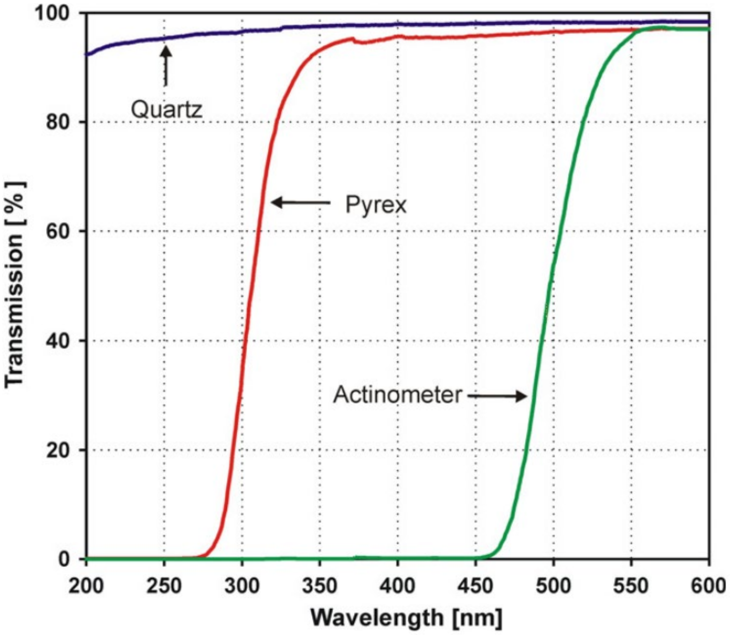

Figure 7.1: Transmission of UV light in various materials. Taken from ref 152

Initial photoacetylation performed in the array of high-pressure mercury lamps (Runs 1 and 2) exhibited low overall conversion of diamantane. This could reasonably be attributed to the use of Pyrex reaction vessels which are not transparent to all UV light. However, the UV transmission of Pyrex at wavelengths above 350 nm is nearly equivalent to of quartz.[152] Although this would block any lower wavelength UVC light, high pressure mercury lamps have strong emission lines at higher wavelengths (e.g. 356.4, 404.7 and 435.8). Considering the UV/Vis spectrum of 2,3-butanedione obtained from NIST Webbook, which shows good absorbance between 400 – 450 nm, the UV reactor should not be attributed to poor conversion.

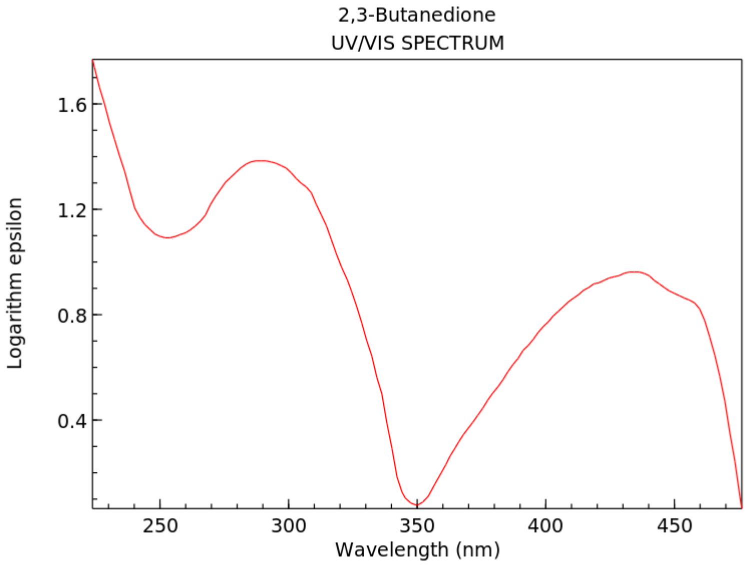

Figure 7.2: UV/Vis spectrum of 2,3-butanedione

The observed increase in conversion with decreased reactor internal diameter (ID) prompted an investigation into the effect of reactor geometry on conversion. Runs 3 and 4 were prepared from a single solution of diamantane and diacetyl in DCM, and ID was the only variable. GC-MS analysis of the reaction products after 66 hours clearly indicated that decreasing the reactor ID from 24 mm to 4.2 mm more than doubled the conversion of diamantane. One explanation for this behavior is that the UV light is not fully penetrating the sample. According to the Beer-Lambert law, the intensity of transmitted light logarithmically decreases with increasing the path length at constant concentration and molar absorptivity. This means that there is an effective penetration depth of the UV light beyond which the intensity of the light is insufficient to initiate acetylation. Though this depth was not rigorously calculated, if a penetration depth of 1.0 mm is assumed (for illustrative purpose only) the percent of total solution being irradiated is 73%, 16%, and 12% for reactor IDs of 4.2, 24, and 31 mm, respectively.

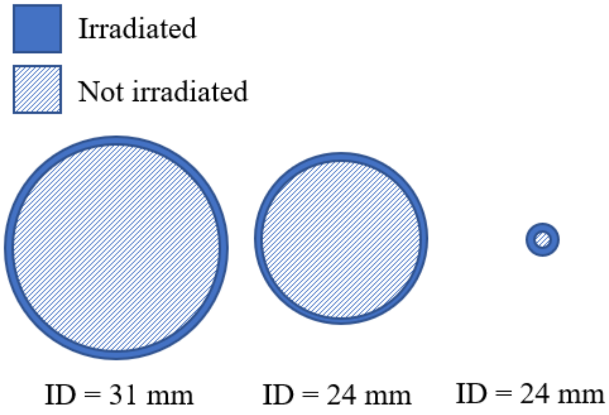

Figure 7.3: Visual comparison of penetration depth at various reactor IDs

Several solvents were tested using standard 7" borosilicate NMR tubes as reaction vessels (Runs 4 - 8). Although higher conversion was observed, chlorinated diamantane was detected in GC-MS (m/z = 222.10 detected, 222.12 actual) when DCM and DCE were used at solvents. Runs 4 and 5 indicate that chlorination may be attributed to increased temperature. Runs 7 and 8 confirm that photo acetylation can be conducted in toluene solution and in bulk diacetyl with no formation of chlorinated products. However, the notably lower solubility of diamantane in diacetyl is limiting.

Table 7.1: UV Acetylation of diamantane[a]

	Run	**solvent**	**Temp (°C)**	**ID (mm)**	**Time (h)**	**[S]**	**conv. (%)[c]**	**x_{cl} (%)[c]**
UV5	1[b]	DCE	60	24	64	0.05	18	2
UV6	2[b]	DCE	60	31	64	0.05	12	5
UV7	3	DCM	54	24	66	0.17	34	26
UV7$_{NMR}$	4	DCM	54	4.2	66	0.17	77	20
UV8$_{DCM}$	5	DCM	38	4.2	65	0.17	74	13
UV8$_{DCE}$	6	DCE	38	4.2	65	0.17	83	10
UV8$_{tol}$	7	toluene-d8	38	4.2	65	0.17	81	0
UV8$_{DAc}$	8	diacetyl	38	4.2	65	0.07	76	0
UV10	9	toluene	38	4.2	64	sat.[d]	72	0
UV15	10	toluene	38	4.2	64	sat.[d]	72	0

[a] All reactions contained 10 eq. of diacetyl and were reacted with 50W LED UV lamps x 2 unless otherwise stated.

[b] High-pressure mercury lamps 75W x 16 used

[c] Conversion determined by GC-MS analysis

[d] Saturated solution at room temperature

With the identification of toluene as an optimal solvent, an attempt to scale up the photoacetylation of diamantane was made. A saturated solution of diamantane in a 2:1 vol:vol mixture of toluene and diacetyl was prepared at room temperature. This solution was then transferred to standard 7" 4.2 mm ID NMR tubes. Runs 9 and 10 consisted of arrays of 5 and 17 total tubes, respectively, and indicate that the reaction can be scaled simply by adding more NMR tubes in the reactor without affecting conversion. After UV irradiation unreacted diamantane was quantitatively recovered by column chromatography (eluent: hexanes). 4-acetyldiamantane was isolated by slowly increasing eluent to 5% vol. ethyl acetate in hexanes followed by recrystallization from hot methanol:water. Overall, 1.55 g of pure 4-acetyldiamantane was isolated.

Monoterpene Characterization

(3R,5R,7R)-1-(1-(4-((3R,5R,7R)-adamantan-1-yl)cyclohex-3-en-1-yl)vinyl)adamantane ***(3a)***

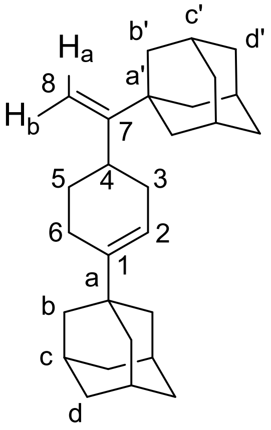

^{1}H NMR: (CDCl$_3$, 500 MHz) δ (ppm) = 5.43 (dt, J = 5.36, 1.83 Hz, 1H, C2), 4.80 (s, 1H, H$_a$) 4.75 (s, 1H, H$_b$) 2.22 (1H, C4), 2.16 (1H, C6**a**), 2.09 (1H, C3**a**), 2.00 (1H, C6**b**), 1.99 (1H, Cc and Cc'), 1.94 (1H, C3**b**), 1.75-1.59 (24H, Cd, Cd', Cb and Cb'), 1.68 (1H, C5**a**), 1.41 (1H. C5**b**)

A note about peak assignments: Due to overlapping and convoluted peaks in the aliphatic region (δ = 2.5 – 0.0 ppm) peak assignments were determined by the midpoint of the peak in HSQC NMR. Although the assignment of an **a** and **b** environment for the CH$_2$ signals of C3, C4, and C6 is to account for the splitting that occurs due to difference in equatorial and axial proton signals, no actual distinction of each is made. Rather all downfield signals were simply denoted **a** while all upfield signals were denoted **b**.

^{13}C NMR: (CDCl3, 500 MHz) δ (ppm) = 165.2 (C7), 145.7 (C1), 118.2 (C2), 105.0 (C8), 41.1 (Cb’), 40.6 (Cb), 38.5 (Ca’), 37.2 (Cd’), 37.0 (Cd), 36.9 (Ca), 35.6 (C3), 34.4 (C4), 32.4 (C5), 28.8 (Cc’), 28.6 (Cc), 24.7 (C6)

GC-MS (EI): m/z (int.) = 376 (6), 240 (5), 214 (49), 200 (9), 155 (6), 136 (10), 135 (100), 134 (10), 107 (20), 93 (21), 93 (21), 91 (24), 79 (25), 77 (18)

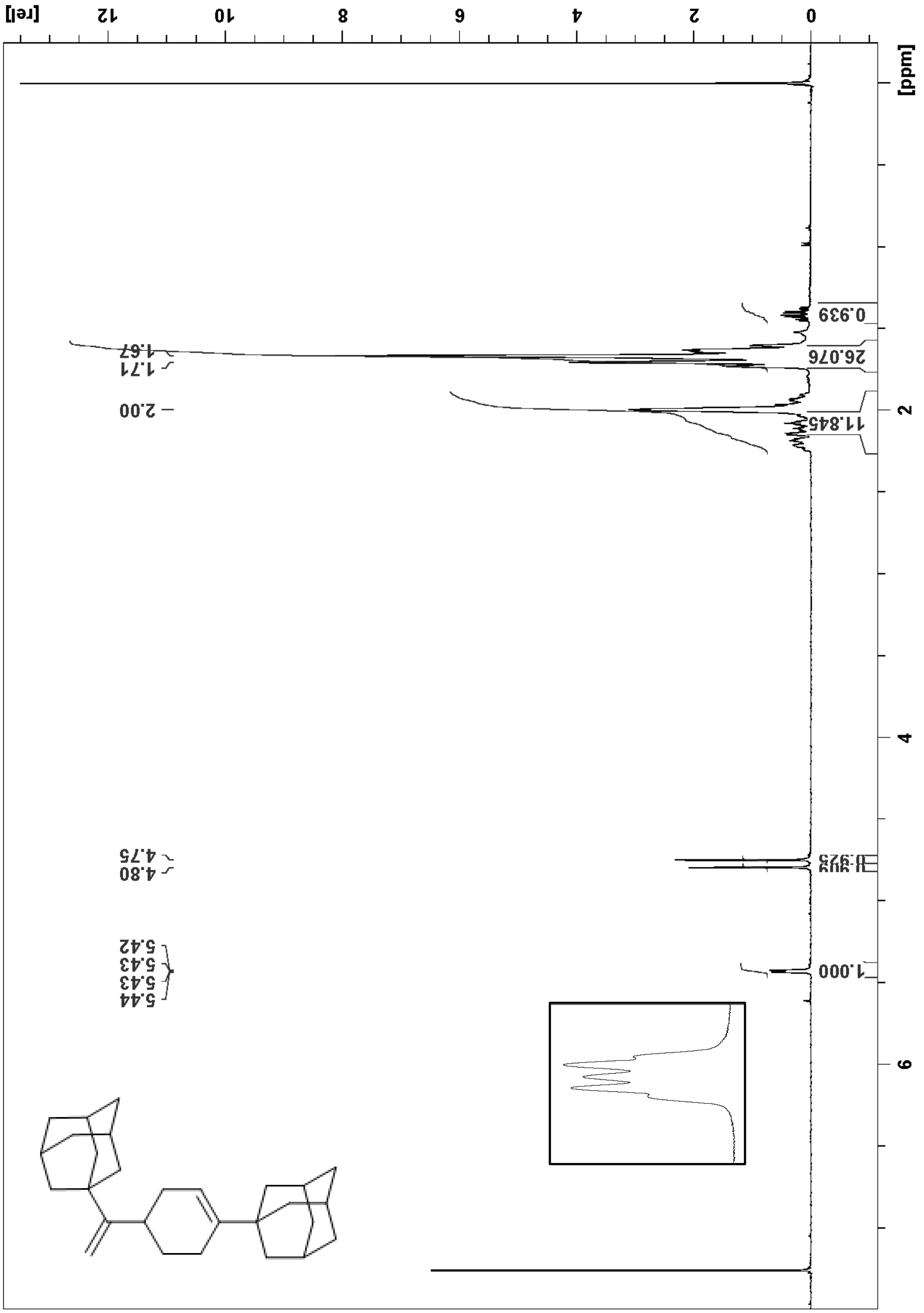
[rel]
12
10
8
6
4
2
0
[ppm]
6
4
2
5.44
5.43
5.43
5.42
4.80
4.75
2.00
1.71
1.67
1.000
0.909
0.925
11.845
26.076
0.939

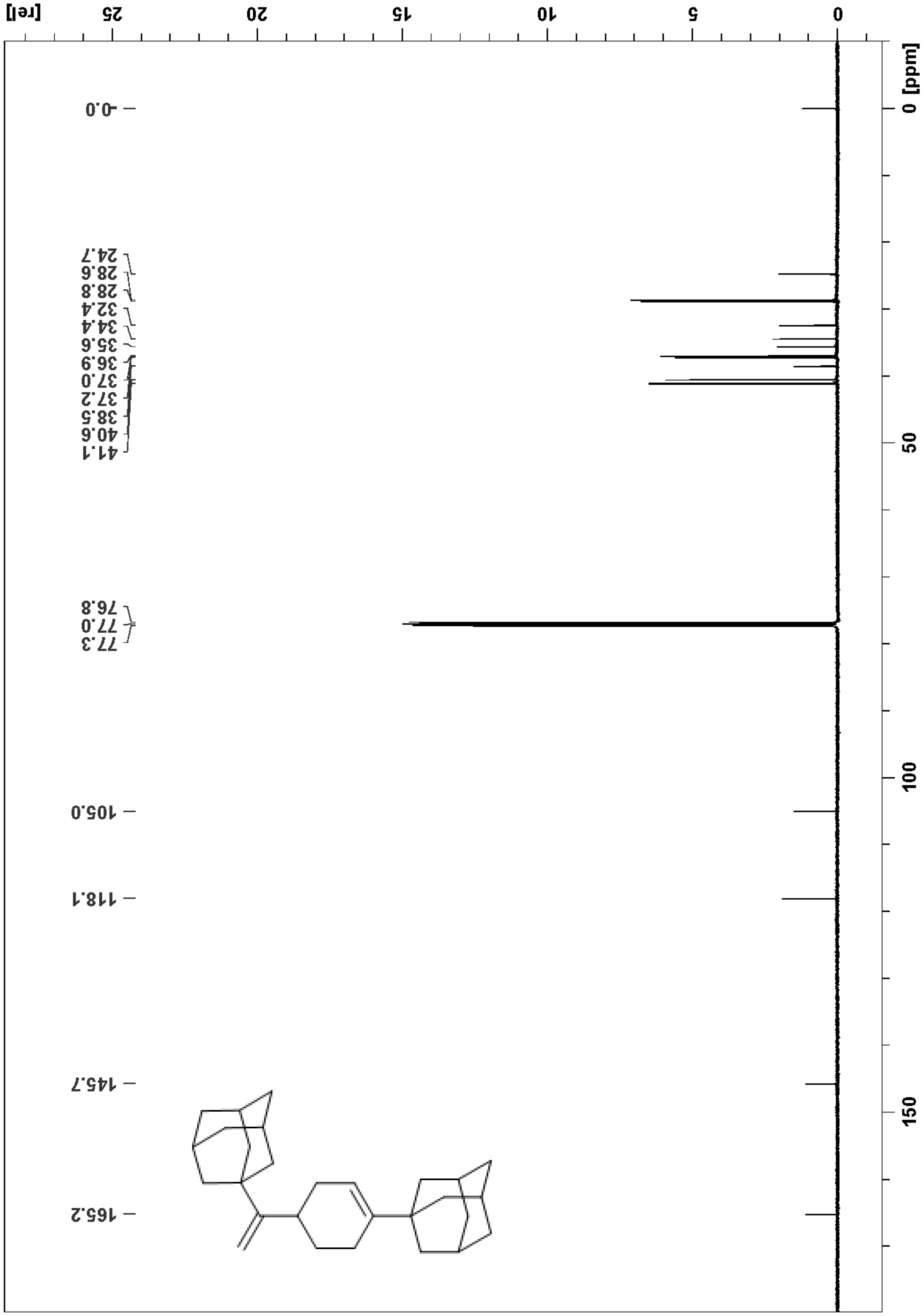
-0.0
24.7
28.6
28.8
32.4
34.4
35.6
36.9
37.0
37.2
38.5
40.6
41.1
76.8
77.0
77.3
105.0
118.1
145.7
165.2
0 [ppm]
50
100
150
[rel]
25
20
15
10
5
0

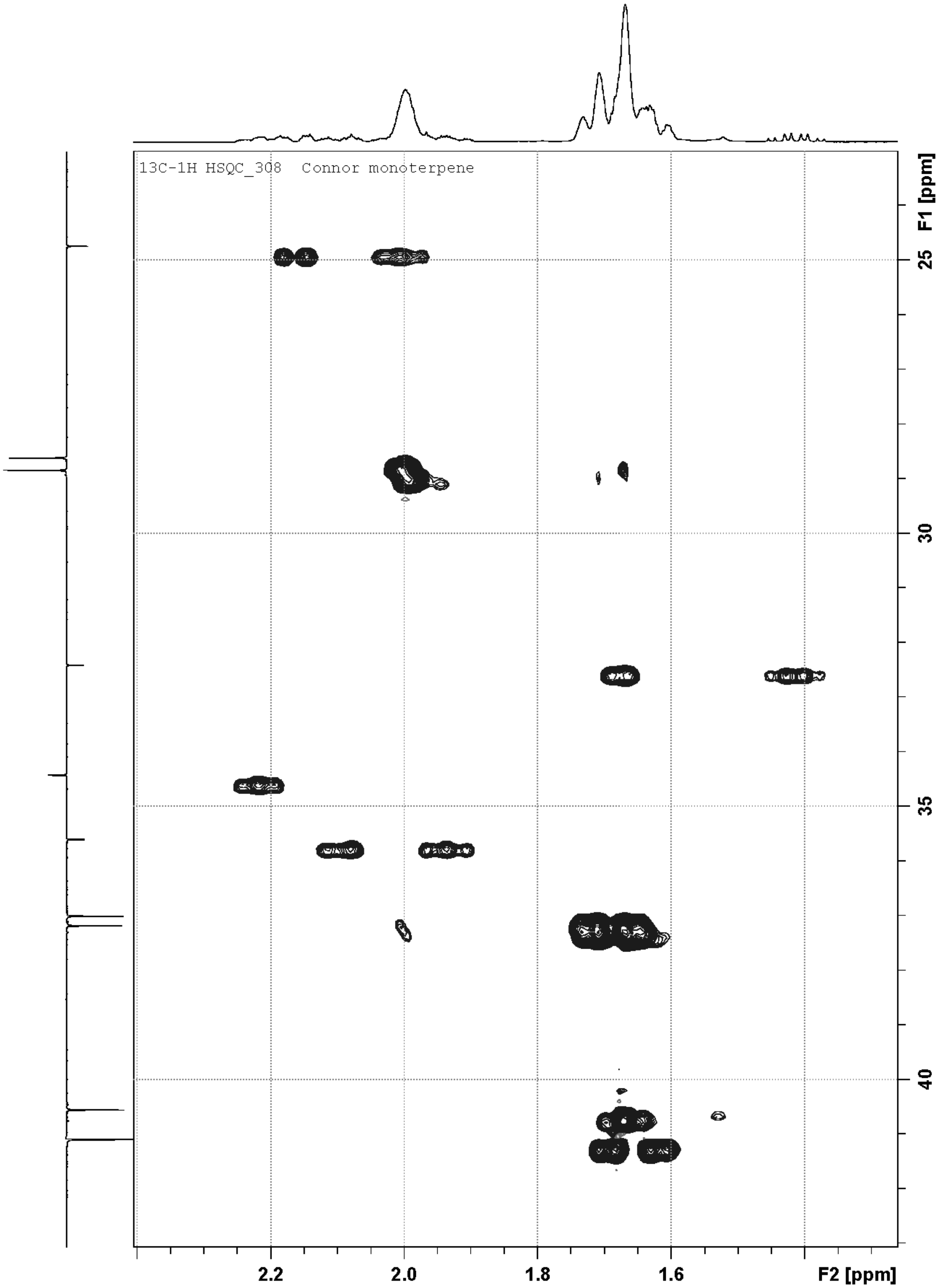

Figure 7.4: HSQC NMR spectrum of **3a** (^{1}H and DEPT 135)

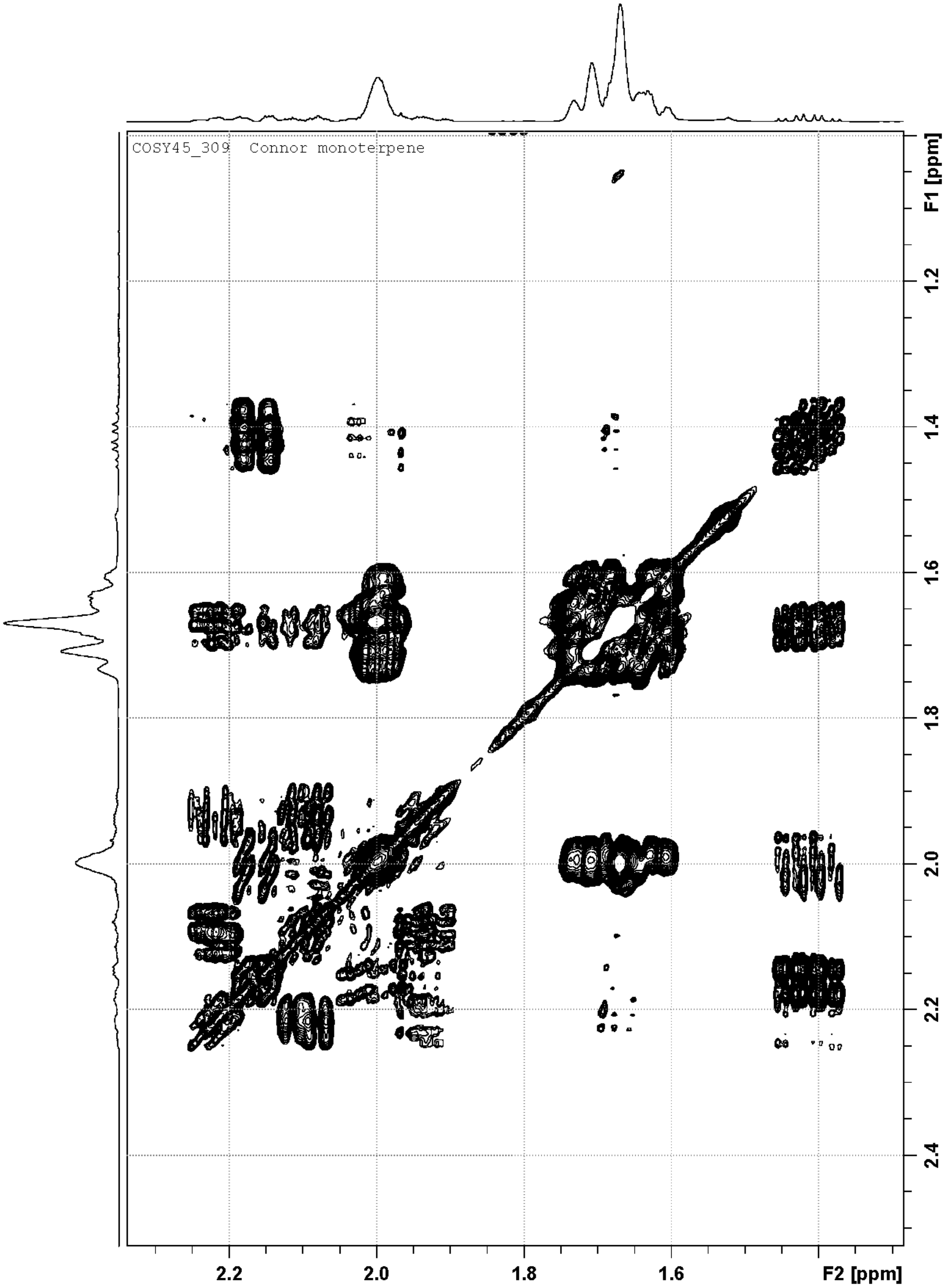

Figure 7.5: COSY NMR spectrum of **3a**

NMR Spectra of Isolated Compounds

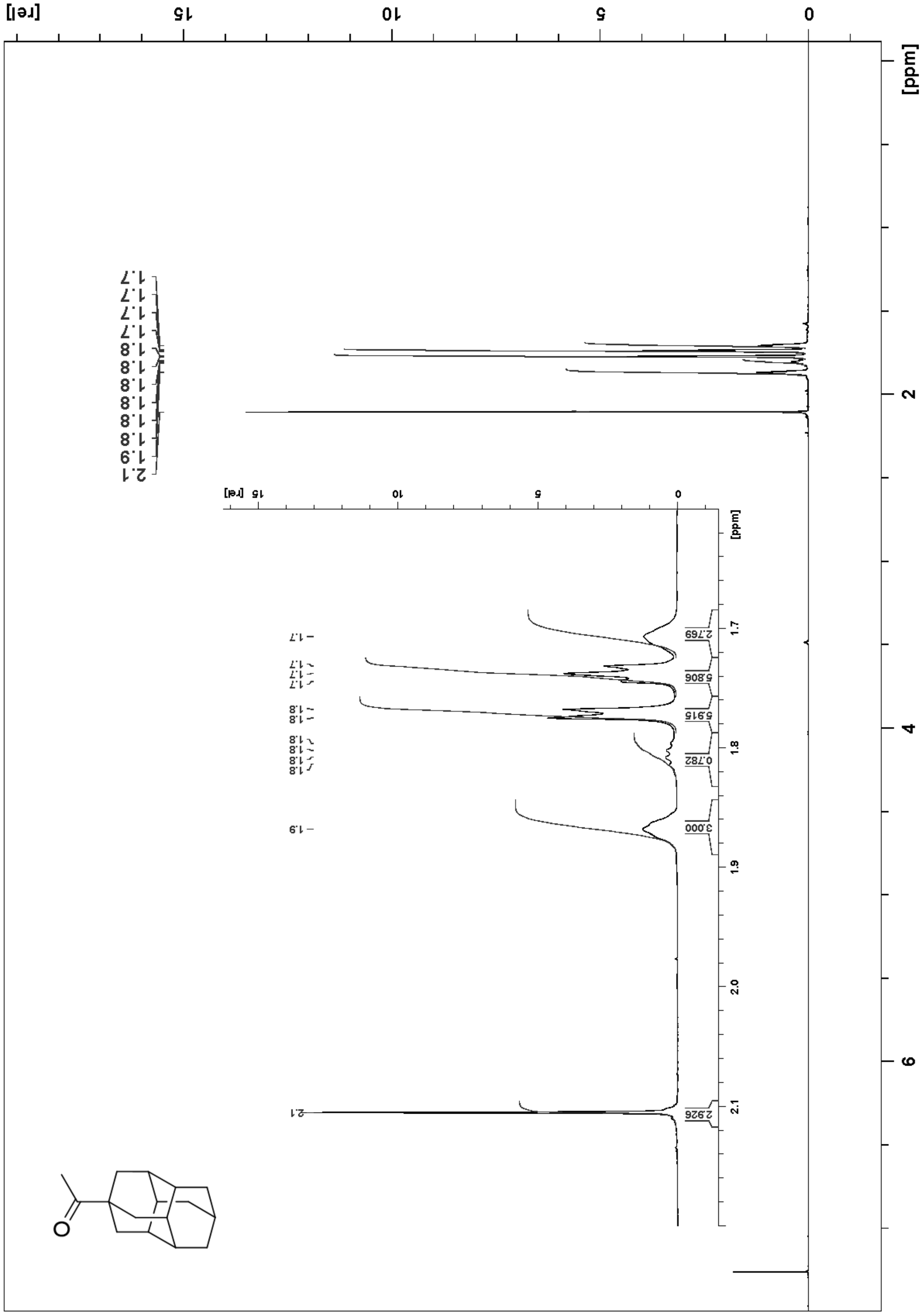

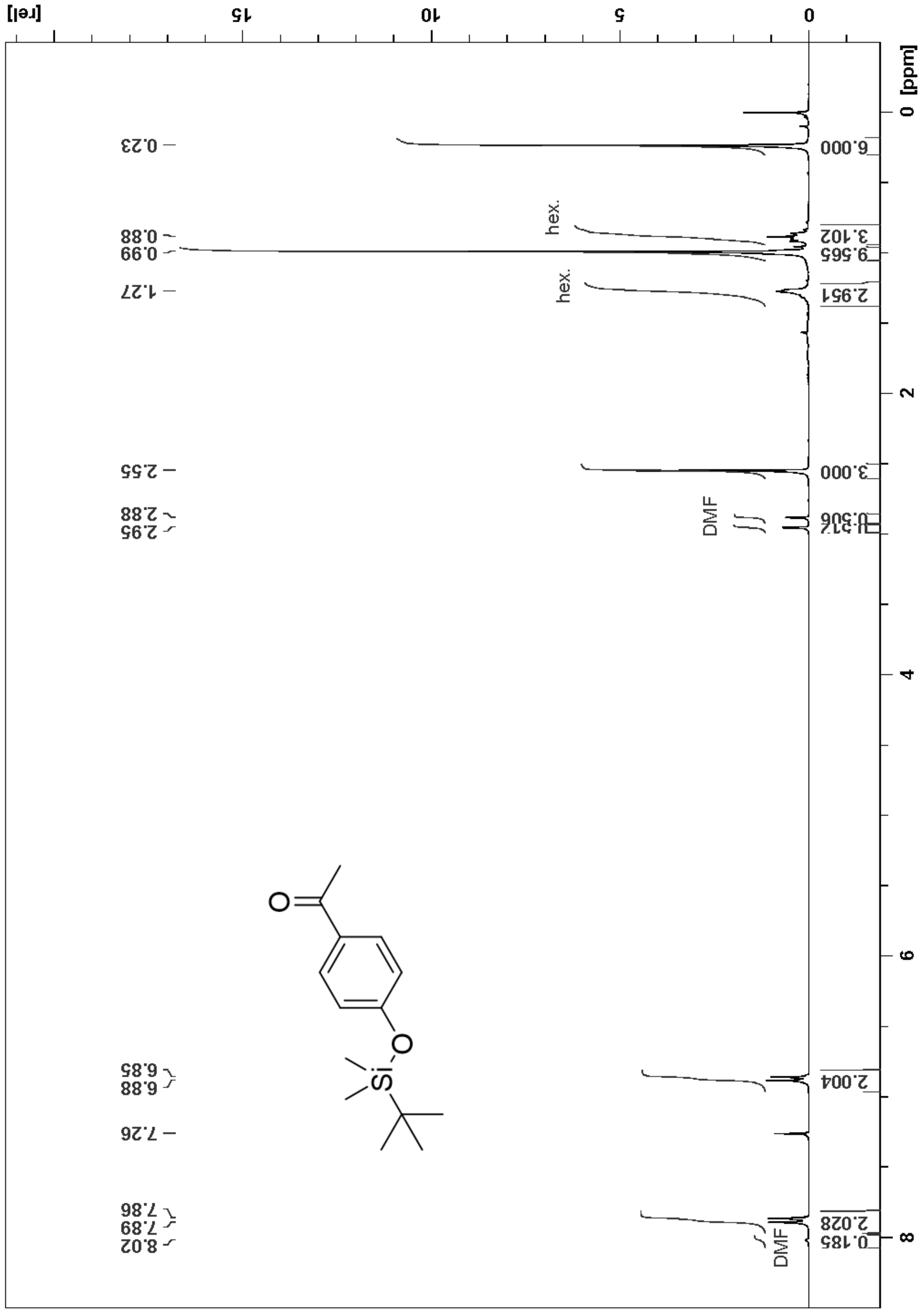
[rel]
15
10
5
0
[ppm]
0
2
4
6
8
0.23
0.88
0.99
1.27
2.55
2.88
2.95
6.85
6.88
7.26
7.86
7.89
8.02
hex.
hex.
DMF
DMF
6.000
3.102
9.565
2.951
3.000
0.306
0.314
2.004
2.028
0.185
O
O
Si

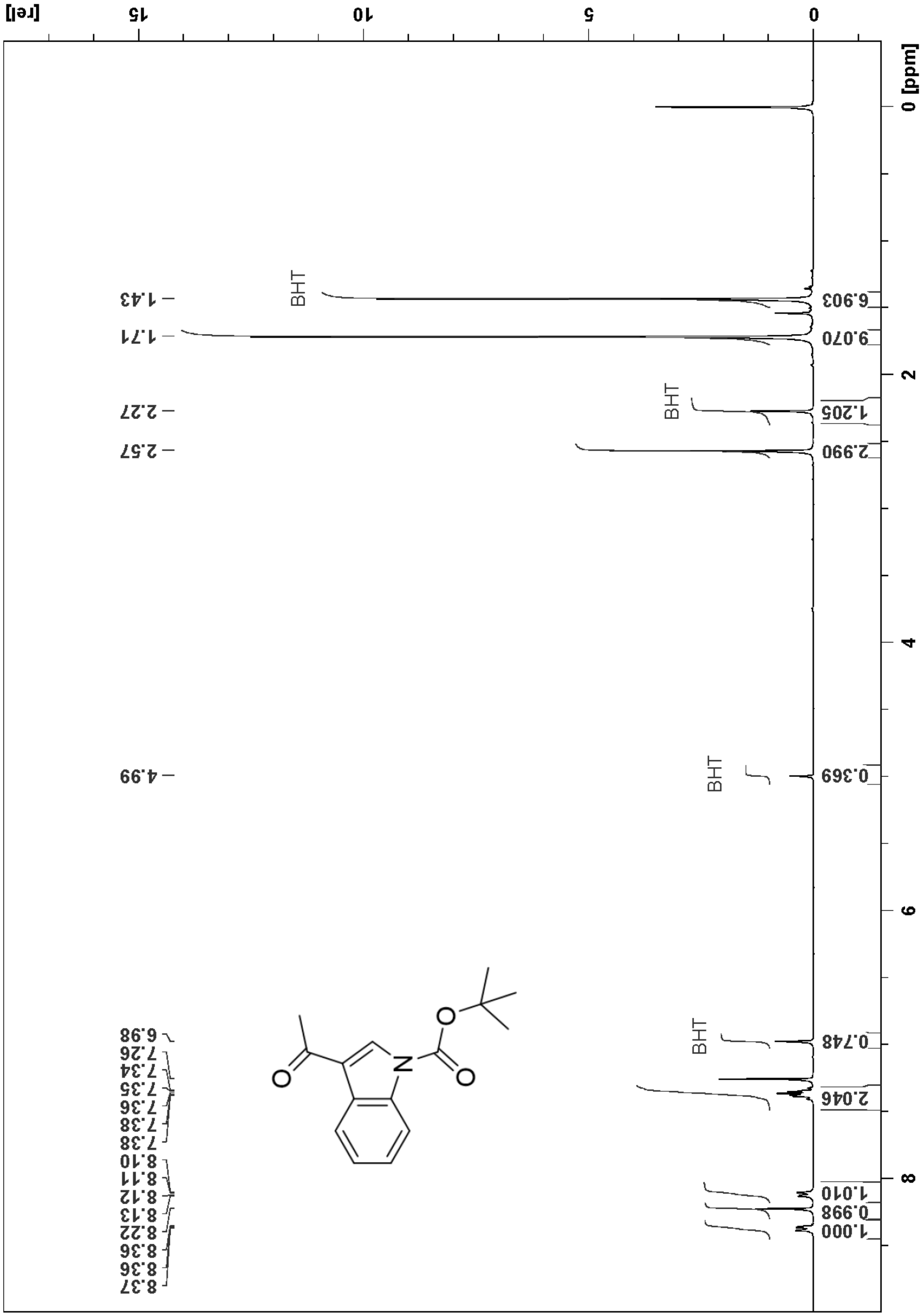
8.37
8.36
8.36
8.22
8.13
8.12
8.11
8.10
7.38
7.38
7.36
7.35
7.34
7.26
6.98
4.99
2.57
2.27
1.71
1.43
BHT
BHT
BHT
BHT
1.000
0.998
1.010
2.046
0.748
0.369
2.990
1.205
9.070
6.903
8
6
4
2
0 [ppm]
0
5
10
15
[rel]
O
N
O
O

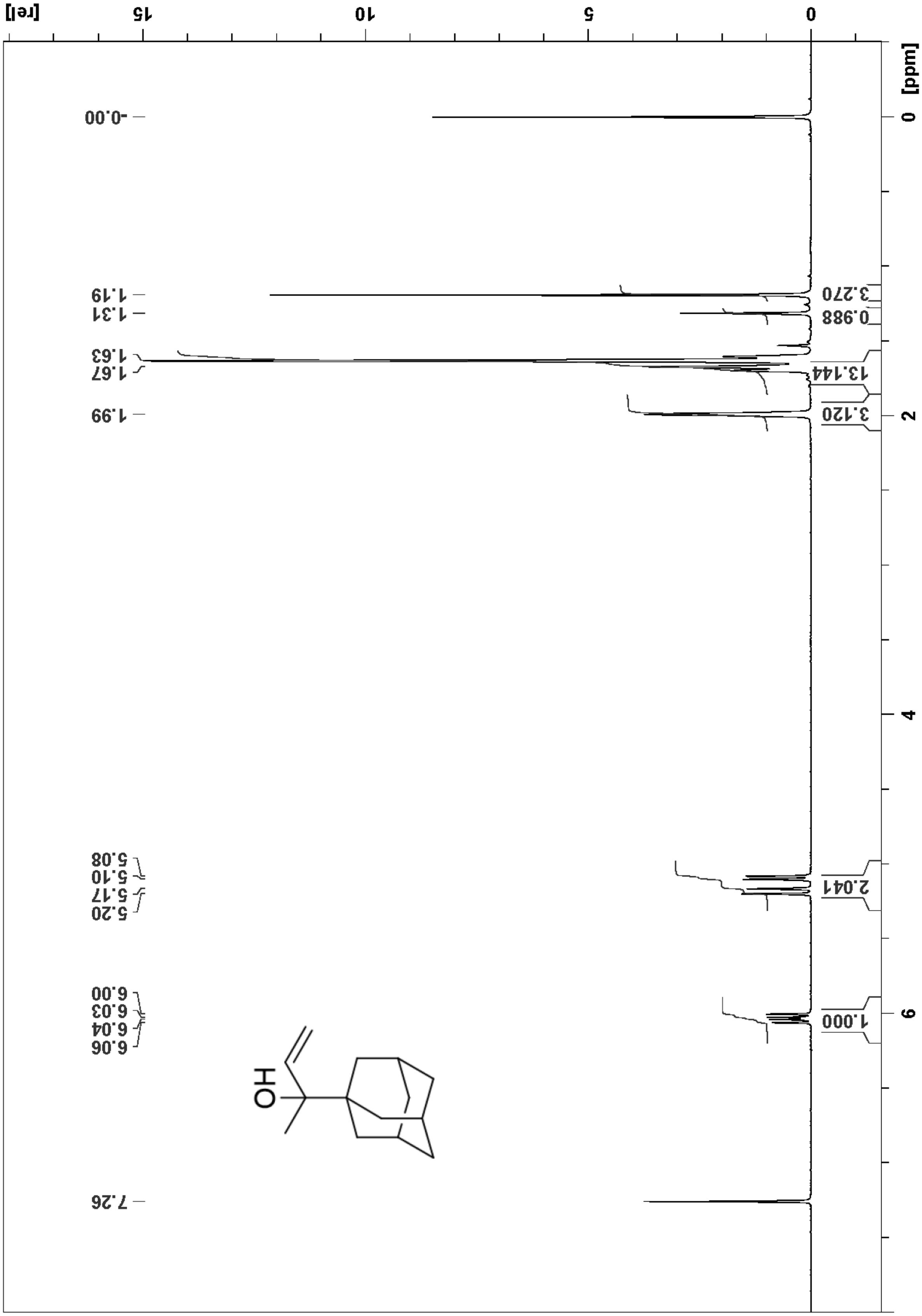
[ppm]
0
2
4
6
[rel]
0
5
10
15
-0.00
1.19
1.31
1.63
1.67
1.99
5.08
5.10
5.17
5.20
6.00
6.03
6.04
6.06
7.26
3.270
0.988
13.144
3.120
2.041
1.000
OH

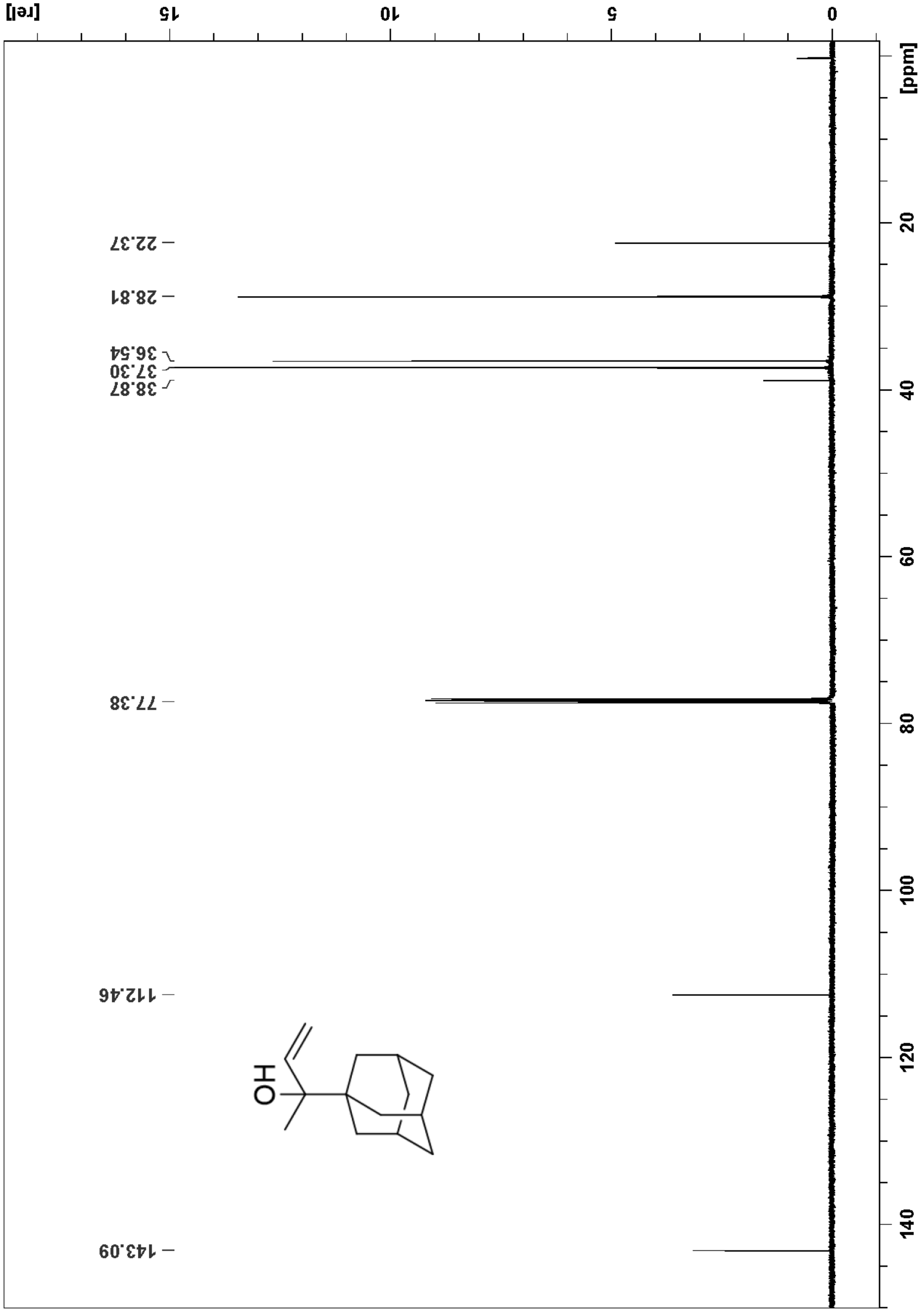
[rel]
15
10
5
0
[ppm]
20
40
60
80
100
120
140
22.37
28.81
36.54
37.30
38.87
77.38
112.46
143.09
OH

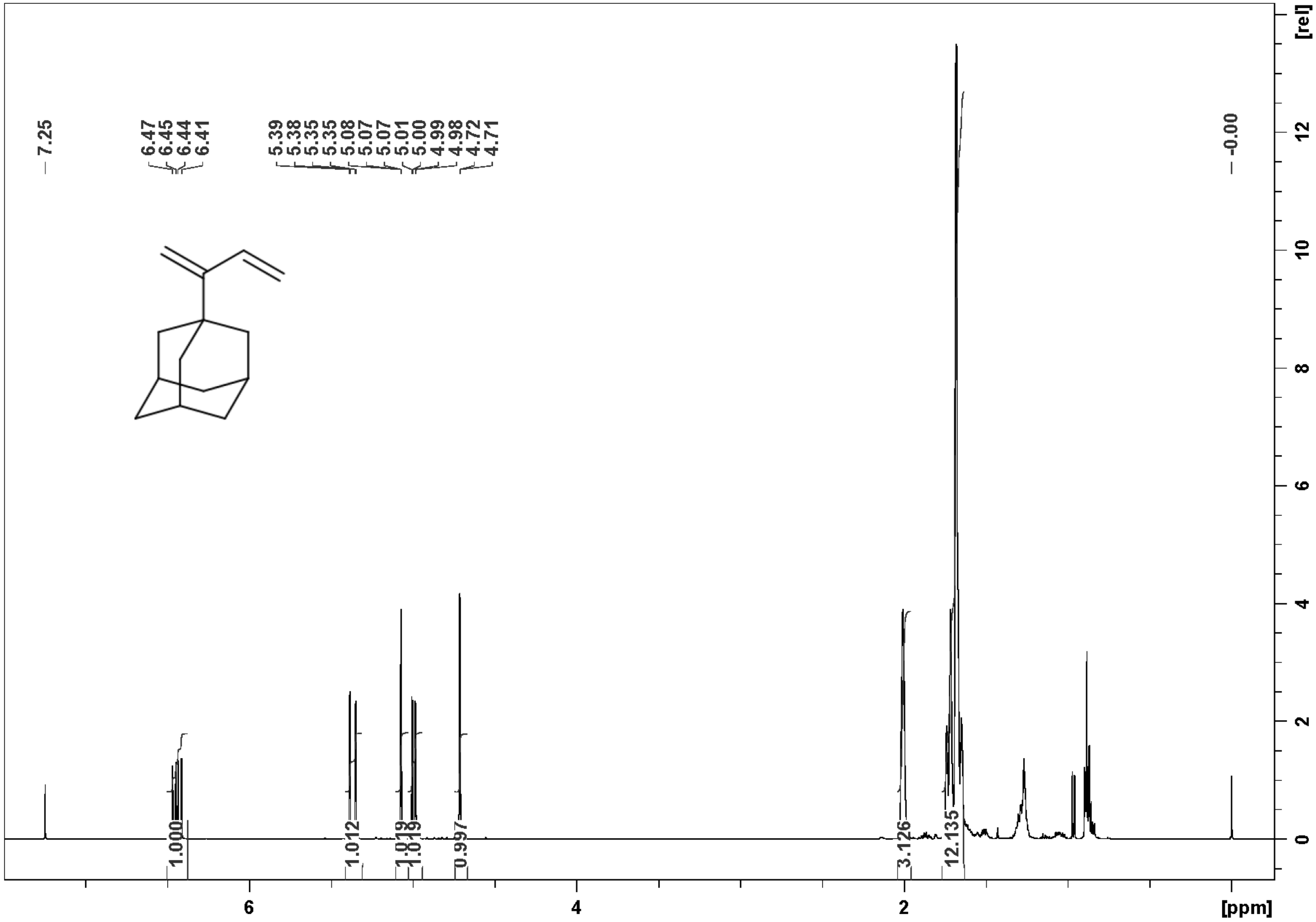
7.25
6.47
6.45
6.44
6.41
5.39
5.38
5.35
5.35
5.08
5.07
5.07
5.01
5.00
4.99
4.98
4.72
4.71
-0.00
1.000
1.012
1.019
1.019
0.997
3.126
12.135
6
4
2
[ppm]
[rel]
12
10
8
6
4
2
0

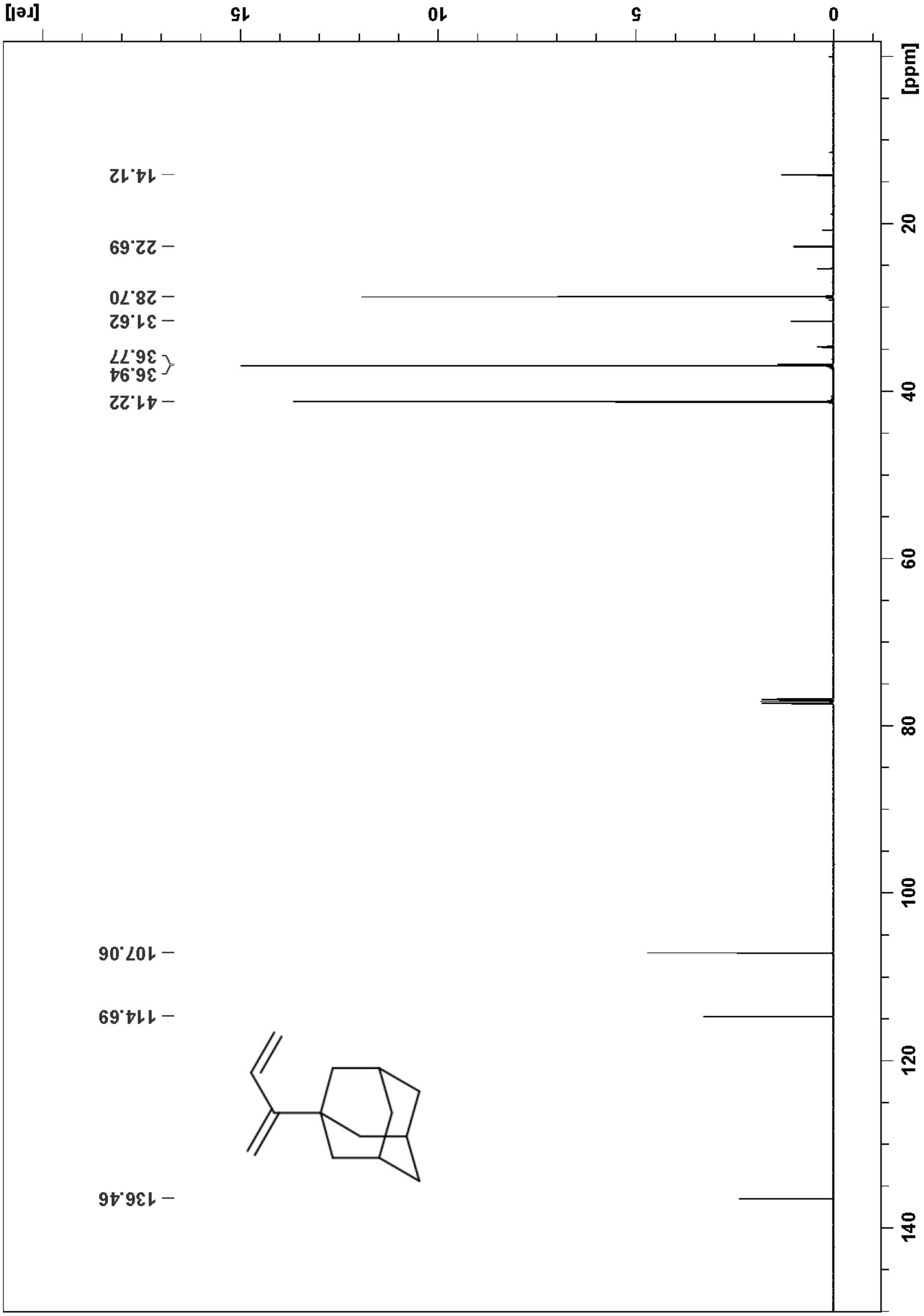
14.12
22.69
28.70
31.62
36.77
36.94
41.22
107.06
114.69
136.46
[rel]
15
10
5
0
[ppm]
20
40
60
80
100
120
140

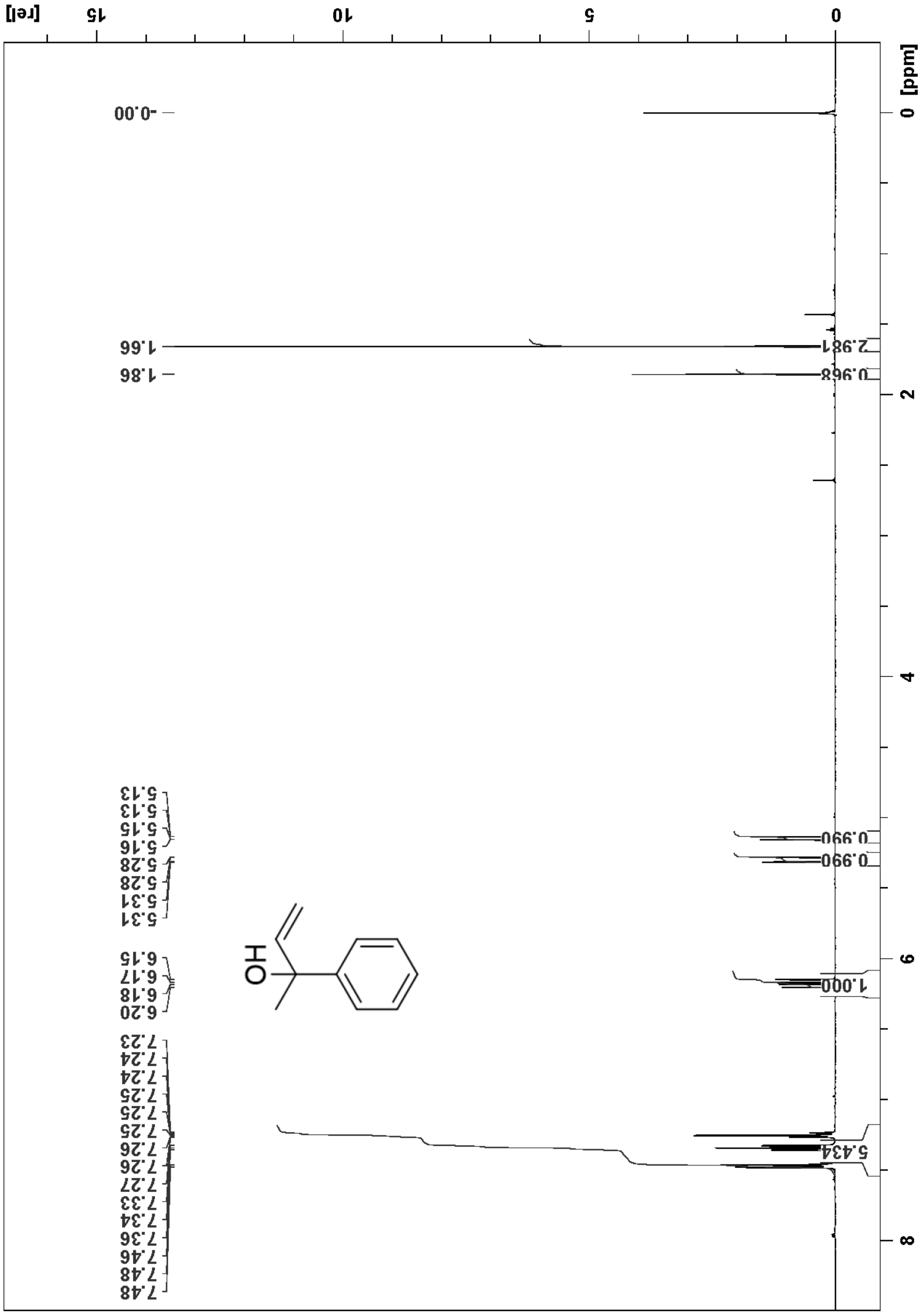
7.48
7.48
7.46
7.36
7.34
7.33
7.27
7.26
7.26
7.25
7.25
7.25
7.24
7.24
7.23
6.20
6.18
6.17
6.15
5.31
5.31
5.28
5.28
5.16
5.15
5.13
5.13
1.86
1.66
-0.00
OH
5.434
1.000
0.990
0.990
0.968
2.981
8
6
4
2
0 [ppm]
15
10
5
0
[rel]

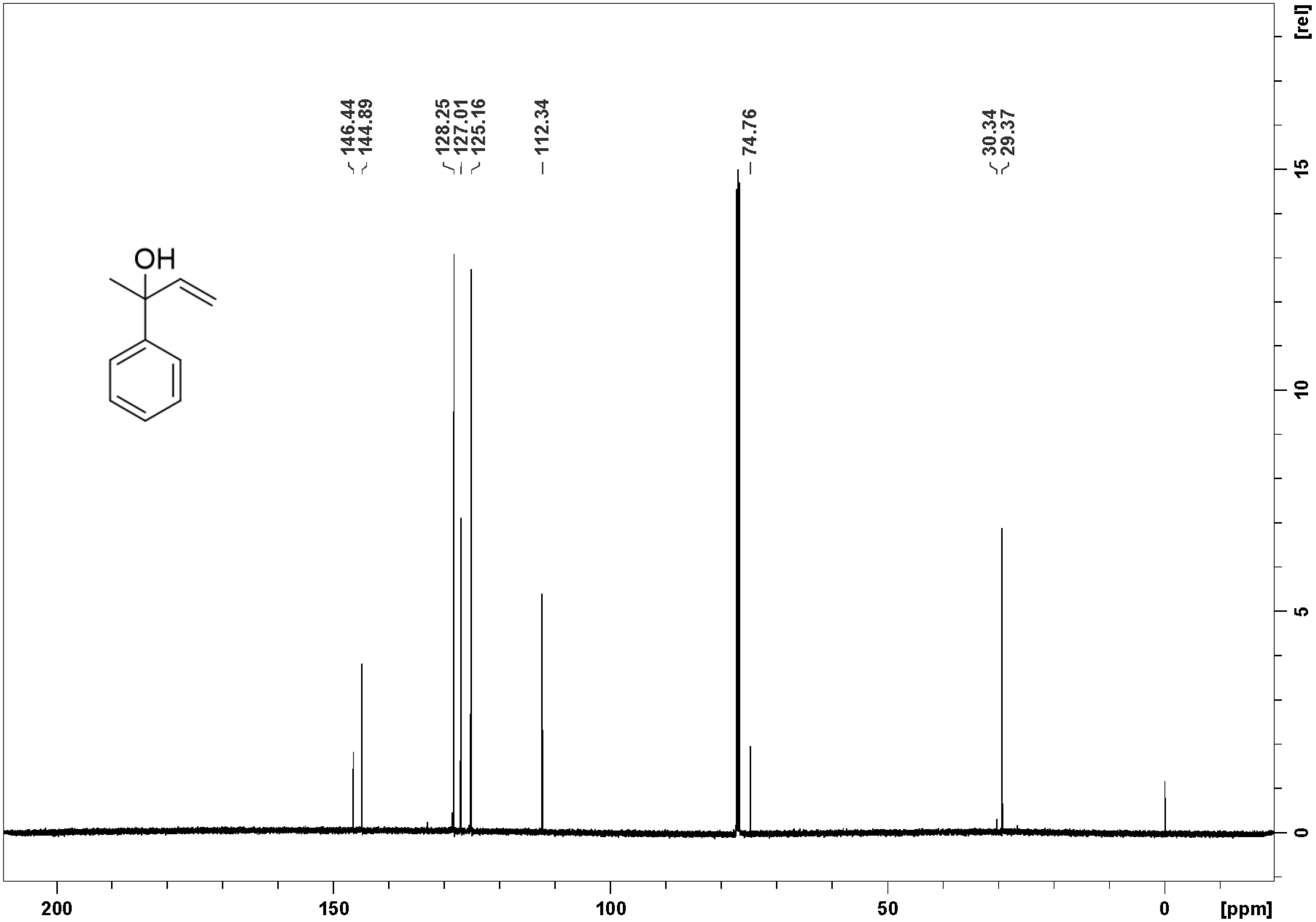
146.44
144.89
128.25
127.01
125.16
112.34
74.76
30.34
29.37
OH
[rel]
15
10
5
0
200
150
100
50
0
[ppm]

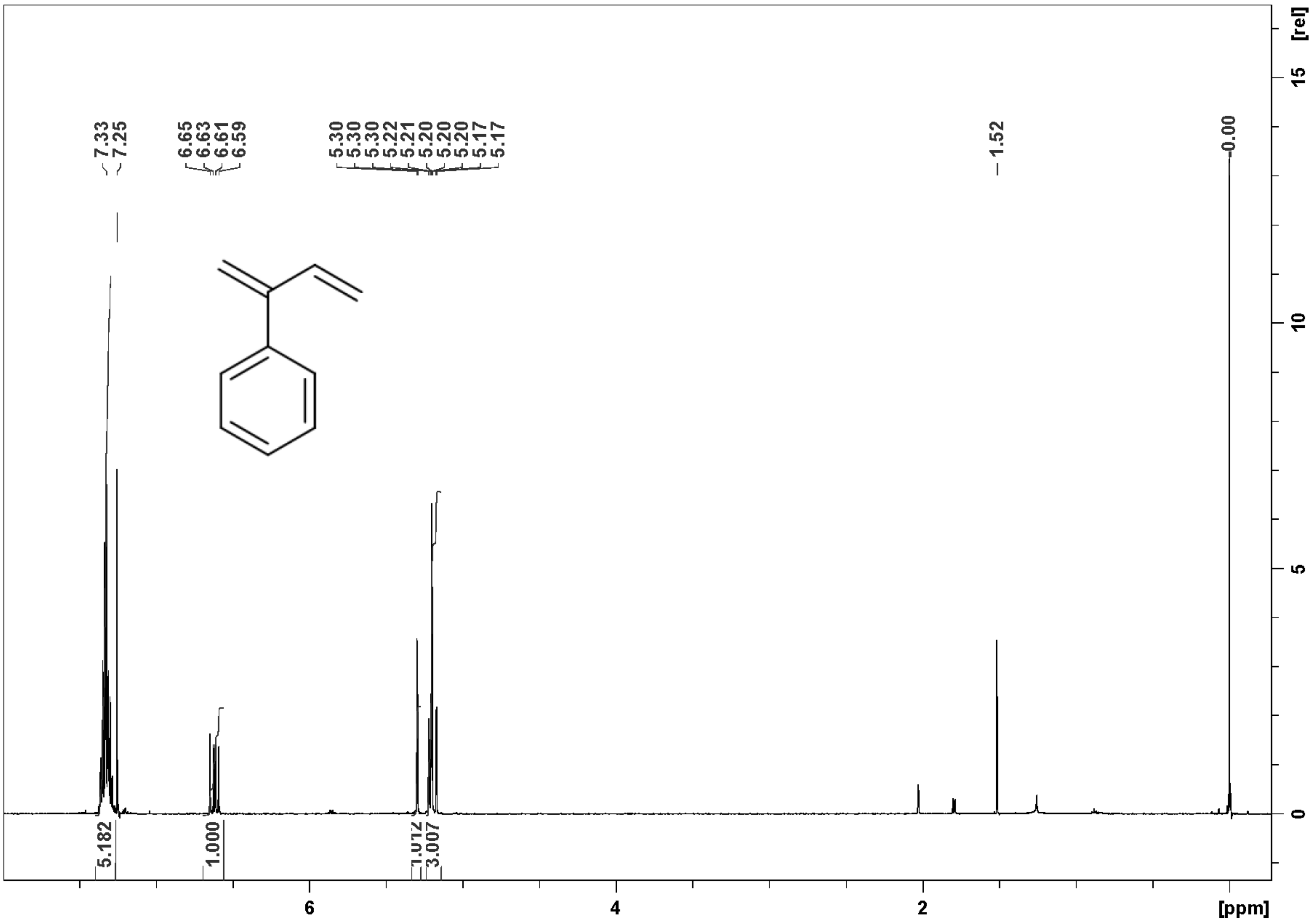
7.33
7.25
6.65
6.63
6.61
6.59
5.30
5.30
5.30
5.22
5.21
5.20
5.20
5.20
5.17
5.17
1.52
-0.00
5.182
1.000
1.012
3.007
[rel]
15
10
5
0
6
4
2
[ppm]

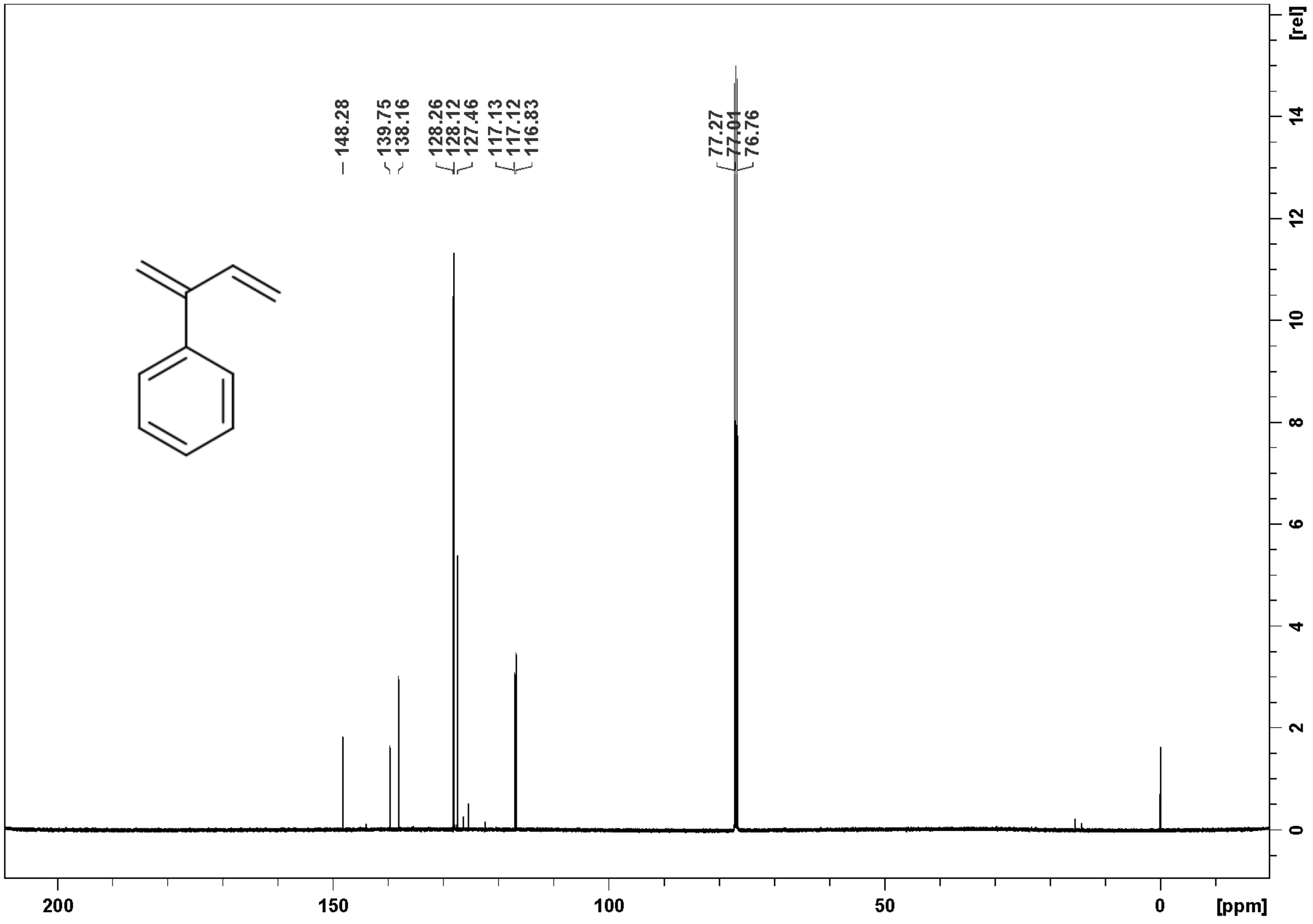
148.28
139.75
138.16
128.26
128.12
127.46
117.13
117.12
116.83
77.27
77.01
76.76
200
150
100
50
0
[ppm]
14
12
10
8
6
4
2
0
[rel]

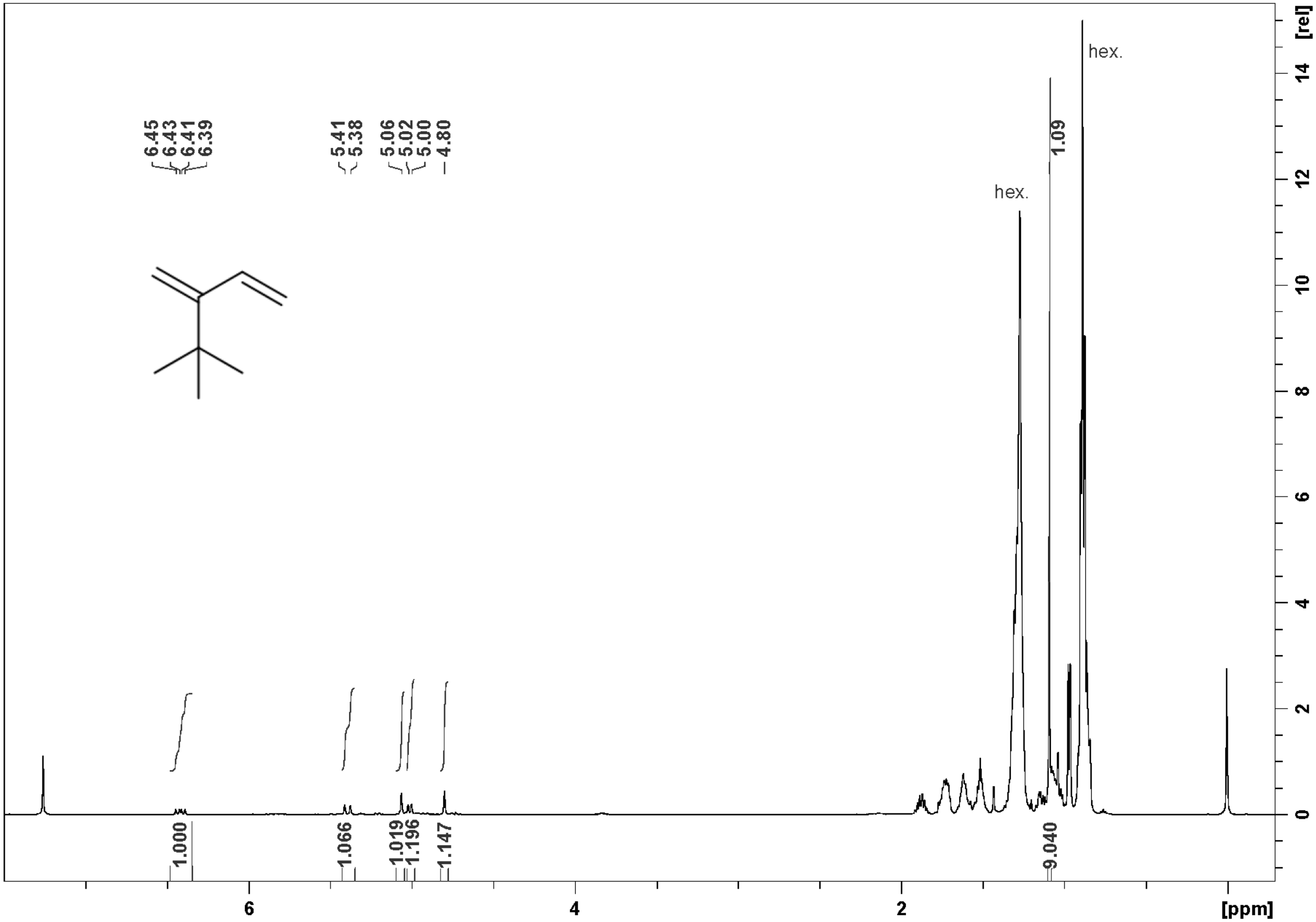
6.45
6.43
6.41
6.39
5.41
5.38
5.06
5.02
5.00
4.80
hex.
1.09
hex.
1.000
1.066
1.019
1.196
1.147
9.040
6
4
2
[ppm]
[rel]
14
12
10
8
6
4
2
0

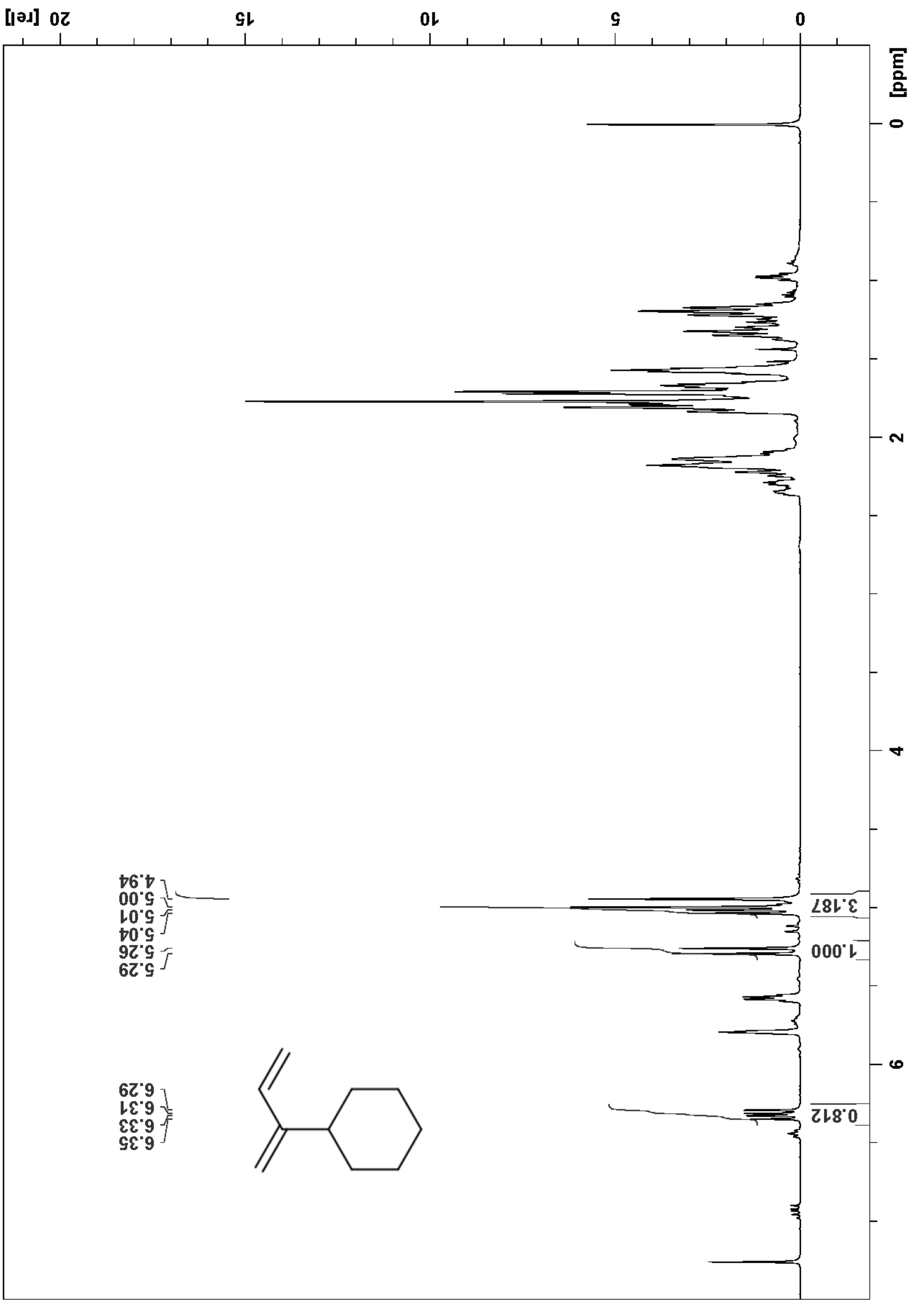

6.35
6.33
6.31
6.29
5.29
5.26
5.04
5.01
5.00
4.94
0.812
1.000
3.187
0
2
4
6
[ppm]
0
5
10
15
20
[rel]

Mass Spectra used for Runs 11 – 18

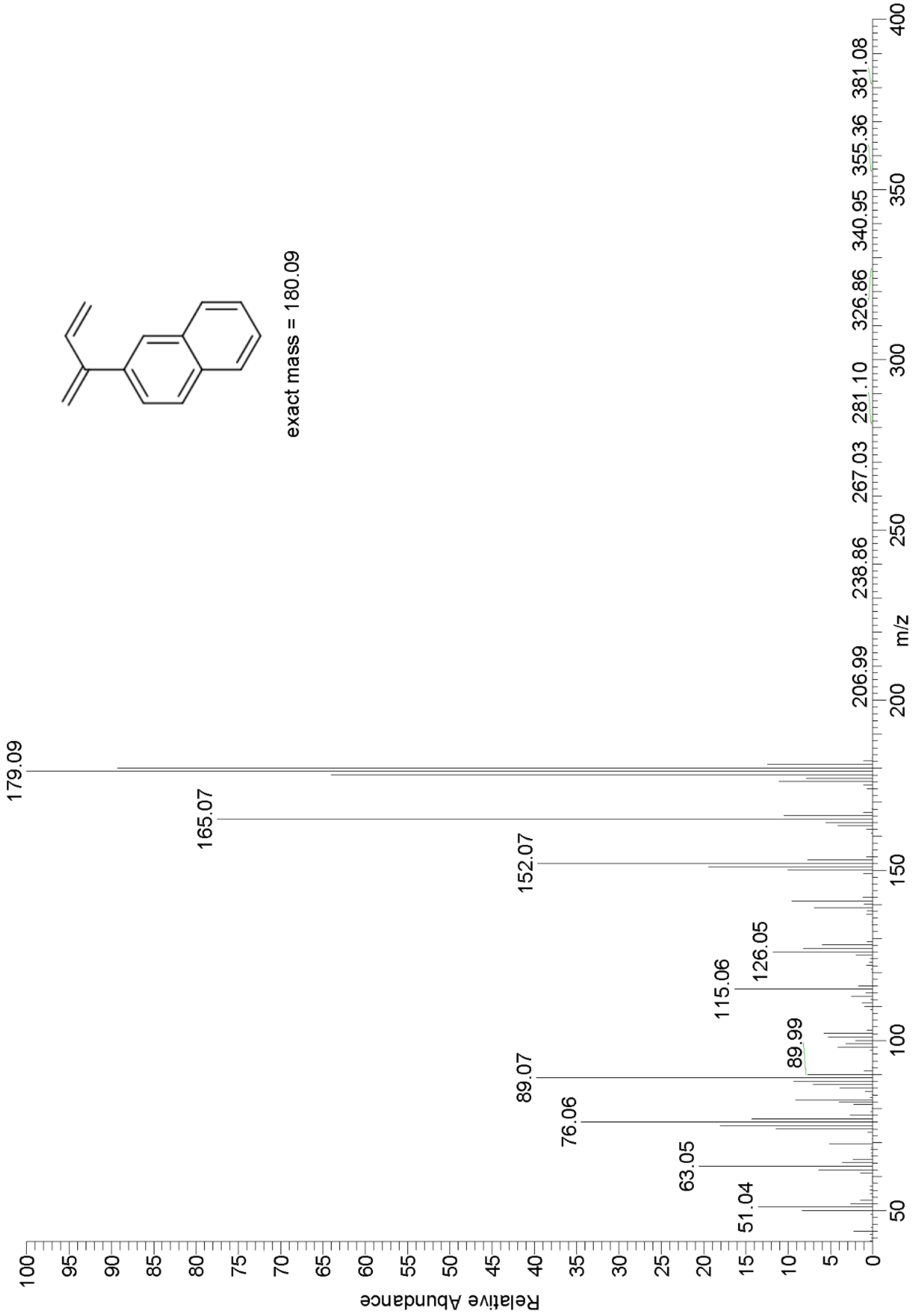

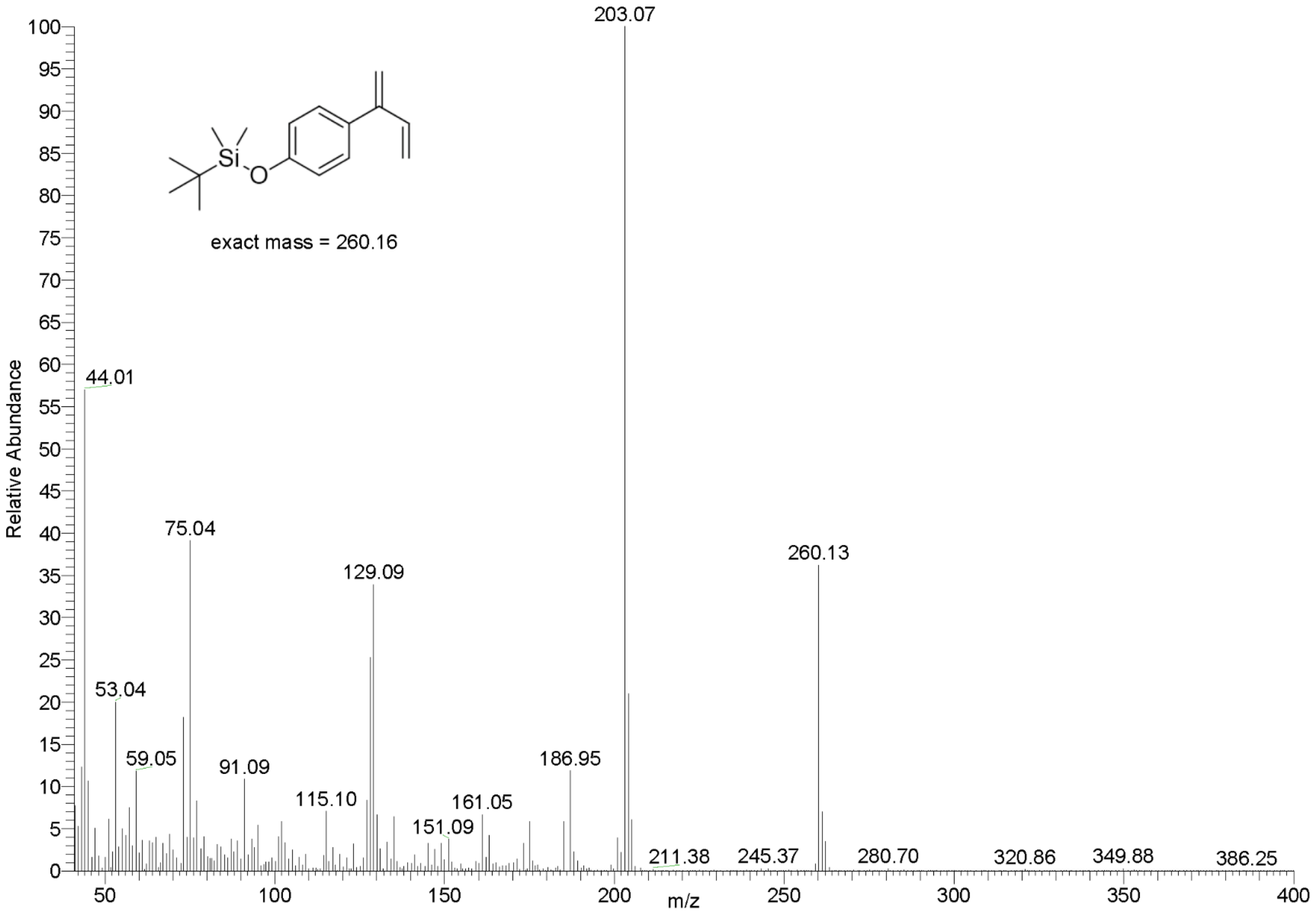
exact mass = 260.16
Relative Abundance
m/z
203.07
44.01
75.04
260.13
129.09
53.04
59.05
91.09
186.95
115.10
161.05
151.09
211.38
245.37
280.70
320.86
349.88
386.25
0
5
10
15
20
25
30
35
40
45
50
55
60
65
70
75
80
85
90
95
100
50
100
150
200
250
300
350
400

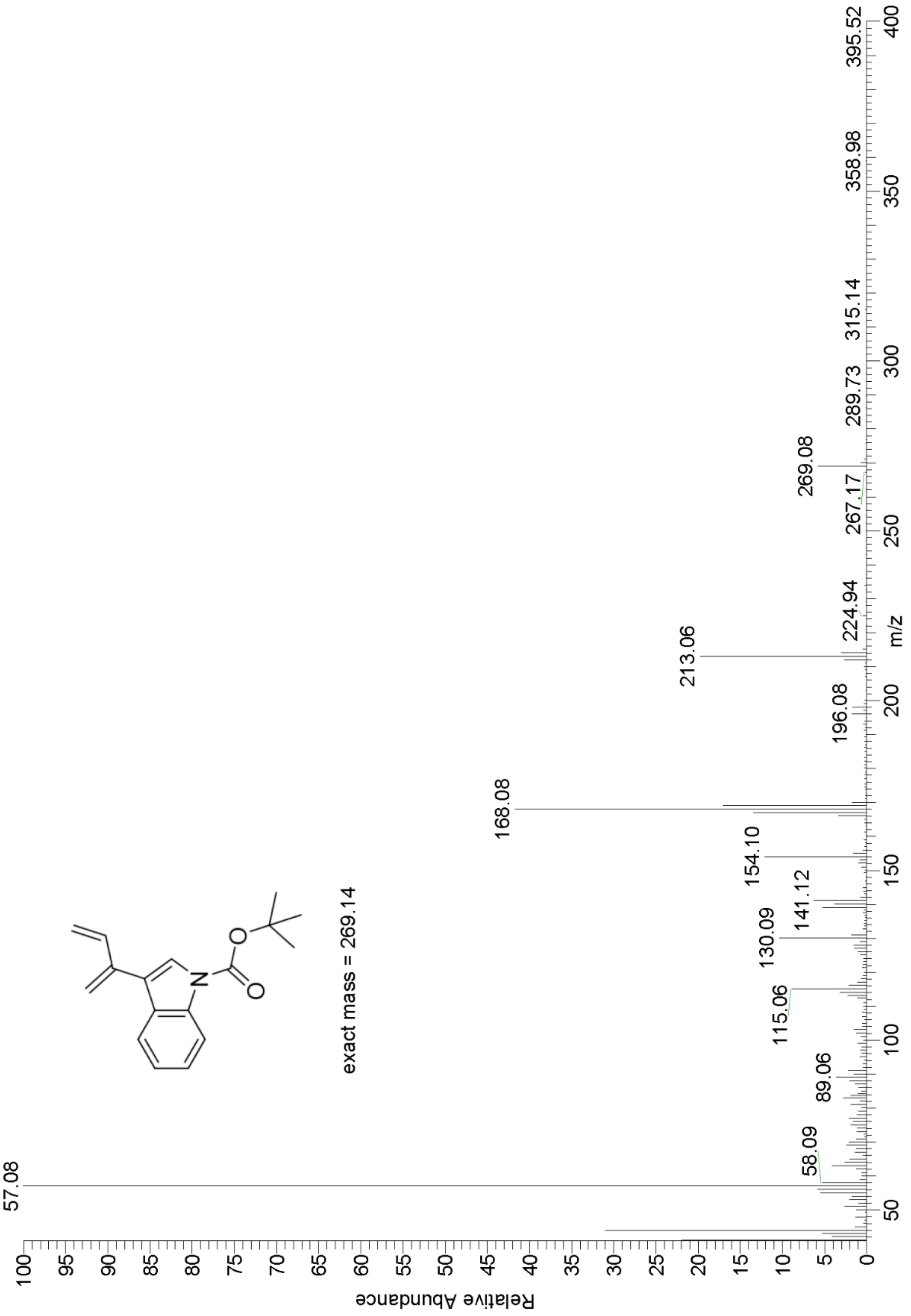
exact mass = 269.14
57.08
58.09
89.06
115.06
130.09
141.12
154.10
168.08
196.08
213.06
224.94
267.17
269.08
289.73
315.14
358.98
395.52
Relative Abundance
m/z
0
5
10
15
20
25
30
35
40
45
50
55
60
65
70
75
80
85
90
95
100
50
100
150
200
250
300
350
400
N
O
O

Appendix B - Chapter 3 Supporting Information

Microstructure Characterization

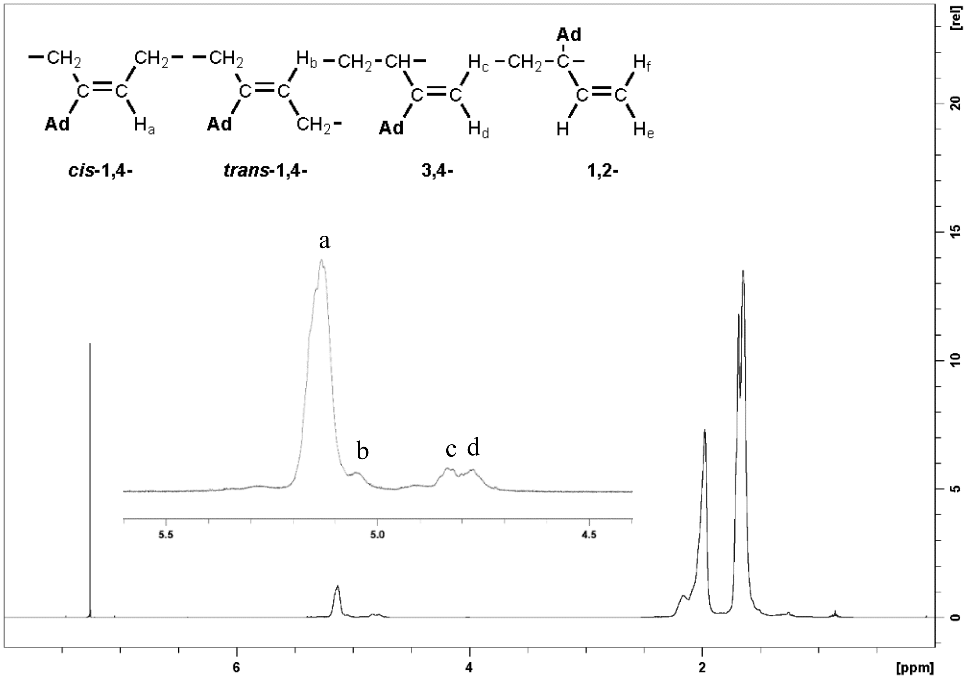

Figure 7.6: ^{1}H NMR spectra of poly(**1**) (Run 3) and microstructure assignments in the olefinic region

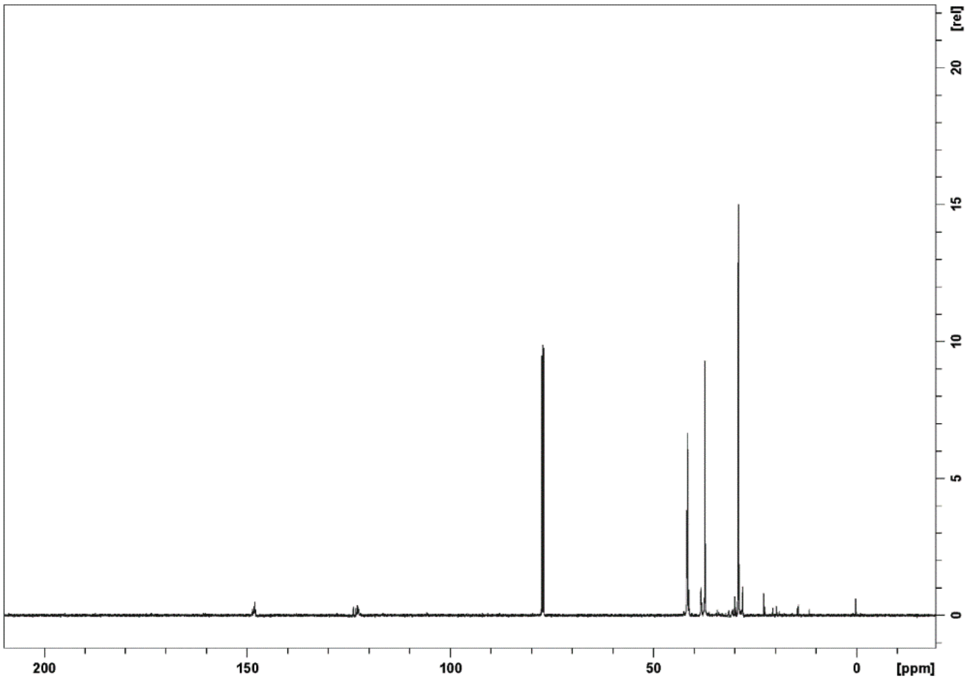

Figure 7.7: ^{13}C NMR spectra of poly(**1**) (Run 3)

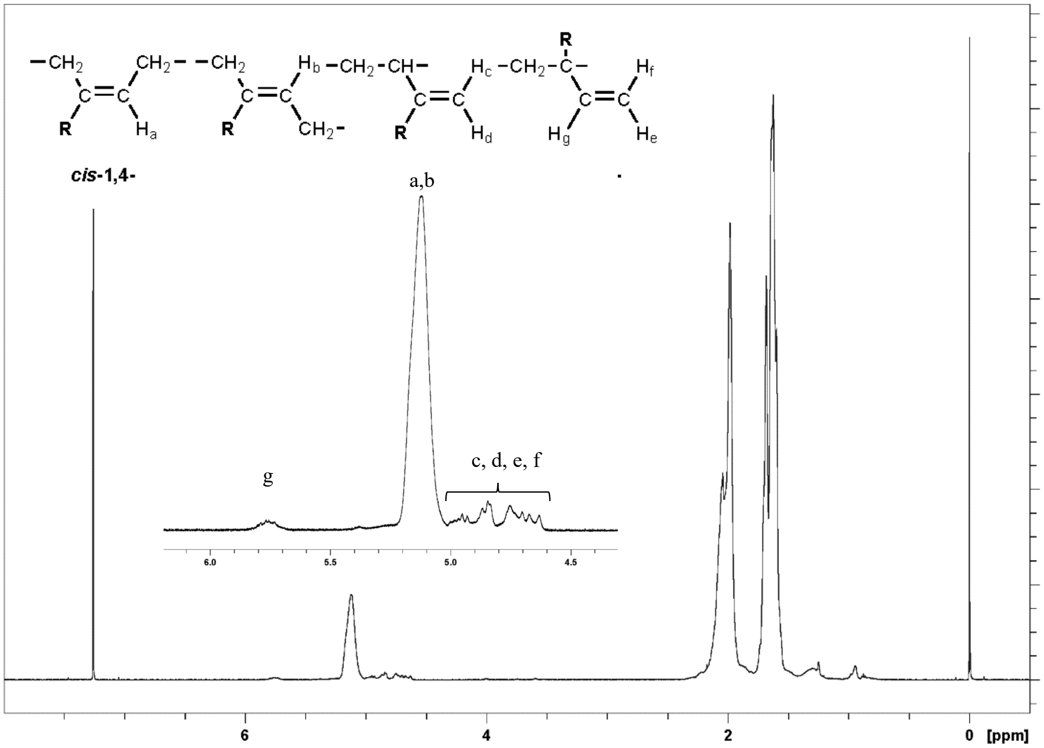

Figure 7.8: ^{1}H NMR spectra of poly(**1**-*ran*-isoprene) (Run 14) and microstructure assignments in the olefinic region

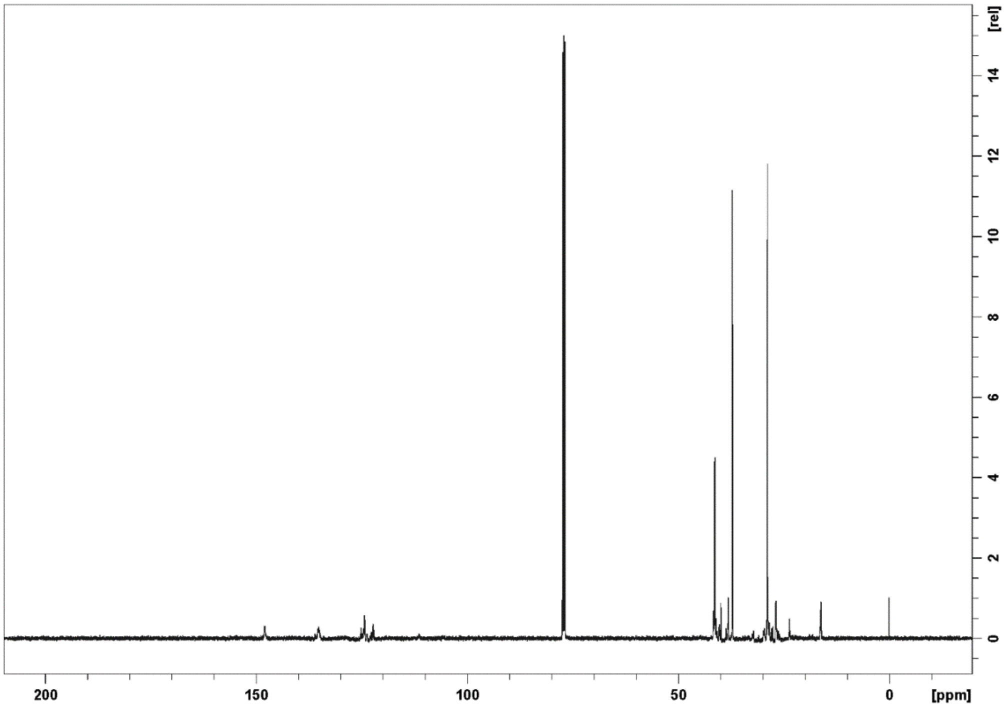

Figure 7.9: ^{13}C NMR spectra of poly(**1**-*ran*-isoprene) (Run 14)

Determination of Adamantyl Content in poly(1-*ran*-isoprene) by ^{1}H NMR

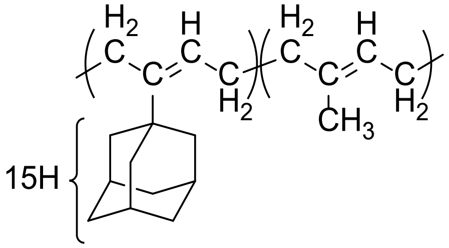

Figure 7.10: poly(**1**-*ran*-isoprene) structure

Considering the structure of poly(**1**-*ran*-isoprene) that is entirely 1,4-units, there are 19 sp^3 protons attributed to each **1** repeat unit and 7 sp^3 protons for each isoprene repeat unit. The average number of sp^3 protons (p_a) in a repeat unit of 1,4-poly(**1**-*ran*-isoprene) can then be expressed in terms of mole fraction by eq. 1.

$$\left(p_{sp^3} = 7x_i + 19x_{\mathbf{1}} \right) \tag{1}$$

Where x_i and $x_{\mathbf{1}}$ are the mole fractions of isoprene and **1**. Each 1,4-repeat unit will contribute 1 sp^2 proton. The number of sp^2 protons (p_v) in a repeat unit of 1,4-poly(**1**-*ran*-isoprene) can then be expressed in terms of mole fraction by eq. 2.

$$p_{sp^2} = x_i + x_{\mathbf{1}} = 1 \tag{2}$$

The presence of 3,4-microstructure, whether from **1** or isoprene, will result in a net loss of 1 sp^3 proton and a net gain of 1 sp^2 proton. Similarly, all 1,2-repeat units result in a loss of 2 sp^3 protons and an increase in 2 sp^2 protons. Therefore, eq. 1 and eq. 2 can be expressed as eq. 3 and eq. 4 to account for the observed microstructure.

$$p_{sp^3} = 7x_i + 19x_{\mathbf{1}} - a - 2b \tag{3}$$

$$p_{sp^2} = 1 + a + 2b \tag{4}$$

Where a and b are the mole fraction of 3,4- and 1,2-microstructure in the sample. These values can be determined by integrating the ^{1}H NMR spectrum. Expressing x_i in terms of $x_{\mathbf{1}}$ gives eq. 5.

$$p_{sp^3} = 7(1 - x_{\mathbf{1}}) + 19x_{\mathbf{1}} - a - 2b \tag{5}$$

The ratio of total sp^3 to total sp^2 protons (p_a/p_v) can be determined by integration of the ^{1}H NMR spectrum and is expressed as eq. 6.

$$\frac{p_{sp^3}}{p_{sp^2}} = \frac{7(1-x_1) + 19x_1 - a - 2b}{1 + a + 2b} \tag{6}$$

Solving for x_1 gives eq. 7.

$$x_1 = \frac{\left(\frac{p_{sp^3}}{p_{sp^2}}\right)(1 + a + 2b) + a + 2b - 7}{12} \tag{7}$$

Differential Scanning Calorimetry of Copolymer and Physical Mixture

The Figure below shows the DSC data for pure poly(**1**) and poly(isoprene)

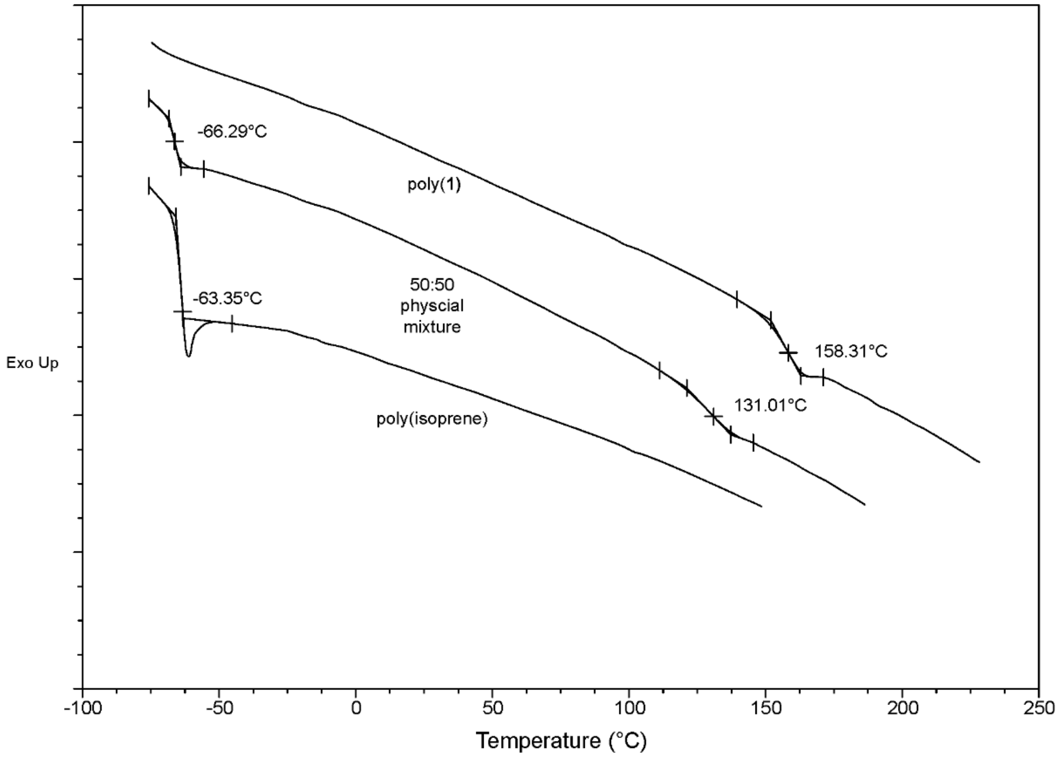

Figure 7.11: Differential Scanning Calorimetry of Copolymer and Physical Mixture

Variation of T_g with M_n for poly(1)

The Figure below shows the variation of T_g for pure poly(**1**) including unpublished data from nitroxide mediated polymerization and thermal/autopolymerization, and data from Kobayashi, et al.

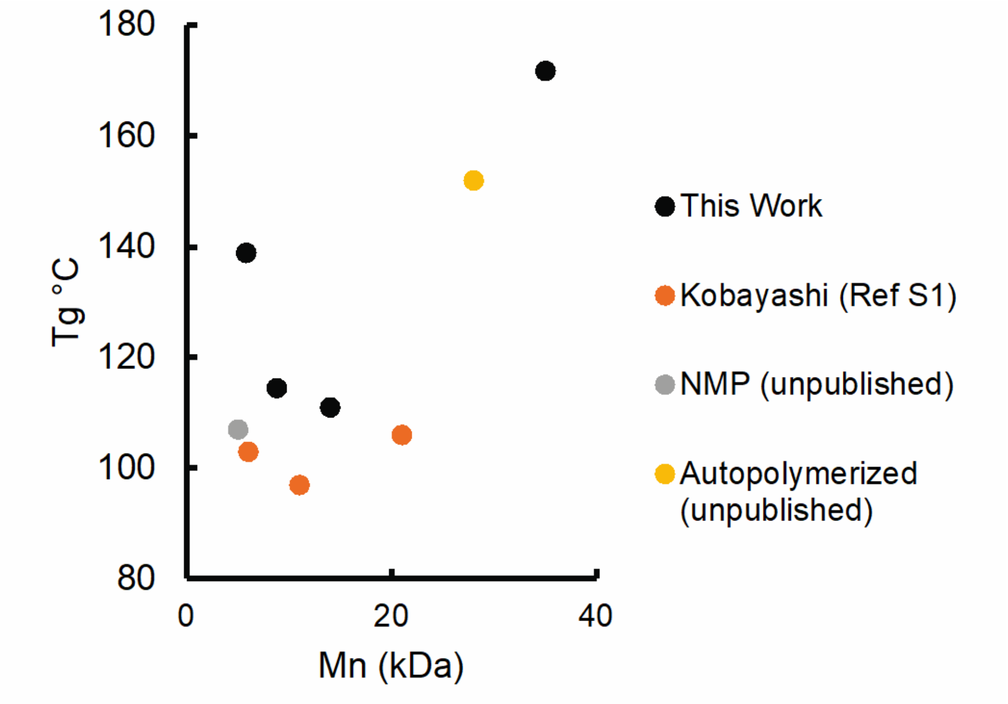

Figure 7.12: Compiled variations of in T_g vs. M_n found for poly(**1**)